Phosphodiesterases 4B and 4D Differentially Regulate cAMP Signaling in Calcium Handling Microdomains of Adult Mouse Cardiomyocytes

Doctoral Thesis

University of Hamburg, Faculty of
Mathematics, Informatics and Natural Sciences
Department of Chemistry

Submitted by

Axel E. Kraft

Hamburg, April 2019

Die Druckfreigabe für die vorliegende Arbeit wurde am 15. April 2019 durch das Studienbüro des Fachbereiches Chemie der Universität Hamburg erteilt.

Reviewer:	Prof. Dr. rer. nat. Viacheslav O. Nikolaev
Second Reviewer:	Prof. Dr. med. Elke Oetjen
Date of Disputation:	April 12, 2019

Die vorliegende Arbeit „*Phosphodiesterases 4B and 4D Differentially Regulate cAMP Signaling in Calcium Handling Microdomains of Adult Mouse Cardiomyocytes*“ wurde am Institut für Experimentelle Herz-Kreislaufforschung des Universitätsklinikums Hamburg-Eppendorf im Zeitraum 1. August 2015 - 31. Dezember 2018 angefertigt.

Acknowledgements

I would like to thank Prof. Dr. Viacheslav Nikolaev for giving me the opportunity to work on this really fascinating topic and for his excellent supervision during the time of my PhD thesis.

I am really grateful for Prof. Dr. Elke Oetjen co-supervising my thesis.

Thanks to Prof. Dr. Marco Conti and Prof. Dr. Thomas Wieland for their valuable and helpful advice for this work.

I would also like to thank the whole Nikolaev working group for the outstanding working atmosphere. Special thanks go to Karina Schlosser, Sophie Sprenger and Annabell Kühl for their excellent technical assistance.

Thanks to the members of the UKE Microscopy Facility for performing the STED microscopy experiments.

My dearest thanks go to my sisters and my parents for their continuous support during the last years. Especially to my sister Mieke for reading and commenting on this work.

My special appreciation goes to Anne for her love and support during the last nine years.

Kurzfassung

Der universelle second messenger 3',5'-cyclisches Adenosinmonophosphat (cAMP) reguliert die kardiale elektromechanische Kopplung, indem es in eigenständig regulierten subzellulären Mikrodomänen wirkt. Die Unterfamilien 4B und 4D der Phosphodiesterase sind maßgeblich an der Regulation der cAMP Signalweiterleitung in Säugetierkardiomyozyten beteiligt. Es konnte gezeigt werden, dass Schwankungen der PDE4 Aktivität im menschlichen Herzen zu Arrhythmien und Herzversagen führen.

Das Ziel dieser Arbeit war die systematische Untersuchung der Einflüsse von PDE4B und PDE4D auf die Regulation der cAMP Signalweiterleitung in drei subzellulären Mikrodomänen, die um die Calcium handling Proteine lokalisiert sind.

Untersucht wurde die Regulation der Mikrodomänen um den L-Typ-Calciumkanal (LTCC), die Calciumpumpe des sarcoplasmatischen und endoplasmatischen Reticulums (SERCA2a) und die kardialen Ryanodin Rezeptoren Typ 2 (RyR2), sodass deren Auswirkungen auf Herzfunktionen und -erkrankungen besser verstanden werden können.

Transgene Mäuse, die Förster Resonanz Energy Transfer (FRET) basierende cAMP spezifische Biosensoren in den Mikrodomänen der Caveolin reichen Plasmamembran, der SERCA und des RyR2 exprimieren, wurden mit globalen PDE4B und PDE4D knockout Mäusen gekreuzt. Durch FRET Mikroskopie in adulten ventrikulären Kardiomyozyten, die aus Wildtyp und PDE4B und PDE4D knockout Mäusen isoliert wurden, konnten spezifische Aussagen über den Einfluss beider PDE Unterfamilien auf diese Mikrodomänen getroffen werden. Die Ergebnisse zeigen, dass alle Mikrodomänen unterschiedlich von PDE Unterfamilien reguliert werden. Selbst innerhalb einer Organelle, dem sarkoplasmatischen Retikulum, konnte die Koexistenz von mindestens zwei verschiedenen cAMP-Mikrodomänen gezeigt werden, die um den RyR2 und der SERCA2a lokalisiert sind und von PDE4B bzw. PDE4D kontrolliert werden. Dies korreliert mit der lokalen Proteinkinase A (PKA) abhängigen Phosphorylierung des Phospholamban (PLN) und des RyR2 sowie der Neigung des Herzens zu Arrhythmien. Stimulated Emission Depletion (STED) Mikroskopie von immungefärbten Kardiomyozyten stärkt die Annahme einer Kokokalisation von PDE4B sowohl mit der Sarkolemma- als auch mit der RyR2 Mikrodomäne.

Mittels Live Cell Imaging konnte bestätigt werden, dass PDE4D an der Regulation der cAMP Signalweiterleitung in der Caveolin reichen Plasmamembran und der SERCA2a Mikrodomäne beteiligt ist. Im Gegensatz zu früheren Publikationen konnte gezeigt werden, dass PDE4B nicht nur in der LTCC Mikrodomäne vorhanden, sondern auch direkt an der Regulation des RyR2 beteiligt ist.

Abstract

The ubiquitous second messenger 3',5'-cyclic Adenosine Monophosphate (cAMP) regulates the cardiac Excitation-Contraction Coupling (ECC) by acting in discrete subcellular microdomains. Phosphodiesterase (PDE) subfamilies 4B and 4D are critically involved in the regulation of cAMP signaling in mammalian Cardiomyocytes (CMs). Alterations in PDE4 activity in human hearts have been shown to result in arrhythmia and heart failure.

In this work, the specific roles of PDE4B and PDE4D in the regulation of cAMP dynamics in three distinct subcellular microdomains were investigated. Microdomains of interest were formed around the caveolin-rich plasma membrane which harbors the L-Type Calcium Channel (LTCC), Sarco/Endoplasmic Reticulum Ca^{2+}-ATPase 2a (SERCA2a) and the cardiac Ryanodine Receptor Type 2 (RyR2).

Transgenic mice expressing Förster Resonance Energy Transfer (FRET)-based cAMP specific biosensors targeted to caveolin-rich plasma membrane, SERCA2a and RyR2 microdomains were crossed with PDE4B-KO and PDE4D-KO mice. By performing FRET imaging in ventricular CM isolated from adult wild type and PDE4B-KO or PDE4D-KO mice, a direct analysis of the specific effects of both PDE subfamilies was performed.

The data demonstrate that all microdomains are differentially regulated by these two PDEs. Even within one organelle, such as the sarcoplasmic reticulum, we could show the co-existence of at least two distinct cAMP microdomains formed around RyR2 and SERCA2a which are preferentially controlled by PDE4B and PDE4D, respectively. This correlated with local cAMP-dependent Protein Kinase A (PKA) substrate phosphorylation and arrhythmia susceptibility. Stimulated Emission Depletion (STED) microscopy of immunostained CM suggested possible co-localization of PDE4B with both sarcolemmal and RyR2 microdomains.

Using live cell imaging, it could be confirmed that PDE4D is involved in the regulation of cAMP dynamics at SERCA2a and at the caveolin-rich plasma membrane. In contrast to previous reports, we provide evidence that PDE4B is regulating not only LTCC associated compartments but is also directly involved in the RyR2 microdomain.

Contents

List of Tables

List of Figures

List of Symbols

Angle of incidence	α
Avogadro's number	N_A
Corrected FRET ratio	$FRET_{corr}$
Dipole orientation factor	κ^2
Distance between donor and acceptor	r
Donor emission spectrum	f_d
Förster distance	R_0
First excited singlet state	S_1
FRET efficiency	E
FRET ratio	$FRET$
Ground state	S_0
Half maximum degradation time	$\tau_{1/2}$
Index of medium	n_m
Lateral resolution	d
Molar acceptor extinction coefficient	ϵ_A
Number of animals	N
Number of experiments	n
Refractive index	n_r
Spectral bleedthrough factor	b
Spectral overlap integral	J
Wavelength	λ

List of Abbreviations

AC	Adenylyl Cyclase
abs	absorbance
AKAP	A-Kinase-Anchoring Protein
AP	Action Potential
Appl	Application
ATP	Adenosine Triphosphate
β-AR	β-Adrenergic Receptor
β_1-AR	β_1-Adrenergic Receptor
β_2-AR	β_2-Adrenergic Receptor
β_3-AR	β_3-Adrenergic Receptor
βArr	β-Arrestin
BCA	Bicinchoninic Acid
BDM	2,3-Butanedione Monoxime
CaM	Calmodulin
CaMKII	Ca^{2+}/Calmodulin-Dependent Kinase Type II
cAMP	3',5'-cyclic Adenosine Monophosphate
Cav1	Caveolin 1
Cav2	Caveolin 2
Cav3	Caveolin 3
CFP	Cyan Fluorescent Protein
cGMP	3'-5'-cyclic Guanosine Monophosphate
CICR	Ca^{2+} Induced Ca^{2+} Release
CM	Cardiomyocyte
CMOS	Complementary Metal-Oxide-Semiconductor
CNBD	Cyclic Nucleotiede Binding Domain
CNG	Cyclic Nucleotide-Gated Ion Channels
Co-IP	Co-Immunoprecipitation
CSQ	Calsequestrin
DAD	Delayed Afterdepolarization
DNA	Desoxyribonucleic Acid
EAD	Early Afterdepolarization

ECC	Excitation-Contraction Coupling
ELISA	Enzyme-Linked Immunosorbent Assay
em	emission
EPAC	Exchange Proteins Activated by cAMP
EPR	Prostaglandin Receptor
ERK	Extracellular Signal-Regulated Kinases
FCS	Fetal Calf Serum
FRET	Förster Resonance Energy Transfer
GAF	cGMP-Activated Phosphodiesterases, Adenylyl Cyclase and Fh1A
GAPDH	Glyceraldehyde 3-Phosphate Dehydrogenase
Gαs	α Subunit of the stimulatory Heterotrimeric G Protein
GFP	Green Fluorescent Protein
GPCR	G Protein-Coupled Receptor
HEPES	4-(2-Hydroxyethyl)-1-Piperazineethanesulfonic Acid
HF	Heart Failure
HSP20	Heat Shock Protein 20
I-1	Inhibitor-1
IBMX	3-Isobutyl-1-Methylxanthine
IF	Immuno Fluorescence
Iso	Isoprenaline
JNC	Junctin
LTCC	L-Type Calcium Channel
mAKAP	Muscle AKAP
ms	mouse
NCX	Sodium-Calcium Exchanger
P	Phosphorylation site
PAS	Period, Aryl-Hydrocarbon Receptor Nuclear Translocator and Single Minded
PBS	Phosphate Buffered Saline
PCR	Polymerase Chain Reaction
PDE	Phosphodiesterase
PKA	Protein Kinase A
PKC	Protein Kinase C
PLN	Phospholamban
Popdc	Popeye domain containing proteins
PP1	Protein Phosphatase 1
PP2B	Calcineurin
rb	rabbit
RyR2	Ryanodine Receptor Type 2

SDS-PAGE	Sodium Dodecyl Sulfate Polyacrylamide Gel Electrophoresis
SEM	Standard Error of Mean
Ser	Serine
Ser-16	Serine-16
Ser-2808	Serine-2808
SERCA2a	Sarco/Endoplasmic Reticulum Ca^{2+}-ATPase 2a
sh	sheep
SNS	Sympathetic Nervous System
Sp	Species
SR	Sarcoplasmic Reticulum
STED	Stimulated Emission Depletion
TAC	Transverse Aortic Constriction
TG	Transgenic
Thr-17	Threonine-17
T-tubule	Transverse tubule
UCR	Upstream Conserved Region
UCR1	Upstream Conserved Region 1
UCR2	Upstream Conserved Region 2
UKE	University Medical Center Hamburg-Eppendorf
WB	Western Blot
WT	Wild Type
YFP	Yellow Fluorescent Protein

1. Introduction

1.1 Physiological Relevance of Cyclic Nucleotides

Second messengers such as calcium or cyclic nucleotides are intracellular signaling molecules that are produced by a cell in response to extracellular factors such as hormones or neurotransmitters [1]. Due to their chemical structures, first messengers often cannot pass the phospholipid bilayer to initiate signaling cascades within the cell [2]. For maintaining homeostasis, the extracellular stimuli are transduced and amplified inside the cell by producing second messengers that allow a fast response to rapidly changing physiological conditions [3].

3',5'-cyclic Adenosine Monophosphate (cAMP) and 3'-5'-cyclic Guanosine Monophosphate (cGMP) are ubiquitous second messengers that are involved in the regulation of numerous independent biological processes, by controlling intracellular signal transduction. After the discovery of cAMP in the 1950s [4, 5], it had become evident that other 3',5' cyclic nucleotides might exist with an importance for regulating cellular physiology [6]. Shortly after, endogenously produced cGMP could be detected in rat urine [7].

cAMP regulates, amongst other very important physiological processes, immune reactions [8, 9], insulin secretion [10, 11], gene expression [12, 13], glucose and lipid metabolism [14], steroidogenesis [15], fluid and electrolyte secretion [16], electrical nerve and muscle excitability [17] as well as memory formation [18, 19]. However, for this work, the most important role of cAMP is the regulation of the heart by controlling the force of contraction and force of relaxation [20] as well as the beating frequency of the myocardium [21, 22].

cGMP is involved in bone growth [23], gastrointestinal motility [24], visual transduction [25], bladder function [26], metabolism [27] and brown fat cell differentiation [28]. Its impact on the cardiovascular system is the regulation of platelet function [29], vascular tone [30], cardiac contractility [31] and vascular remodeling [32]. cGMP formation is catalyzed by guanylyl cyclases, in particular by the soluble guanylyl cyclases that are located mainly in the cytosol and can be activated by nitric oxide [33]. Membrane-associated guanylyl cyclases are the receptors for the natriuretic peptides, ANP, BNP and CNP [34].

1.1.1 The Role of cAMP in the Heart

In mammalian hearts, cAMP is responsible for controling the beating frequency and the force of contraction and relaxation, also known as positive chronotropic, inotropic and lusitropic effects [35]. The formation of cAMP is achieved for example by the β adrenergic pathway. This pathway is a G Protein-Coupled Receptor (GPCR)-triggered signaling cascade which is crucial in cell communication. GPCRs are a family of integral membrane proteins with 7 transmembrane domains that bind extracellular substances and transmit the signals to an intracellular molecule called G protein (guanine nucleotide-binding protein). This further leads either to the activation or the inhibition of the cAMP-synthesizing enzymes Adenylyl Cyclases (ACs). cAMP synthesis is stimulated by catecholamine-induced activation of stimulatory G-proteins (G_s) or suppressed via inhibitory G-proteins (G_i).

1.1.2 β Adrenergic Signaling

β-Adrenergic Receptors (β-ARs) are the most important family of GPCRs in the heart. They are targets of many endogenously produced catecholamines such as epinephrine or norepinephrine [36], which is a powerful mean to increase the pumping function in the heart. Catecholamines originating from the Sympathetic Nervous System (SNS) lead to an β-AR induced modulation of heart rate and myocardial contractility [37]. Furthermore, they are targets for many medications like beta blockers or selective β agonists, that used to treat cardiovascular diseases [38, 39]. Isoprenaline (Iso), for example, is a non-selective β-AR agonist and the isopropylamine analog of epinephrine [40]. It is a drug used for the treatment of heart block [41] and bradycardia [42]. Propranolol is medication of the beta blocker class. It could be used to treat high blood pressure, capillary hemangiomas and essential tremors [43].

The binding of catecholamines to the receptors generally stimulates the SNS, which is responsible for the fight-or-flight response [44]. The fight-or-flight response tends acutely to increase physical performance. It dilates pupils, mobilizes energy, increases heart rate and diverts blood flow from non essential organs to skeletal muscles [45].

Cardiomyocytes (CMs) express all three subtypes of β-ARs, β_1-AR, β_2-AR and at least in some species, β_3-AR whereas the majority of the β-ARs is represented by β_1-AR and β_2-AR [46]. The structural motif of these receptors include seven hydrophobic transmembrane domains, which are linked by hydrophilic loops [47]. In human and mouse heart tissue, the amount of β_1-AR is 3-4 times as high as β_2-AR [48, 49]. Although β_3-AR are relatively minor it may contribute to normal and diseased myocardial regulation [50].

β-ARs are coupled to stimulatory G proteins which activate ACs, an enzyme family

that catalyzes the conversion of Adenosine Triphosphate (ATP) to cAMP [51]. Increased concentrations of cAMP lead to the activation of Cyclic Nucleotide-Gated Ion Channels (CNG), Popeye domain containing proteins (Popdc), Exchange Proteins Activated by cAMP (EPAC) and Protein Kinase A (PKA). EPAC is a protein that consists of a catalytic domain and a regulatory cAMP binding site [52]. Its role in the intracellular signaling is the GTP-loading of small G-proteins such as Rap1. Thus, it mediates numerous PKA independent effects of cAMP [53]. The predominantly expressed isoform EPAC1 has minor effects on the basal regulation of the myocardium [54]. In Heart Failure (HF), however, EPAC expression is increased and involved in cardiac hypertrophy induced by chronic catecholamine stimulation of β_1-Adrenergic Receptors (β_1-ARs) [55]. PKA is the main mediator of cAMP signaling in CMs and consists of two regulatory and two catalytic subunits [56]. The binding of cAMP to the regulatory subunit causes a dissociation of the catalytic subunits and leads to the phosphorylation of several downstream targets involved in the Ca^{2+}-cycling [57, 58].

The predominant subtype β_1-AR, but not β_2-AR, is mainly responsible for positive chronotropic and inotropic effects of CMs by activating PKA [59]. β_2-Adrenergic Receptors (β_2-ARs) were shown to have anti apoptotic effects [60]. β-AR subtype specific responsibilities are based on distinct pattern of cAMP compartmentation [61]. It could be uncovered that β_1-ARs are localized across the whole membrane, whereas β_2-ARs are located exclusively in the Transverse tubules (T-tubules) of healthy CMs [62]. Those are cell membrane invaginations that penetrate into the center of CMs. They permit a rapid transmission of the action potential into the cell and also play an important role in the regulation of the cellular Ca^{2+} handling [63].

As already mentioned, short time acute stimulation of β-ARs is associated with beneficial effects, while long-term stress results in non mitotic pathological growth of CMs [64], also known as cardiac hypertrophy, which leads ultimately to heart failure [65].

1.1.3 cAMP Compartmentation in the Heart

Receptor dependent cAMP stimulation often results in different downstream responses. In CMs, cAMP is produced by both β-ARs and Prostaglandin Receptors (EPRs). Yet, only β-AR derived cAMP regulates the electrical and mechanical properties [66, 67]. Those observations were the first hint that cAMP signaling must be compartmentalized. This means that mechanisms have to exist that prevent cAMP from moving freely throughout the cell. Although activation of EPRs leads to elevated intracellular cAMP levels, this signaling pathway is not considered in detail within this work due to the lack of relevance for the calcium cycling within

CMs [68].

In the fluid mosaic model published in 1972, it was proposed that membrane proteins are able to diffuse freely throughout the lipid bilayer [69], which suggested that signal transduction of those proteins occurs through the random process of collision coupling [70]. The weakness of this theory is that the density of signaling proteins is too low to explain the rapid and reliable responses that occur upon extracellular stimuli. This leads to the hypothesis of an existence of mechanisms that restrict the movement of membrane proteins [71]. This proposes that there must be some mechanisms separating the plasma membrane into different microdomains in which different signaling proteins are concentrated. An important factor in maintaining the accuracy of receptor-mediated responses is the formation of signaling complexes that combine effectors of cAMP, such as PKA, with target proteins. This combination is often achieved by the interaction with scaffolding proteins that belong to the A-Kinase-Anchoring Protein (AKAP) family [72]. It was shown that the destruction of the PKA-AKAP interaction results in altered cAMP signaling in the heart [73]. AKAPs are crucial for building up functionally relevant signaling complexes due to their ability of subcellular localization [74]. The highly specific localization can be achieved by electrostatic attraction of positively charged amino acids to negatively charged membrane lipids [75, 76]. At least 15 cardiac AKAPs were identified. Most of them are involved in recruiting PKA, Phosphodiesterases (PDEs) and protein phosphatases in order to form relevant signaling complexes in the heart. It was shown that the specific localization is mediated through interaction of PKA subunits with different endogenous AKAPs that result in distinct cAMP compartments controlled by specific PDE subsets [77]. AKAP9, also known as Yotiao, anchors PKA to the K^+ channel [78]. This regulation is highly important in terms of rapid cardiac repolarization of CMs [79]. The potassium channel phosphorylation by PKA is controlled by PDE4D3 [80]. AKAP18α directs PKA to the LTCC which is critical for increased Ca^{2+} influx in response to β-AR stimulation [81]. It was shown that the cardiac LTCC also forms a complex with another anchoring protein named AKAP79/150 [82]. Muscle AKAP (mAKAP) anchors PKA and PDE4D3 to the RyR2 complex, which controls a signaling unit that regulates the Ca^{2+} release from the Sarcoplasmic Reticulum (SR). Phosphorylation and dephosphorylation of Phospholamban (PLN), which is part of the SERCA2a complex is regulated by AKAP18δ and plays a critical role in Ca^{2+} reuptake into the SR [83]. Beside AKAPs, PDEs are most important for controlling subcellular microdomains by shaping intracellular cAMP and cGMP gradients [84]. The detailed roles of AKAPs on the regulation of the LTCC-, SERCA2a- and RyR2- complex will be explained in chapter 1.3.

β-Arrestin (βArr) is another important family of scaffolding proteins that are crucial

for compartmentation [85]. Their influence on the regulation of cellular signaling in CMs is not only limited to the impact on β-AR signaling by desensitizing the receptors [86]. It could be shown, that by recruiting PDE4D isoforms, βArrs contribute to the composition of β-AR associated submembrane microdomains [87]. βArr binds PDE4D to initiate PKA phosphorylation that controls β-AR signaling [88].

1.2 Phosphodiesterases

By hydrolyzing cyclic nucleotides, the super family of cyclic nucleotide Phosphodiesterases (PDEs) plays a critical role in regulating cyclic nucleotide signaling events by shaping intracellular gradients of cAMP and cGMP to disable random diffusion [89]. 21 genes encode for at least 100 isoforms that can be classified in 11 families [90, 91] (see Figure 1.1). The isoforms are grouped according to their structure, function and affinity for cAMP and cGMP [92], each family with a different selectivity and affinity for their substrates. Five PDE families (PDE1, PDE2, PDE3, PDE4 and PDE8) hydrolyze cAMP in mammalian myocardium [93, 94]. PDE1, PDE2 and PDE3 are hydrolyzing both cAMP and cGMP, whereas PDE4 and PDE8 are exclusively degrading cAMP [95]. The N-terminal regions have several functional roles like targeting the isoforms to specific subcellular locations and signalosomes, the modulation of responses to signals from regulatory molecules or post-translational modifications [96].

PDE 1 is believed to be responsible for the crosstalk between cyclic nucleotide signaling and calcium [97]. The activity of Calmodulin (CaM)-stimulated PDEs that belong to the PDE family 1 show an increase in activity up to 1000% upon CaM binding [98]. All three subfamilies (PDE1A, PDE1B and PDE1C) are expressed in CMs. PDE1A and PDE1B show a higher affinity to cGMP [99] and PDE1C binds both cyclic nucleotides with equal affinity [100].

Each of the three isoforms (PDE2A1, PDE2A2 and PDE2A3 [101]) of the cGMP-stimulated PDE family 2 harbors a pair of cGMP-Activated Phosphodiesterases, Adenylyl Cyclase and Fh1A (GAF) domains with a cGMP binding site [102]. Activation by cGMP leads to a hydrolysis of cAMP, which is why PDE2 plays a crucial role in the crosstalk between the individual cyclic nucleotides [103]. PDE2A1 was found to be located in the cytosol whereas PDE2A2 and PDE2A3 are membrane-associated [104]. Furthermore, PDE2A2 was shown to regulate mitochondria morphology [105].

PDE3 is also involved in the cAMP cGMP crosstalk. In contrast to PDE2, the PDE3 family (PDE3A and PDE3B) gets inhibited by cGMP [106, 107]. PDE3A, represented by three isoforms [107], is the predominant cAMP degrading PDE in human hearts [108] and second most important in rodent CMs [109]. Further, PDE3B was shown to be protective against ischemia/reperfusion injuries [110].

The cAMP specific PDE8 family is encoded by two genes, whereas only PDE8A could be detected in human and rodent hearts [111]. It could be identified that PDE8A is involved in the calcium homeostasis since it is responsible for the regulation of LTCC Ca^{2+} currents. It was reported that PDE8A knockout CMs showed a 'leaky' RyR2 phenotype [112]. Further, it is worth mentioning that PDE8 is insensitive to the non selective PDE inhibitor 3-Isobutyl-1-Methylxanthine (IBMX) [113].

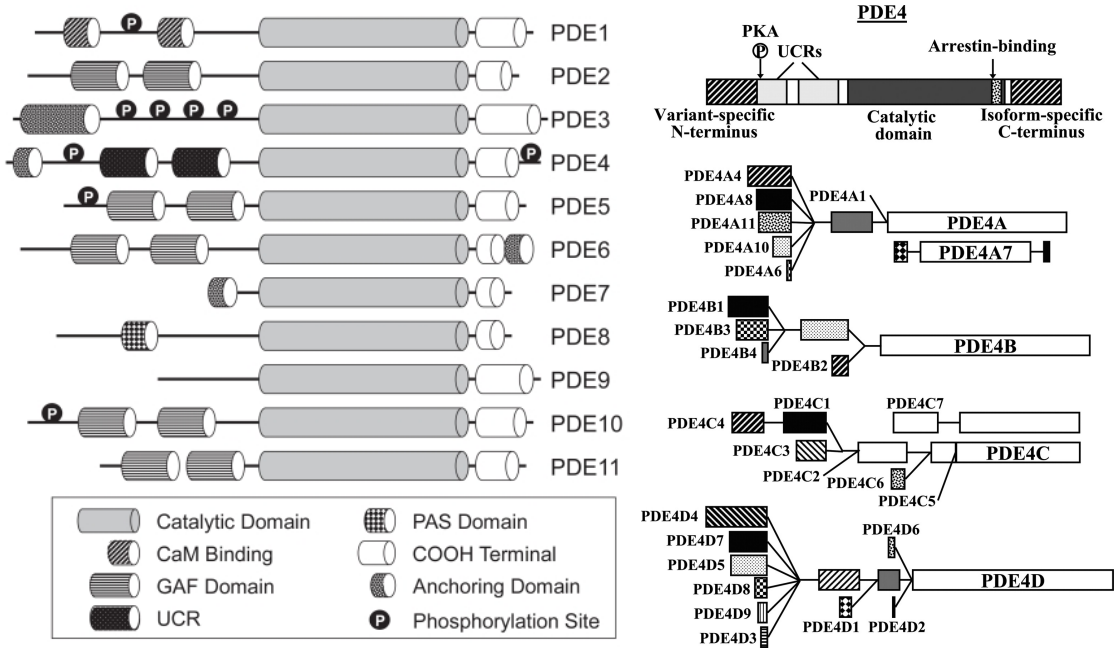

Figure 1.1: PDE Superfamily, Structure of PDE4 Family. Left, Schematic representation of the structure of the 11 Phosphodiesterase (PDE) families that give rise to over 100 isoforms. The conserved catalytic domain is located at the C-terminus. N-terminal regions are crucial for subcellular localization, in the incorporation of PDEs into compartmentalized signalosomes. Calmodulin (CaM), cGMP-Activated Phosphodiesterases, Adenylyl Cyclase and Fh1A (GAF), Upstream Conserved Region (UCR), Period, Aryl-Hydrocarbon Receptor Nuclear Translocator and Single Minded (PAS) and Phosphorylation site (P). Figure adapted from [114]. **Right**, PDE4 long isoforms are harboring 2 UCRs, whereas UCR1 is lacking in the short forms. UCR1 has a PKA phosphorylation site. Protein Kinase A (PKA). Figure adapted from [115].

1.2.1 Phosphodiesterase 4 Family

The PDE4 family is the largest PDE family and one of the most studied. It gives rise to over 20 isoforms encoded by four genes (*pde4a*, *pde4b*, *pde4c* and *pde4d*) [116] (see Figure 1.1). The PDE4 variants arise due to differences in their N-termini as these encode regulatory domains and phosphorylation sites. They can be classified

according to the size of the N-terminal regions, dependent on the presence and size of the Upstream Conserved Region (UCR) 1 and 2 (Upstream Conserved Region 1 (UCR1) and Upstream Conserved Region 2 (UCR2)), which are unique modules composed of loops and amphipathic helices [90]. UCR1 is harboring a PKA phosphorylation site [117]. PDE4 long forms have both UCR1 and UCR2, whereas the short forms are lacking UCR2. Super-short isoforms have a truncated UCR2 and dead-short isoforms lack both UCR domains [118]. The phosphorylation of the site within UCR1 causes a conformational change and an increased activity of the catalytic domain up to 250% [119]. The catalytic domains of PDE4B, PDE4C and PDE4D contain sites for Extracellular Signal-Regulated Kinases (ERK) phosphorylation [120]. ERK phosphorylation leads to an inhibited activity, which can be overcome by PKA phosphorylation of the UCR1 site [120]. Both phosphorylation steps probably form a timing loop for controlling the duration of the cAMP signal transduction [121]. The presence or absence of these domains has a significant impact on PKA and ERK phosphorylation [122]. The catalytic domains of each PDE4 gene exhibit 75% of sequence identity to any other PDE4 family member [119]. PDE4B1, the major PDE4B isoform in adult and neonatal CMs, belongs to the PDE4 long forms [123]. PDE4D is mainly represented in mouse CMs by PDE4D3 and PDE4D5, both classified as PDE4 long forms [124]. X-ray crystal structures of the catalytic domain have uncovered that the active site for cAMP hydrolysis is made of a deep hydrophobic pocket of numerous helices [125]. This domain is of essential importance for designing specific PDE inhibitors that are widely used for clinical and experimental approaches [126]. As already mentioned, the subcellular location of PDEs is integral to their function in shaping cAMP gradients and their involvement in intracellular signaling events. The localization of PDE4 isoforms is directed by the highly varied N-terminal targeting domains [127] as well as the multi functional docking domain positioned at the C-terminal end of the catalytic unit [128].

1.2.2 PDE4 in Cardiomyocytes

PDE4 is a major player not at basal cAMP levels but during β-AR stimulation since it was shown that inhibition of this family has very limited effects on basal cardiovascular parameters, such as blood pressure, heart rate and contractility [129]. Three out of the four PDE4 genes (*pde4a*, *pde4b* and *pde4d*) are expressed in CMs. As described in section 1.3, β-AR-signaling is a major part of the fight-or-flight response. Activated β-ARs affect ACs which catalyze the reaction from ATP to cAMP. The increased cAMP concentration activates PKA, which in turn phosphorylates a number of important substrates for the Excitation-Contraction Coupling (ECC) that lead to positive inotropic and lusitropic effects. This PKA phosphorylation is tightly

regulated by isoforms belonging to the PDE4 family, which associate directly within signalosomes that modify the signaling not due to global signaling but in tight compartments [92]. PDE4B is involved in the regulation of the cardiac LTCC, whereas PDE4D is associated with the SERCA2a and RyR2 complex. The sections 1.3.1-1.3.3 cover the detailed interaction of PDE4 isoforms with calcium handling proteins of CMs.

Although PDE4 inhibition has beneficial effects on CM function [130], chronic PDE inhibition resulted in increased mortality, often due to cardiac side effects [131]. As already indicated in the previous section, PDE4D has an essential role in regulating β-AR signaling in CMs by desensitizing β_2-AR [132]. Upon β_2-AR stimulation, its coupled G_s protein affects ACs which catalyzes the reaction from ATP to cAMP resulting in locally activated PKA. The receptor gets desensitized by the negative feedback loop as PKA phosphorylates the receptor. This causes a switch in the receptor's signaling from G_s to G_i resulting in an AC inhibition [133]. Interaction of PDE4D5 and βArr and thus direct impact on the regulation of this feedback loop could be uncovered by using PDE inhibitors and specific knockdown of PDE4D5 [134, 135].

The small Heat Shock Protein 20 (HSP20) is an ubiquitously expressed family of small chaperone proteins that can protect other proteins against heat-induced denaturation and aggregation [136]. In its phosphorylated state, HSP20 has been shown to be cardioprotective [137]. Phosphorylation at Serine-16 (Ser-16) leads to cell protective switching off of harmful and protective signaling, inhibiting necrosis, apoptosis and stabilizing the cell's cytoskeleton [138, 139]. By performing FRET microscopy experiments and co-immunoprecipitation studies, direct interaction between HSP20 and the catalytic region of PDE4D5 could be shown [140, 141].

In PDE4D deficient mice a dilated cardiomyopathy could be observed at the age of 9 months which had many characteristics consistent with human chronic heart failure as well as exercise-induced ventricular arrhythmia [142]. This phenotype was associated with hyperphosphorylation of the PKA phosphorylation site (Serine-2808 (Ser-2808)) of the RyR2 and diminished levels of calstabin-2, which prevents calcium leak from the SR [143]. The responsible isoform was identified to be PDE4D3.

The slowly activating potassium channel is a major repolarising current in the cardiac action potential [144]. It exists as a macromolecular complex including AC9, PKA and Protein Phosphatase 1 (PP1) [145]. Immunoprecipitation experiments identified a direct interaction of PDE4D3 with AKAP9 [146].

Both PDE4B and PDE4D were shown to coimmunoprecipitate with the LTCC which is responsible for the Ca^{2+} influx [147]. Yet, PDE4B exhibits the dominant functional role in regulating the LTCC phosphorylation and is thereby protective against

cardiac arrhythmia [148]. Furthermore, it was shown that cardiac hypertrophy was associated with decreased activity of PDE4B [107].
Unlike many other cardiac signalosomes, the SERCA2a microdomain was shown to be under control of PDEs that belong to two different families, PDE4D and PDE3A [149]. Both PDEs seem to have comparable effects since genetic deletion of respective PDEs resulted in an increased PLN phosphorylation, increased SERCA2a activity, increased SR calcium load and increased contractility [150, 151].

1.3 Cardiac Excitation-Contraction Coupling

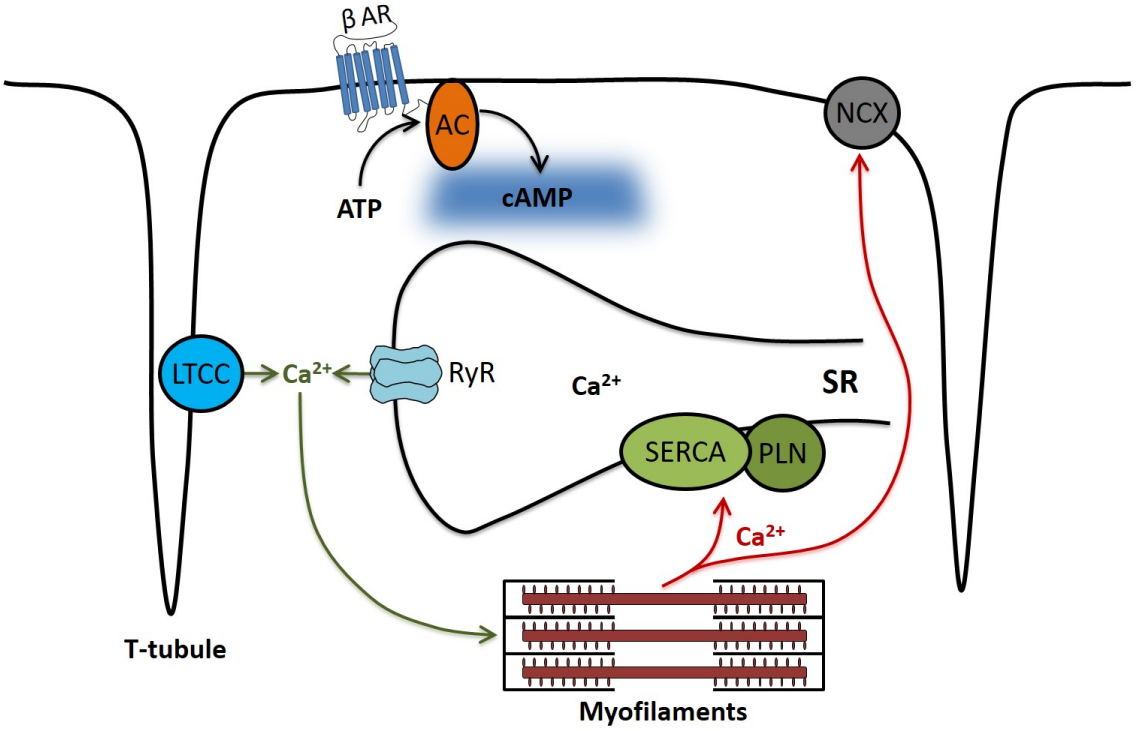

Figure 1.2: Schematic Representation of the Cardiac Excitation-Contraction Coupling. Ca^{2+} cycling is crucial for a proper Excitation-Contraction Coupling (ECC) of a Cardiomyocyte (CM). At depolarization, Ca^{2+} influx through the L-Type Calcium Channel (LTCC) causes a Ca^{2+}-induced Ca^{2+}-release from the Sarcoplasmic Reticulum (SR) through the Ryanodine Receptor Type 2 (RyR2) which activates the myofilaments, resulting in a contraction. Ca^{2+} is either transferred back into the SR by Sarco/Endoplasmic Reticulum Ca^{2+}-ATPase 2a (SERCA2a) that is negatively regulated by Phospholamban (PLN) or extruded from the CM via the Sodium-Calcium Exchanger (NCX). 3',5'-cyclic Adenosine Monophosphate (cAMP) is formed upon β-Adrenergic Receptor (β-AR) stimulation which via G_s protein activates ACs, catalyzing the reaction from Adenosine Triphosphate (ATP) to cAMP. Increased levels of cAMP activate Protein Kinase A (PKA).

The cardiac ECC is a physiological process that bridges electrical excitation of the membrane potential to the consequent mechanical CM contraction [152, 153] (see Figure 1.2).
Action potential-induced excitation of the cellular membrane results in an opening of the voltage gated LTCCs that lead to a Ca^{2+} influx into the cytoplasm. The RyR2s are sensitive to Ca^{2+} in the dyadic space, the space between T-tubules and SR. This triggers additional Ca^{2+} release from the CM's internal storage, a process called Ca^{2+} Induced Ca^{2+} Release (CICR) [154, 155]. During diastole, most of the intracellular Ca^{2+} is stored in the SR. CICR allows the stored Ca^{2+} to diffuse throughout the sarcomere, where it binds to the Ca^{2+} binding protein troponin in the myofilaments which initiates cell contraction. Ca^{2+}, the intracellular second messenger, is released from the SR in the cytosol at every beat to directly activate the myofilaments. Relaxation is initiated by a reduction of the sarcoplasmic Ca^{2+} concentration through an active transport of calcium ions into the lumen of the SR by SERCA2a. Furthermore, Ca^{2+} is removed from the cytosol by the NCX. It uses the energy that is stored in the gradient of extracellular sodium by allowing Na^{+} to flow down its gradient across the plasma membrane in exchange for the countertransport of calcium ions.
A tight regulation of Ca^{2+} handling is essential for the maintenance of a proper electrical and contractile function in CMs. This process becomes fundamentally dysregulated in almost all forms of cardiac pathology. It is now appreciated that AKAPs associate with each of these Ca^{2+} transporters and favor their regulation by PKA [79].

1.3.1 L-Type Calcium Channel (LTCC)

As already described in section 1.3, the balance of intra- and extracellular Ca^{2+} concentration is crucial for a proper ECC. In CMs, it is the L-Type Calcium Channel (LTCC), also named Ca_v1, that is responsible for the Ca^{2+} influx into the cell which triggers calcium release from the SR through the RyR2s [156, 157]. The voltage dependent LTCCs are essential to many cellular processes including ECC, excitability, hormone secretion and regulation of gene expression [158]. Within the LTCC family, four subtypes ($Ca_v1.1$ - $Ca_v1.4$) have been identified by their sensitivity to dihydropyridines [159, 160]. Each subtype exists as a multimeric protein complex consisting of one of four different corresponding α_1 subunits ($\alpha_{1.1}$ - $\alpha_{1.4}$) together with auxiliary β, $\alpha_2\delta$ and γ subunits [160, 161]. The specific type of a Ca^{2+} channel is defined by the α_1 formed ion-conducting pore. The subunit consists of four homologous domains, each containing six transmembrane segments. The predominantly expressed LTCC in ventricular CMs is $Ca_v1.2$ [162]. The regulation of $Ca_v1.2$ is of a central role for the regulation of the myocardium due to its con-

tribution to the electrical and mechanical properties. Influxing Ca^{2+} is responsible for maintaining membrane depolarization during the plateau of the cardiac action potential [163].
To maintain the mentioned diverse cellular functions of the LTCC, the influxing Ca^{2+} current is tightly controlled and compartmentalized within the CMs [164].
Lipid rafts are areas in the lipid bilayer of higher rigidity compared to the more fluid bulk of the bilayer [165]. They harbor several ion channels, including the LTCC [166]. Caveolae are a special type of lipid rafts [167] which are flask-shaped invaginations of the plasma membrane of a size of 50-100 nm. This structure is achieved by the scaffold protein caveolin [168] that is present in a variety of cell types and involved in a large amount of signaling processes [169]. Three caveolin isoforms (Caveolin 1 (Cav1), Caveolin 2 (Cav2) and Caveolin 3 (Cav3)) are known to be expressed in the myocardium to target appropriate proteins to caveolae [170]. Cav3, the predominant isoform in the heart, was shown to colocalize with the cardiac LTCC [171]. As previously mentioned in 1.1.3, AKAP18α (also known as AKAP15) is a membrane-associated anchoring protein that directs PKA to the LTCC through a direct interaction between a leucine zipper located in its COOH-terminal region and the cytoplasmic domain of the channel [172, 173]. Functional experiments were performed with cultured CMs and showed that disruption of PKA anchoring using competing peptides derived from APKAP18α might facilitate PKA-mediated regulation of the channel [174]. Beside AKAP18α, the LTCC can form a complex with AKAP79/150 (human form: AKAP79, murine form: AKAP150) [175]. By mediating PKA dependent phosphorylation of the LTCC, AKAP79/150 is critically involved in the increased Ca^{2+} influx upon β-AR stimulation. In Cav3-rich membrane compartments of CMs, a functional complex was detected comprising AKAP79/150, AC5 and AC6, PKA and LTCC [176] (see Figure 1.3).

1.3.2 Sarco/Endoplasmic Reticulum Ca^{2+}-ATPase 2a (SERCA2a)

The Sarco/Endoplasmic Reticulum Calcium transport ATPase (SERCA) is a pump that transports Ca^{2+} from the cytoplasm into the SR and is present in both plants and animals [177, 178]. The SERCA pump is encoded by three genes: *serca1*, *serca2* and *serca3* which give rise to at least two differentially spliced isoforms [179, 180]. Being the most common isoform in the heart, SERCA2a is responsible for the reuptake of 90% of Ca^{2+} during diastole in ventricular cardiomyocytes [181, 182]. SERCA2a, a transmembrane pump of 110 kDa [183], is activated by cytosolic Ca^{2+} concentrations of greater than 100 nM and pumps Ca^{2+}, against a concentration gradient, under ATP consumption back to the SR [184]. As already stated in section 1.3, SERCA2a is crucial for the contractile function in CMs since after each contraction

cycle, Ca^{2+} is pumped back by SERCA2a to the intracellular Ca^{2+} storage SR. PLN, a transmembrane protein consisting of 52 amino acids [185], is a key regulator of the SR. By inhibiting SERCA2a activity in an unphosphorylated state, it is ultimately the effector of adrenergic lusitropy [186]. The negative regulation mechanism of PLN is regulated by Ca^{2+} concentrations [187]. Increasing concentrations in cytosolic Ca^{2+} lead to dissociation of the SERCA2a-PLN interaction [188, 189]. Furthermore, PLN activity is regulated by specific phosphorylation [190] of the PKA dependent phosphorylation site Ser-16 [191, 192] and the Ca^{2+}/Calmodulin-Dependent Kinase Type II (CaMKII) dependent phosphorylation site Threonine-17 (Thr-17) [193, 194]. Catecholamine dependent stimulation of β-AR results in phosphorylation of both sites, Ser-16 and Thr-17, whereas Thr-17 phosphorylation requires an influx of Ca^{2+} through the LTCC [195, 196]. However, Ser-16 phosphorylation is sufficient to relieve PLN dependent inhibition of SERCA2a and for mediating maximal cardiac response [197]. As explained in 1.2, PDEs are crucial for cAMP-PKA signaling by creating local cAMP pools. Both PDE3A and PDE4D have been shown to interact with the SERCA2a complex by regulating PLN phosphorylation [198, 199]. It could be shown in mice that a knockout of PDE3A or PDE4D results in increased PLN phosphorylation-associated with increased SERCA2a activity, SR Ca^{2+} load and increased contractility, that suggests a major role of those PDE subfamilies in the regulation of the SERCA2a microdomain.
AKAP18δ was identified to be the anchoring protein controlling the SERCA2a complex [200]. It has a critical impact on the regulation by enabling PKA dependent phosphorylation of PLN which leads to enhanced Ca^{2+} uptake into the SR [201]. Further it was shown that AKAP18δ interacts with protein phosphatase 1(PP1) and its inhibitor-1 (I-1) [83]. PP1 can inhibit the SERCA2a activity by dephosphorylating PLN. Thus, AKAP18δ has a big impact on the cardiac ECC [202] (see Figure 1.3).

1.3.3 Ryanodine Receptor Type 2 (RyR2)

Ryanodine receptors are a class of intracellular calcium channels of excitable animal tissue like neurons and muscles [203, 204]. Three isoforms of the ryanodine receptor are found in different tissues and contribute to different signaling pathways involving Ca^{2+} release from intracellular organelles [205, 206]. Cardiac RyR2s are intracellular ion channels in the SR membrane that provide a pathway for release of calcium ions from the intracellular Ca^{2+} storage SR into the cytosol. They consist of four monomers, each with a size of approximately 5000 amino acids [207]. The N-terminal cytoplasmic part of the RyR2 comprises of 80-90% of amino acids. It serves as a scaffold for proteins including kinases (PKA, CaMKII and phosphatases) and contains a multitude of regulatory ligand-binding- and phosphorylation sites [208,

209]. The transmembrane C-terminal region that comprises of the remaining 10-20%, is responsible for the channel function of the homotetramer [210, 211].

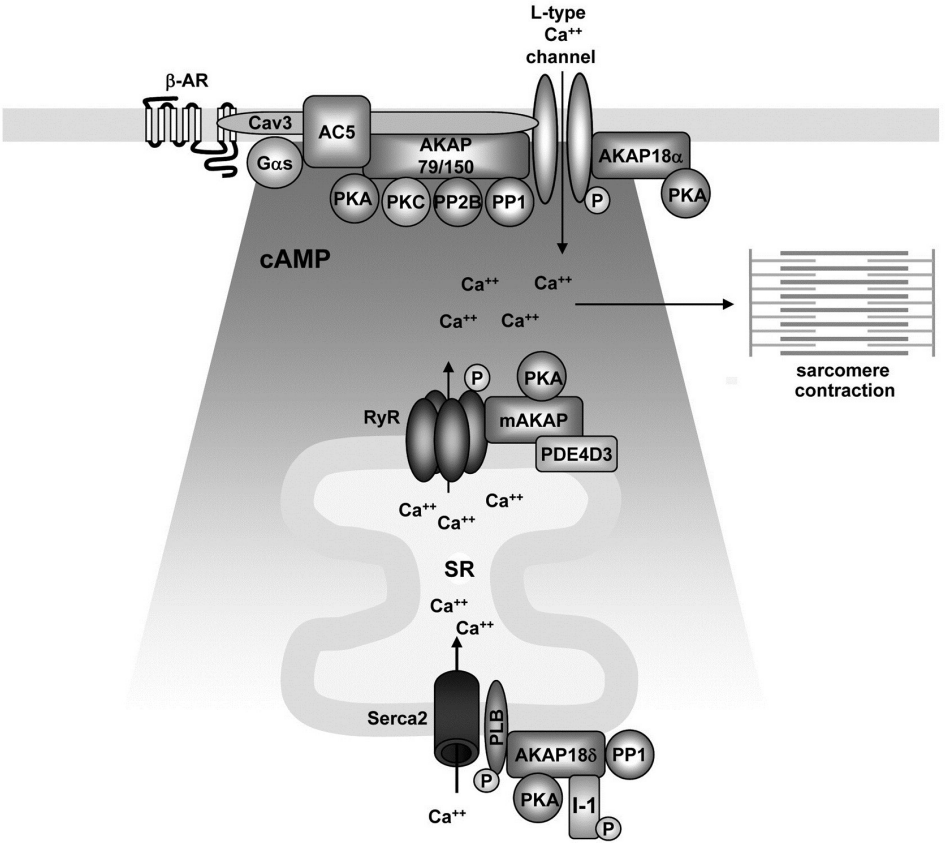

Figure 1.3: AKAPs controlling Calcium Handling in Cardiomyocytes. A-Kinase-Anchoring Protein (AKAP)18α favors Protein Kinase A (PKA) mediated phosphorylation (P) of the L-Type Calcium Channel (LTCC). AKAP79/150 assembles a large protein complex including β-Adrenergic Receptor (β-AR), Caveolin 3 (Cav3), α Subunit of the stimulatory Heterotrimeric G Protein (Gαs), Adenylyl Cyclase (AC)5, Protein Kinase A (PKA), Protein Kinase C (PKC), Calcineurin (PP2B), Protein Phosphatase 1 (PP1) and LTCC. Muscle AKAP (mAKAP) directs PKA to regulate the phosphorylation of the Ryanodine Receptor Type 2 (RyR2) which is under control of Phosphodiesterase (PDE)4D3. AKAP18δ anchors PKA, PP1 and Inhibitor-1 (I-1) to the Sarco/Endoplasmic Reticulum Ca^{2+}-ATPase 2a (SERCA2a) microdomain which is under negative control of Phospholamban (PLN). Extracellular Ca^{2+} fluxing into the Cardiomyocyte (CM) causes a Ca^{2+} release from the Sarcoplasmic Reticulum (SR) resulting in a sarcomeric contraction. Ca^{2+} is pumped into the SR via SERCA2a. Figure adapted from [79].

Cardiac RyR2s are Ca^{2+} sensitive channels in the SR membrane and are located in close proximity to the LTCCs. They are the main Ca^{2+} releasing mechanism of the SR in the myocardium. RyR2s interact with a large number of additional

protein such as triadin, Junctin (JNC), Calsequestrin (CSQ) and anchoring proteins for kinases and phosphatases. Together with triadin, JNC and CSQ, RyR2s form a junctional quaternary complex. JNC and triadin have a single transmembrane-spanning domain and interact directly with the RyR2s [212, 213].
In 2005 it was shown that PDE4D3 is the only PDE isoform in the RyR2 complex and it was shown that the PDE4D3 levels were reduced in the RyR2 complex of failing human hearts [142]. There is evidence that the targeting of PDE4D3 to the RyR2 complex is achieved by the muscle-specific anchoring protein mAKAP [214]. mAKAP forms a signaling unit to regulate the Ca^{2+} release from the SR by anchoring PKA and PDE4D3 to the RyR2 complex in close proximity to the sites of interaction with protein phosphatases PP1/PP2 and calstabin [214, 215].
Three phosphorylation sites have been identified: Serine (Ser)-2808, Ser-2814 and Ser-2030 [216]. Ser-2808 in human and rodents or Ser-2809 in rabbit, the first identified phosphorylation site of RyR2 was originally described as CaMKII phosphorylation site. Later it was shown that PKA could phosphorylate this site as well [217, 218]. The second phosphorylation site Ser-2814 (Ser-2815 in rabbit) is exclusively phosphorylated by CaMKII [219]. The latest identified phosphorylation site Ser-2030 (Ser-2031 in rabbit) has been described to be phosphorylated by PKA [220].
HF is a leading world-wide cause of mortality and morbidity. Patients with HF either die of progressive failure of cardiac mechanical function or of ventricular arrhythmia [221]. Much of the impaired contractile function in HF is caused by reduced Ca^{2+} transient in CMs that is mainly dependent on the Ca^{2+} content of the SR [222]. The defective SR Ca^{2+} handling is characterized by 'leaky' RyR2 channels due to stress-induced dissociation of the stabilizing RyR2 subunit calstabin2, resulting in a diastolic SR Ca^{2+} leak, reduced SR Ca^{2+} content and decreased Ca^{2+} transient [223, 224, 225, 226] (see Figure 1.3).

1.4 Afterdepolarization

Afterdepolarization is an abnormal depolarization of the CM membrane potential that follows a cardiac action potential [227]. It may lead to cardiac arrhythmia which leads ultimately to heart failure [228]. During the resting potential of the cardiac action potential (Phase 4) the voltage of the membrane potential is about -90 mV and is associated with outfluxing potassium ions.
Phase 0 is initiated by the activation of Na^+ current. This happens when an action potential from an adjacent cell arrives through gap junctions. If the voltage of the membrane gets increased to a certain threshold potential of -70 mV, it causes the Na^+ channels to open, which results in an influxing sodium current into cell that rapidly increases the voltage to 50 mV [229].
Phase 1 begins with the inactivation of the Na^+ channels. This causes a very short

opening of potassium channels, which leads to a brief flow of potassium ions out of the cell, leading to a slight reduction of the membrane potential [230].
The membrane potential slowly begins to repolarize but remains almost constant during the plateau phase (Phase 2) since there is a steady state of charge moving into and out of the cell. The opening of the LTCCs causes an influx Ca^{2+}, that results in the ECC, as described in section 1.3 [231].
The rapid repolarization Phase 3 is characterized by closing the LTCCs. The sodium-potassium pump restores the ion concentrations back to basal conditions [232].

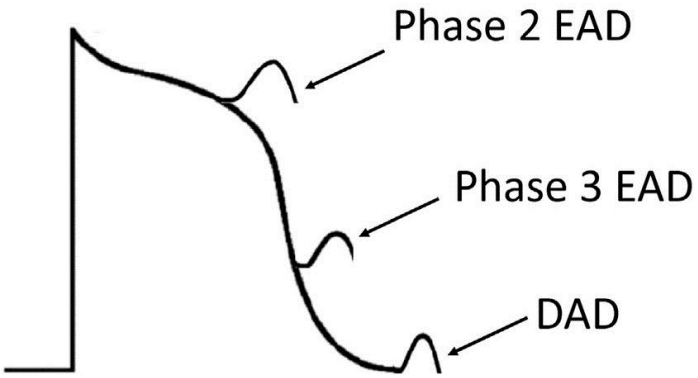

Figure 1.4: Afterdepolarization Phenomena. Early Afterdepolarization (EAD) occurs early in Phase 2 or late in Phase 3, whereas Delayed Afterdepolarization (DAD) occurs during Phase 4 of a cardiac action potential. Figure adapted from [233].

EADs are abnormal depolarization during phase 2 or phase 3. Phase 2 EADs are mostly based on the opening of calcium channels, while phase 3 EADs occur due to opened sodium channels [234] (see Figure 1.4).
DADs appear during phase 4 of the cardiac action potential after the repolarization is completed but before the next regular action potential via the conduction system of the heart occurs. The reason for DADs is an intracellular Ca^{2+} release from the SR [235, 236] (see Figure 1.4).

1.5 Förster Resonance Energy Transfer (FRET)

FRET is a physical phenomenon describing energy transfer between two light sensitive chromophores. It is named after the German scientist Theodor Förster, who discovered this mechanism in 1948 [237]. The principle of FRET is based on an energy transfer between an excited donor chromophore and an acceptor chromophore. Accordingly for FRET to take place, the donor emission spectrum has to overlap with the excitation spectrum of the acceptor (see Figure 1.5). The energy of the excited donor is not transferred via photons but radiationless via dipole-dipole interactions.

The molecular processes of absorption and emission are illustrated in the Jablonski diagram (see Figure 1.5). The donor, excited with light of a specific wavelength, which is usually close to the maximum of the absorption spectrum, absorbs energy which moves the donor electron from the ground state S_0 to the higher level of the first excited singlet state S_1. Due to vibrational relaxation, the electron rapidly returns to the lowest energy level of S_1. If in close enough proximity to the associated acceptor, the donor transfers part of its excitation energy to the acceptor via dipole-dipole coupling [239, 240, 241].
The FRET efficiency E, as described in equation 1.1, is dependent on the distance r between donor and acceptor as well as R_0, the Förster distance of the used chromophore pair describing the distance at which the energy transfer efficiency is 50% [242].

$$E = \frac{1}{1 + \left(\frac{r}{R_0}\right)^6} \tag{1.1}$$

R_0 is specific for each pair of chromophores and is calculated according to equation 1.2 with the dipole orientation factor κ^2, the medium's refractive index n_r, Avogadro's number N_A and J as spectral overlap integral [242].

$$R_0^6 = \frac{9 \cdot (ln10) \cdot (\kappa^2 n_r^{-4} Q_0 J)}{128\pi^5 N_A} = 8.8 \cdot 10^{-28} \cdot (\kappa^2 n_r^{-4} Q_0 J) \tag{1.2}$$

J is calculated as shown in equation 1.3 as a function of the wavelength λ, the donor emission spectrum f_d and the acceptor molar extinction coefficient ϵ_A [242].

$$J = \int f_D(\lambda) \cdot \epsilon_A(\lambda) \cdot \lambda^4 d\lambda \tag{1.3}$$

Since the FRET efficiency is inversely proportional to the sixth power of the distance between the chromophores, it is a very sensitive and accurate tool for detecting smallest changes in the distance between donor and acceptor. In combination with the Dexter electron transfer, FRET is responsible for sunlight harvesting during photosynthesis of plants [243].

1.5.1 Applications of FRET in Science

FRET microscopy became a well-established method to investigate many novel signaling mechanisms and biochemical processes in living cells. Typical unimolecular fluorescent biosensors consist of a binding domain for the molecule of interest, which is flanked between two fluorescent proteins that act as energy donor and acceptor

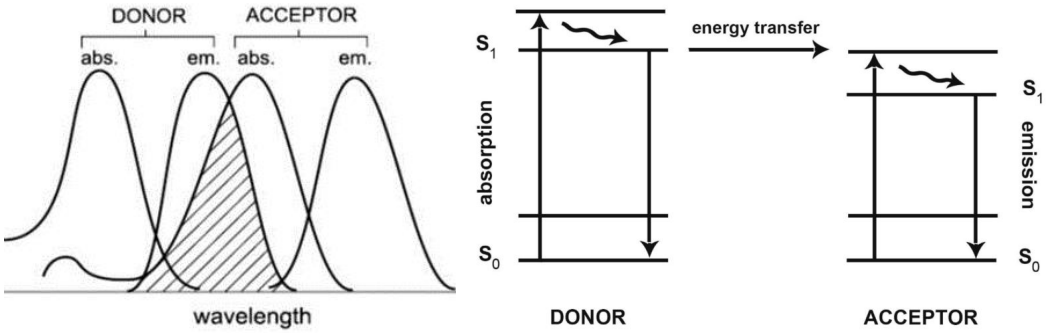

Figure 1.5: Donor and Acceptor Spectra, Jablonski Diagram. Left, Schematic illustration of the overlapping donor-emission and acceptor-excitation spectra. The overlapping spectra are striped. absorbance (abs), emission (em).
Right, Jablonski diagram, illustrating energy states and transitions between donor and acceptor molecules. Vertical lines illustrate energy state transitions due to absorption or emission of photons. Wavy arrows illustrate vibrational relaxation. Figures adapted from [238].

[244]. The excited donor protein emits energy that can be partially transferred to the neighboring acceptor protein, which also emits fluorescence light without being directly excited. Energy transfer can occur within a distance of 10 nm. The binding of the molecule of interest to the binding domain leads to a conformational change of the biosensor that results in an altered distance between donor and acceptor. With increased distance between the two fluorophores, the emitted light of the donor looses the ability to excite the acceptor which leads to a reduction of transferred energy [245, 246]. By monitoring the ratio of acceptor/donor fluorescence, changes in concentration of the molecule of interest can be recorded and analyzed in real-time.
Alternatively, bimolecular sensors can consist of two interacting proteins, one fused to the donor and another one to the acceptor fluorophore, to monitor changes in protein-protein interaction over time [247, 248]. FRET biosensors can be introduced into living cells by plasmid transfection, viral gene transfer or they can be expressed in transgenic animal models [249]. The great advantage of FRET microscopy is the ability to visualize temporal and spatial changes of for example second messengers, not only within a single cell but in subcellular compartments [245]. This technique is widely used for e.g. pH-measurements [250, 251, 252], Ca^{2+}-measurements [253, 254, 255], ATP-measurements [256], detection of disease related molecules [257] and visualization of compartmentation of second messengers such as cyclic nucleotides in CMs [258, 259, 260, 261].

1.5.2 cAMP Specific FRET Biosensors

The first cAMP specific FRET biosensor was published in 1991. The sensor consists of cAMP-dependent protein kinase in which the catalytic and regulatory subunits were each labeled with a different fluorescent dye, such as fluorescein or rhodamine [262]. Since then, FRET has become a powerful tool for real-time monitoring of signaling events in living cells and tissues [263, 264]. Classical biochemical techniques require thousands of cells to analyze a limited number of time points without any spatial resolution at the cellular level. During the last decades, a series of more compact FRET biosensors has been generated that could easily be introduced into cells by transfection of the DNA construct [265, 266, 267]. To gain a higher spatial resolution, targeted versions of FRET biosensors were developed which can be expressed specifically in certain tissues and even in specific microdomains. These achievements resulted in a monitoring of cAMP with significant improved resolution in space and time. Chromophores that are often used for cAMP specific FRET biosensors are derivatives of the Green Fluorescent Protein (GFP) flanking a single Cyclic Nucleotiede Binding Domain (CNBD). A commonly used chromophore pair, that meets the requirements explained in 1.5, is Cyan Fluorescent Protein (CFP) and Yellow Fluorescent Protein (YFP).

For this work, the Epac1-camps sensor was used (see Figure 1.6). Originally, to generate the Epac1-camps sensor, human EPAC 1 was fused to CFP and YFP [266]. The binding of cAMP to the CNBD results in a conformational change of the biosensor, which results in an increased distance between donor and acceptor. Due to the increased distance between CFP and YFP, the emitted donor energy can no longer transfer the energy to the acceptor fluorophore accordingly, the rate of transferred energy is reduced.

Targeted versions of the Epac1-camps biosensor were used to make statements about cAMP dynamics in Ca^{2+} handling microdomains of adult mouse CMs. Fusing the biosensor to the caveolin-rich plasma membrane microdomain, is a suitable model to analyze changes in cAMP levels in the LTCC microdomain due to the high density of Ca^{2+} channels in the caveolin-rich plasma membrane [268]. This was achieved by anchoring the Epac1-camps sensor to the well-established N-terminal 10 amino acid sequence from the Lyn kinase encoding palmitoylation and myristoylation motifs [268]. SERCA2a microdomain specificity was achieved by fusing the biosensor to PLN, which regulates Ca^{2+} reuptake into SERCA2a. The cytosolic cAMP sensor Epac1-camps was fused to the 5'-end of the PLN encoding sequence via a flexible linker [269]. JNC, a protein directly interacting with the RyR2 was utilized to target the E1-camps sensor to the RyR2 microdomain. This was achieved by fusing the FRET biosensor to the N-terminal region of JNC [270].

The CM specificity of the targeted FRET biosensors was achieved by the expression

under the control of the Cardiomyocyte specific α-MHC promoter. This mechanism is demonstrated by the example of the RyR2 microdomain specific FRET biosensor E1-JNC, in Figure 1.7.

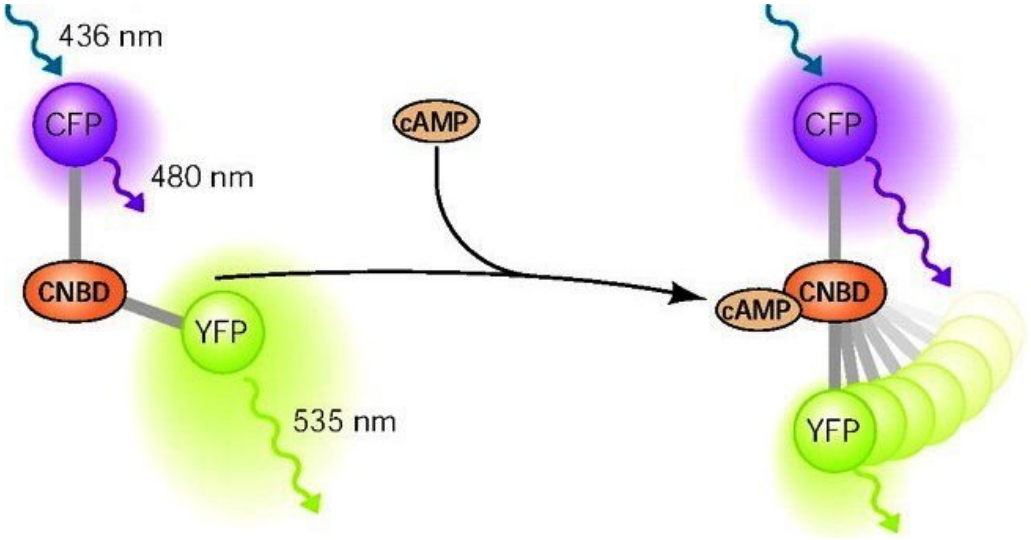

Figure 1.6: Structure of the Epac1-camps FRET Biosensor. The Epac1-camps Förster Resonance Energy Transfer (FRET) biosensor is based on a Cyclic Nucleotiede Binding Domain (CNBD) from EPAC1 that is flanked by a pair of fluorophores. Cyan Fluorescent Protein (CFP) acts as energy donor, Yellow Fluorescent Protein (YFP) as energy acceptor. The donor is excited with light of 436 nm, the wavelength of maximum emission, leading to emission of 480 nm light. Due to the close distance between donor and acceptor, the emitted donor can transfer its energy to the acceptor, which results in emitting light of 535 nm. The binding of 3',5'-cyclic Adenosine Monophosphate (cAMP) causes a conformational change resulting in an increased distance between CFP and YFP. Due to the increased distance, the emitted donor energy looses its ability to excite the acceptor. Figure adapted from [246].

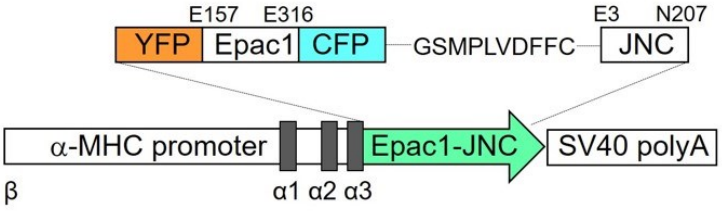

Figure 1.7: Expression of the Epac1-JNC Biosensor. Schematic representation of the Epac1-JNC FRET biosensor which includes two fluorophores, Yellow Fluorescent Protein and Cyan Fluorescent Protein flanking the cAMP binding domain from Epac1 and fused to the N-terminal region of Junctin (JNC). Epac1-JNC was transgenically expressed in mice under the control of the Cardiomyocyte specific α-MHC promoter.

1.6 Stimulated Emission Depletion (STED) Microscopy

STED microscopy is one of several techniques that enable to perform super resolution microscopy [271]. Normal resolution of a light microscope is fundamentally limited to diffraction limit of light. In 1873, Ernst Abbe reported that by using conventional light microscopy, the smallest resolvable distance between two objects may never be smaller than half the wavelength of the imaging light (≈200 nm) [272]. The lateral resolution of conventional light microscopes d is limited by the Abbe diffraction limit, as described in equation 1.4, where λ is the wavelength of the excitation laser, n_m the index of the medium and α the angle of incidence [273].

$$d = \frac{\lambda}{2n_m \cdot sind\alpha} \tag{1.4}$$

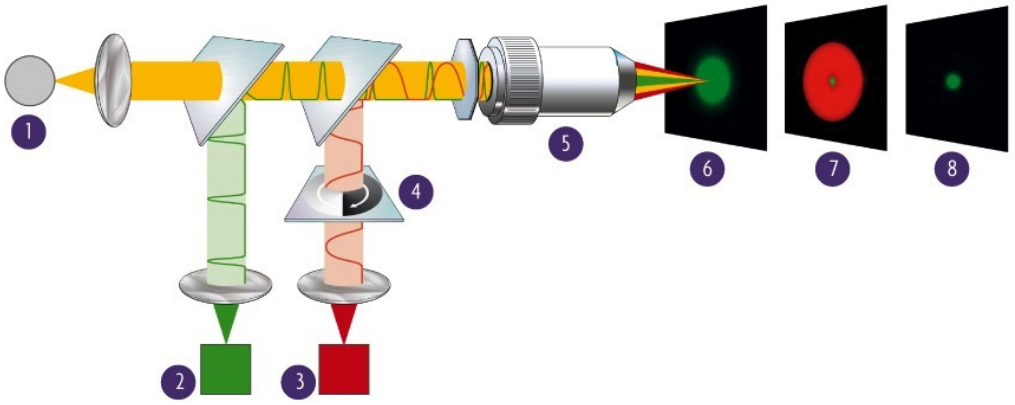

Figure 1.8: Principle of STED Microscopy. The principle of Stimulated Emission Depletion (STED) microscopy is the coupling of an excitation laser with a slightly defocused depletion laser beam resulting in a donut shaped depletion. The limiting effects of light diffraction can be overcome by aligning the two lasers, whereas the size of the fluorescent spot is minimized. 1 Detector, 2 Excitation laser, 3 Depletion laser, 4 Phase filter, 5 STED objective, 6 Focused excitation spot, 7 Overlay, 8 Resulting fluorescence spot. Diagram adapted from [274].

Electron microscopy was invented to overcome this limit. Due to the high resolution, electron microscopy led to many very important discoveries. However, with this technique it is not possible to analyze three dimensional structures of living cells or tissues [275]. This is only possible by using focused visible light. STED microscopy overcomes this resolution limit imposed by diffraction and allows fluorescence imaging of nanoscale features. The resolution of STED microscopy images is improved up to 12 fold compared to classical confocal microscopy [276].

The basic idea of STED microscopy is based on two lasers to downsize the fluorescent spot that scans the sample which leads to resolutions that are by far higher than described in the Abbe equation. One laser excites the fluorophores of the sample of interest the same way as in conventional confocal microscopy [277]. By using a pair of perpendicularly polarized beams from a stimulating depletion laser, a depletion of the excited dye molecules is induced. The dye molecules get de-excited before they can emit any fluorescent light. Due to the doughnut shaped depletion beam, the fluorescence is inhibited in the outer regions which results in a small, super resolution spot that is scanned across the sample (see Figure 5.1).

1.7 Aim of this Work

Alterations in PDE4 activity in human hearts have been shown to result in heart diseases as arrhythmia and heart failure. That's why the aim of this PhD thesis was to uncover the individual roles of PDE subfamilies 4B and 4D on the regulation of the cAMP signaling in calcium handling microdomains of adult mouse CMs.

Major goals of the thesis:

1. To uncover the impact of PDE4B and PDE4D on the regulation of cAMP dynamics in the caveolin-rich plasma membrane microdomain which harbors the L-Type Calcium Channel.
2. To identify the roles of Phosphodiesterase subfamilies 4B and 4D on the cAMP signaling in the Sarco/Endoplasmic Reticulum Ca^{2+}-ATPase 2a microdomain.
3. To determine the structural and functional contribution of PDE4B and PDE4D on the Ryanodine Receptor Type 2 microdomain.

2. Materials and Methods

2.1 Materials

Unless otherwise stated, all solutions and buffers were prepared with ultra pure water from RiOs^{TM} 3 Water Purification System (MilliporeSigma, Burlington, USA).

2.1.1 Animals

The mouse lines used for this project are listed in Table 2.1.

Table 2.1: Mouse Lines.

Mouse line	Genetic Background	Origin
pm-Epac1	FVB/N1	V. Nikolaev [268]
E1-PLN	FVB/N1	V. Nikolaev [269]
E1-JNC	FVB/N1	V. Nikolaev [270]
PDE4B-KO	C57/BL6	M. Conti [278]
PDE4D-KO	C57/BL6	M. Conti [279]

2.1.2 Chemicals

Table 2.2: Chemicals.

Chemical	Manufacturer, Item Number
β-Mercapthoethanol	Sigma Aldrich, #M6250
(-)-Isoproterenol hydrochloride	Sigma Aldrich, #I6504
2,3-Butanedione monoxime	Sigma Aldrich, #B0753
2-Propanol	Chem Solute, #11361000
3-Isobutyl-1-Methylxanthine	AppliChem, #A0695
Ammonium persulfate	Sigma Aldrich, #A3678

Chemical	**Manufacturer, Item Number**
Ampuwa	Fresenius Kabi, #40676.00.00
Bovine serum albumin	Sigma Aldrich, #A8806
Bromophenol blue sodium salt	Carl Roth, #A512.1
Calcium chloride	Sigma Aldrich, #C8106
Calcium chloride dihydrate	Sigma Aldrich, #C7902
di-8-ANEPPS	Molecular Probes, #F1221
Dimethyl sulfoxide	Sigma Aldrich, #D8418
di-Sodium hydrogen phosphate dihydrate	Merck, #1065800500
Ethanol absolute for molecular biology	PanReac AppliChem, #A3678
Ethylenediaminetetraacetic acid (0.5 M)	Sigma Aldrich, #3690
Fetal Calf Serum	Biochrom, #S0615
Forskolin	Sigma Aldrich, #F6886
Glucose	Sigma Aldrich, #G7528
Glycerol	Sigma Aldrich, #G5516
Glycine	Carl Roth, #3908.2
HEPES	Applichem, #A1069
Hydrochloric acid 37%	Carl Roth, #9277.1
Insulin-Transferrin-Selenium-X (ITS)	Gibco, #51500-056
Laminin	Sigma Aldrich, #L2020
L-Ascorbic acid	Sigma Aldrich, #A0278
L-glutamine	Biochrom, #K0282
Liberase DH Research Grade	Roche, #5401089001
Magnesium chloride hexahydrate	Merck, #1058330250
Magnesium sulfate heptahydrate	Merck, #1058861000
MEM, no glutamine, no phenol red	Gibco, #51200038
Methanol	Carl Roth, #4627.2
Moviol	Sigma Aldrich, #81381
N,N-Dimethylformamide	Sigma Aldrich, #D-4551
N.N,N',N'-Tetramethylethylenediamine	Sigma Aldrich, #T9281
PBS Dulbecco	Merck, #L1820
Penicillin/Streptomycin	Biochrom, #A2213
Potassium chloride	Merck, #1049330500
Potassium dihydrogen phosphate	Merck, #1048731000
Potassium hydrogen carbonate	Merck, #1048540500
Powdered milk	Carl Roth, #T145.1
Propranolol hydrochloride	Sigma Aldrich, #P0884
Rotiphorese Gel 30 (Acrylamide)	Carl Roth, #3029.2

Chemical	Manufacturer, Item Number
Sodium azide	Sigma Aldrich, #S20002
Sodium chloride	Merck, #1064041000
Sodium dodecyl sulfate solution (20%)	Sigma Aldrich, #5030
Sodium hydrogen carbonate	Merck, #1063291000
Sodium hydroxide solution	Chem Solute, #1340
Sodium pyruvate	Sigma Aldrich, #P8574
Taurine	Applichem, #A1141
Technical Buffer Solution pH 4.01	Mettler-Toledo AG, #51350004
Technical Buffer Solution pH 7.00	Mettler-Toledo AG, #51350006
Tergitol solution Type NP-40	Sigma Aldrich, #NP40S
Tris	Carl Roth, #4855.2
Triton X-100 Solution 10%	AppliChem, #A1287
Trypsin 2.5%	Gibco, #15090-046
Tween 20	Sigma Aldrich, #P1379

2.1.3 Consumables

Table 2.3: Consumables.

Consumable	Manufacturer, Item Number
20 G Sterican	Braun, #4657519
6 Well Plate	Falcon, #351146
96 Well Plates	Thermo Fisher Scientific, #167008
Compitips advanced 5 mL	eppendorf, #0030 089.456
Filterpaper	Hahnemüle, #FP598
Gauze	Th Geyer, #9.068291
Gelloader Pipette Tips	Sarstedt, #70.1190.100
Kimtech	Kimberly-Clark, #7558
Leukosilk	BSN medical, #09567-00 AP
Microscope Cover Glasses 25 mm	Assistent, #41001125
Microscope Slides	Thermo Fisher Scientific, #J1800AMNZ
Micro-Touch	Ansell, #700124
MiniFlex Round Tips	Biozym, #728014
Multiply μStrip Pro 8-strip	Sarstedt, #72.991.002
Nonabsorbable Braided Silk Suture	FST, #18020-50
Quality Pipette Tips 1000 μL	Sarstedt, #70.762.100

Consumable	Manufacturer, Item Number
Rotilabo reaction vials 5 mL	Carl Roth, #PE68.1
SafeSeal tube 1.5 mL	Sarstedt, #72.706
Serological Pipette 10 mL	Sarstedt, #86.1254.001
Serological Pipette 2 mL	Sarstedt, #86.1252.001
Serological Pipette 25 mL	Sarstedt, #86.1255.001
Serological Pipette 5 mL	Sarstedt, #86.1253.001
Serological Pipette 50 mL	Sarstedt, #86.1256.001
Spitzen, 10 mL	Biozym, #725064
Steritop 0.22 μm 1000 mL	Merck, #SCGPT10RE
Tip StackPack 10 μL	Sarstedt, #70.760.502
Tip StackPack 100 μL	Sarstedt, #70.760.502
Transfer pipette	Sarstedt, #86.1172.001
Tube 15 mL	Sarstedt, #62.554.002
Tube 50 mL	Sarstedt, #62.574.004
U-40 Insulin 30Gx1/2	Braun, #40012525
U-40 Insulin Omnifix Solo	Braun, #9161309V

2.1.4 Devices

Table 2.4: Devices.

Devices	Manufacturer
accu-jet pro	Brand
Beamsplitter DV2	Photometrix
Centrifuge Fresco 17	Thermo Fisher Scientific
Class II Biological Safety Cabinet	Labgard
CO_2 Incubator	Sanyo
Contractility and calcium transient analysis system	IonOptix
Developer SRX-101A	Konica Minolta
E-Box	Vilber Lourmat
Filter Cube 05-EM	Photometrix
FlexStation 3	Molecular Devices
Freezer Comfort	Liebherr
Fridge Comfort	Liebherr
Gene Touch	Bioer
Glacier Ultralow Temperature Freezer	Nuaire

Devices	Manufacturer
ISM831C	Ismatec
LABOKLAV	HSP
LED KL 1600	Schott
LED pE-100 440 nm	CoolLED
Leica DMI3000 B	Leica
Leica TCS SP5	Leica
LX 320A scs	Precisa
Mupid-One	Advance
my FUGE	Benchmark
optiMOS	Q imaging
PCB1000-2	KERN
pH Level 1	inoLab
PowerPac	Bio Rad
RCT standard	IKA
Research plus (10 μL - 10 mL)	eppendorf
Scanner LiDE 220	Canon
Shaker DRS-12	ELMI
SMZ 745T	Nikon
ThermoMixer C	eppendorf
Vortex-Genie 2	Scientific Industries
Water Bath	Julabo
Western Blotting System	Bio Rad
Zeiss LSM 800	Zeiss

2.1.5 Kits and Others

Table 2.5: Kits and Others.

Consumable	Manufacturer, Item Number
cAMP ELISA Kit	Sigma Aldrich, #CA200
Chemiluminescent Substrate	Thermo Fisher Scientific, #34580
cOmplete Tablets	Roche, #04 693 116 001
Developerconcentrate	Adeofodur, #00176
Fixerconcentrate	Adeofodur, #01176
Forene	abbvie, #B506
Fuji Medical X-Ray Film	Fujifilm, #47410 19284

Consumable	Manufacturer, Item Number
Immersion liquid type F	Leica, #11513859
Nitrocellulose Blotting Membrane	GE Healthcare, #10600002
pECFP-N1 Vektor	pECFP-N1
PhosphoSTOP	Roche, #04 906 837 001
Pierce BCA Protein Assay Kit	Thermo Fisher Scientific, #23227
Ponceau S solution	Sigma Aldrich, #P7170
Protein Marker V	Peqlab, #27-2211

2.1.6 Software

Table 2.6: Software.

Software	Version	Manufacturer
Excel	Professional Plus 2013	Microsoft
Fiji	1.52e	National Institutes of Health
GraphPad Prism	6.01	GraphPad
ImageJ	1.44n9	National Institutes of Health
Ion Wizzard	6.5.1.92	IonOptix
Mendeley Desktop	1.15.2	Mendeley
Micro-Manager	1.4.5	Open Imaging
Origin	8.5.0G SR1	OriginLab Corporation
Picture Manager	14.0.7010.1000	Microsoft
PowerPoint	Professional Plus 2013	Microsoft
R	3.3.2	The R Foundation
SoftMax Pro	5.4.6.005	Molecular Devices
Texmaker	5.0.2	Free Software Foundation
Word	Professional Plus 2013	Microsoft
ZEN (blue edition)	2.5	Carl Zeiss

2.1.7 Antibodies

Table 2.7: Primary Antibodies for Western Blot. Primary antibodies for Western Blot (WB) analysis. Antibody dilutions were prepared in 5% powdered milk in TBS-T Buffer. Species (Sp), rabbit (rb) and mouse (ms).

Antibody	Dilution	Sp	Manufacturer
Anti GAPDH	1:160000	ms	HyTest Ltd, #5G4
Anti PDE2A	1:500	rb	FabGennix, #PDE2A-101AP
Anti PDE3A	1:1000	rb	Yan Lab, [280]
Anti PDE4A	1:500	rb	abcam, #ab14607
Anti PDE4B	1:2500	rb	abcam, #ab170939
Anti PDE4D	1:2500	rb	abcam, #ab171750
Anti PLN	1:2500	rb	Badrilla, #ab126174
Anti PLN Phospho-Ser16	1:5000	rb	Badrilla, #A010-12
Anti RyR2	1:5000	rb	Sigma Aldrich, #HPA020028
Anti RyR2 Phospho-Ser2808	1:2500	rb	Badrilla, #A0-10-30

Table 2.8: Secondary Antibodies for Western Blot. Secondary antibodies for Western Blot (WB) analysis. Antibody dilutions were prepared in 5% powdered milk in TBS-T Buffer.

Antibody	Dilution	Manufacturer
Immun-Star Goat Anti-Mouse (GAM)-HRP	1:5000	Bio Rad, #170-5047
Immun-Star Goat Anti-Rabbit (GAR)-HRP	1:5000	Bio Rad, #170-5046
Rabbit anti Sheep IgG (H/L)-HRP	1:5000	Bio Rad, #5184-2504

Table 2.9: Primary Antibodies for Immunofluorescence Staining. Primary antibodies for Immuno Fluorescence (IF) staining. Antibody dilutions were prepared in Blocking Buffer. Species (Sp), rabbit (rb) and sheep (sh).

Antibody	Dilution	Sp	Manufacturer
Anti PDE4B	1:200	sh	Baillie Lab, [281]
Anti PDE4D	1:200	sh	Baillie Lab, [134]
Anti RyR2	1:300	rb	Sigma Aldrich, #HPA020028

Table 2.10: Secondary Antibodies for Immunofluorescence Staining. Secondary antibodies for Immuno Fluorescence (IF). Antibody dilutions were prepared in Blocking Buffer.

Antibody	Dilution	Manufacturer
Alexa Fluor 568 Goat Anti-Rabbit	1:500	Thermo Fisher, #A-11011
Alexa Fluor 594 Donkey Anti-Sheep	1:250	abcam, #ab150180
Alexa Fluor 633 Donkey Anti-Sheep	1:500	Thermo Fisher, #A-21100
Goat Anti-Rabbit IgG-Abberior Star RED	1:250	Sigma Aldrich, #41699

2.1.8 Buffers and Solutions

Table 2.11: Perfusion Buffer. Prepared with H_2O Ampuwa, aliquots of 35 mL were stored at -20°C.

Ingredient	Concentration
NaCl	1.13 M
KCl	47 mM
KH_2PO_4	6 mM
$Na_2HPO_4 \cdot 2H_2O$	6 mM
$MgSO_4 \cdot 7H_2O$	12 mM
$NaHCO_3$	120 mM
$KHCO_3$	100 mM
HEPES	100 mM
Taurine	300 mM
Glucose	5.55 mM
BDM	9.89 mM

Table 2.12: Calcium Chloride Solution. Stored at 4°C.

Ingredient	Concentration
$CaCl_2$	100 mM

Table 2.13: BSA Stock Solution (10%). Aliquoted and stored at -20°C.

Ingredient	Concentration
BSA	10% (w/v)

Table 2.14: Liberase Solution. Aliquoted and stored at -20°C.

Ingredient	Mass/Volume
Liberase DH	50 mg
H_2O	12 mL

Table 2.15: Digestion Buffer. Enzymes were thawed immediately before use.

Ingredient	Volume
Perfusion Buffer	2.25 mL
$CaCl_2$	3.75 µL
Liberase Solution	300 µL
Trypsin 2.5%	300 µL

Table 2.16: Stopping Buffer 1. Prepared freshly before use.

Ingredient	Volume
Perfusion Buffer	2.25 mL
FCS	250 µL
Calcium chloride solution	1.25 µL

Table 2.17: Stopping Buffer 2. Prepared freshly before use.

Ingredient	Volume
Perfusion Buffer	9.5 mL
FCS	500 µL
Calcium chloride solution	3.75 µL

Table 2.18: Myocyte Culture Medium. Prepared freshly before use.

Ingredient	Volume
MEM without L-glutamine	48 mL
BSA stock solution (10%)	500 μL
Pencililin/Streptomycin	500 μL
L-glutamine	500 μL
ITS-Supplement	500 μL

Table 2.19: FRET Buffer. Stored at room temperature, pH 7.4.

Ingredient	Concentration
NaCl	144 mM
KCl	5.4 mM
$MgCl_2 \cdot 7H_2O$	1 mM
$CaCl_2$	1 mM
HEPES	10 mM

Table 2.20: SDS Stop 3x. Stored at room temperature, pH 6.7.

Ingredient	Concentration
Tris	200 mM
20% SDS solution	6% (v/v)
Glycerol	15% (v/v)
Bromphenol Blue	1-2 mg
β-Mercapthoethanol	10% (v/v)

Table 2.21: 4xTris/SDS pH 6.8. Stored at room temperature, pH 6.8.

Ingredient	Concentration
Tris	500 mM
20% SDS solution	0.4% (v/v)

Table 2.22: 4xTris/SDS pH 8.8. Stored at room temperature, pH 8.8.

Ingredient	Concentration
Tris	1.5 M
20% SDS solution	0.4% (v/v)

Table 2.23: 10% APS Solution. Aliquoted and stored at -20°C.

Ingredient	Concentration
APS	10% (w/v)

Table 2.24: 10x SDS Running Buffer. Stored at room temperature, pH 8.3.

Ingredient	Concentration
Tris	250 mM
Glycine	1.9 M
20% SDS solution	1% (v/v)

Table 2.25: 1x SDS Running Buffer. Stored at room temperature.

Ingredient	Concentration
10x SDS Running Buffer	10% (v/v)

Table 2.26: 10x Transfer Buffer. Stored at room temperature.

Ingredient	Concentration
Tris	325 mM
Glycine	1.9 M

Table 2.27: 1x Transfer Buffer (20% Methanol). For separating gel (15%) and separating gel (10%), stored at 4°C.

Ingredient	Concentration
10x Transfer Buffer	10% (v/v)
Methanol	20% (v/v)

Table 2.28: 1x Transfer Buffer (5% Methanol). For separating gel (5%), stored at 4°C.

Ingredient	Concentration
10x Transfer Buffer	10% (v/v)
Methanol	5% (v/v)

Table 2.29: 10x TBS Buffer. Stored at room temperature.

Ingredient	Concentration
Tris	100 mM
NaCl	1.5 M

Table 2.30: 1x TBS-Tween Buffer. Stored at room temperature.

Ingredient	Concentration
10x TBS Buffer	10% (v/v)
Tween 20	0.1% (v/v)

Table 2.31: Stacking Gel. 3.8 mL, for 2 gels.

Ingredient	Volume
30% Acrylamide solution	500 μL
4xTris/SDS pH 6.8	940 μL
H_2O	2.31 mL
10% APS solution	18.8 μL
TEMED	7.5 μL

Table 2.32: Separating Gel 5%. 15 mL, for 2 gels.

Ingredient	Volume
30% Acrylamide solution	2 mL
4xTris/SDS pH 8.8	3 mL
H_2O	7 mL
10% APS solution	48 μL
TEMED	18 μL

Table 2.33: Separating Gel 10%. 15 mL, for 2 gels.

Ingredient	Volume
30% Acrylamide solution	4 mL
4xTris/SDS pH 8.8	3 mL
H_2O	5 mL
10% APS solution	48 μL
TEMED	18 μL

Table 2.34: Separating Gel 15%. 15 mL, for 2 gels.

Ingredient	Volume
30% Acrylamide solution	6 mL
4xTris/SDS pH 8.8	3 mL
H_2O	3 mL
10% APS solution	48 μL
TEMED	18 μL

Table 2.35: IonOptix Buffer. Stored at 4°C, Glucose and $CaCl_2$ were added before use, pH 7.54.

Ingredient	Concentration
NaCl	149 mM
KCl	1 mM
$MgCl_2{\cdot}6H_2O$	1 mM
HEPES	5 mM
Glucose	10 mM
$CaCl_2$	1 mM

Table 2.36: Langendorff Perfusion Buffer. Stored at 4°C up to two days, $CaCl_2$ was added after 15 min of carbogenation.

Ingredient	Concentration
NaCl	118 mM
KCl	4.7 mM
$MgSO_4 \cdot 7H_2O$	0.8 mM
$NaHCO_3$	25 mM
KH_2PO_4	1.2 mM
Glucose	5.0 mM
Sodium pyruvate	110 mM
$CaCl_2$	2.5 mM

Table 2.37: Lysis Buffer. Stored at -20°C, Protease Inhibitor Cocktail Tablets cOmplete Tablets and Phosphatase Inhibitor Cocktail Tablets, PhosSTOP were added according to manufacturer information.

Ingredient	Concentration
Tris	30 mM
EDTA	1 mM
NaCl	150 mM
NP-40	1% (v/v)
20% SDS solution	0.1% (v/v)

Table 2.38: Blocking Buffer. Stored at 4°C up to one week.

Ingredient	Volume
PBS	43.5 mL
FCS	5 mL
10% Triton X-100 solution	1.5 mL

Table 2.39: Genotyping PCR Reaction Mix.

Ingredient	Volume
Tail/Ear lysate	0.5 µL
H_2O	14.7 µL
5xGoTaq Buffer	4.0 µL
dNTPs 10 mM	0.5 µL
MHCseqford primer	0.05 µL
YFPnewrev primer	0.05 µL
GoTaq Polymerase	0.2 µL

Table 2.40: Formamide Solution. Prepared freshly before use in FRET Buffer.

Ingredient	Concentration
N,N-Dimethylformamide	1.5 M

2.2 Methods

2.2.1 Mouse Breeding

Transgenic (TG) and Wild Type (WT) mice were bred and accommodated in the animal facility of the University Medical Center Hamburg-Eppendorf (UKE). All animals had constant access to food and water. Tail or ear biopsies were used for genotyping by Polymerase Chain Reaction (PCR), as described in section 2.2.2. For CM isolation and whole heart perfusion experiments, animals were sacrificed at the age of 8-20 weeks. All animal experiments were performed in accordance with institutional and governmental guidelines.
PDE4B-KO and PDE4D-KO mouse lines were mated with pm-Epac1, E1-PLN and E1-JNC animals that result in the mouselines pm-Epac1/PDE4B-KO, pm-Epac1/PDE4D-KO, E1-PLN/PDE4B-KO, E1-PLN/PDE4D-KO, E1-JNC/PDE4B-KO and E1-JNC/PDE4D-KO. Mice were kept on mixed FVB/N1;C57/BL6 background. The mouse lines used for this project are listed in table 2.1. Heterozygous knockout mice (+/d) were mated with each other and result, according to Mendel's law of segregation [282], in 25% WT mice (+/+), 50% heterozygous mice (+/d) and 25% knockout (d/d) mice. To rule out possible influences of fluctuations in the genetic background, all results obtained for knockout animals were directly compared to WT littermates. Heterozygous mice (+/T) harboring a FRET biosensor were bred with WT mice for the biosensor. Samples for WB experiments were prepared using mice without a biosensor.

2.2.2 Genotyping

Bred mice were genotyped by a standard PCR to check for the sensor, PDE4B and PDE4D expression. Tail or ear biopsies were digested over night in 200 μL DirectPCR-Tail Buffer containing Protein kinase K 500 μg/mL at 55°C and 1000 rpm in a thermo cycler. Boiling at 85°C for 45 min terminated the reaction. The lysate was directly used for PCR reaction with the Genotyping-PCR reaction mix as shown in the table below.

94°C	4 min	
94°C	30 sec	} 35x
62°C	30 sec	
72°C	50 sec	
72°C	7 min	

The PCR reaction was analyzed on a 2% agarose gel in TAE Buffer. A 100 bp DNA ladder was used as a DNA marker. Genotyping experiments were performed by Karina Schlosser, Sophie Sprenger and Annabell Kühl.

2.2.3 Cardiomyocyte Isolation

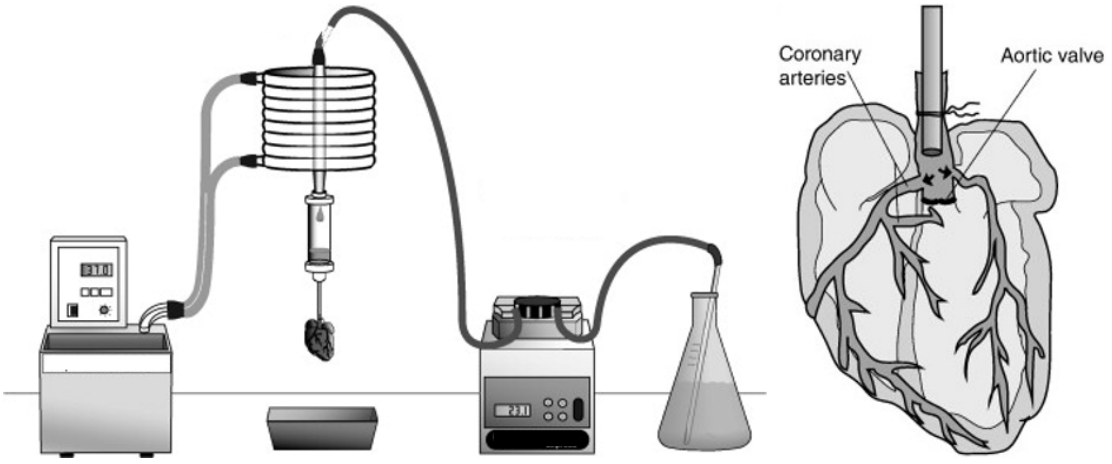

Figure 2.1: Langendorff Perfusion System. Left, Langendorff perfused heart including the associated Langendorff perfusion system that contains a heating system, a peristaltic pump that guarantees a constant flow, tubing and a holding device for the cannulated heart. **Right**, Illustration of a cannulated heart, allowing a retrograde perfusion with Digestion Buffer via the coronary arteries. Figures modified from Louch *et al.* [283].

Adult ventricular mouse CMs were isolated via retrograde Langendorff perfusion as described by Börner *et al.* [284]. Before starting the isolation process, the water bath was heated up and the tubing was rinsed with warm H_2O for at least 10 min. Mice were anesthetized by isoflurane inhalation and sacrificed by cervical dislocation. The heart was rapidly explanted and washed in a petri dish with ice-cold PBS. It was mounted via the aorta on a blunted 20 G cannula, allowing a retrograde perfusion at 37°C via the coronary arteries with a constant flow of 3 mL/min. After 3 min perfusion with Perfusion Buffer, the heart was digested with Digestion Buffer for 9 min. Digestion Buffer was prepared during the 3 min perfusion with Perfusion Buffer to reduce the enzyme degradation to a minimum level. The atria were carefully excised and discarded, whereas the digested ventricles were dissected for 30 s in 2.5 mL Digestion Buffer. 2.5 mL Stopping Buffer 1 was added to stop the digestion. The cell suspension was homogenized by using a 1 mL syringe without a cannula for 3 min. The suspension was filtered through a gauze with a mesh diameter of 200 μm. After 10 min of sedimentation, the supernatant was discarded and the cell pellet was resuspended in 10 ml Stopping Buffer 2. To achieve a final Ca^{2+} concentration of 1 mM, CMs were recalcified in five steps, with 4 min adaption time between each step.

50 µL	$CaCl_2$ 10 mM	final concentration	62 µM
50 µL	$CaCl_2$ 10 mM	final concentration	112 µM
100 µL	$CaCl_2$ 10 mM	final concentration	212 µM
30 µL	$CaCl_2$ 100 mM	final concentration	500 µM
50 µL	$CaCl_2$ 100 mM	final concentration	1000 µM

2.2.4 Langendorff-perfused Whole Heart Stimulation

Mouse handling and heart extraction was performed as described in section 2.2.3. After cannulation of the mouse heart onto a blunted 20 G cannula, the heart was perfused with Langendorff Perfusion Buffer. The buffer was carbogenated (5 Vol% CO_2 in O_2) throughout the whole experiment to prevent calcium from precipitating. Control hearts were perfused with Langendorff Perfusion Buffer for 25 min. Iso-stimulated whole hearts were equilibrated with Langendorff Perfusion Buffer for 10 min. For pharmacological stimulation, the heart was perfused for 15 min with Langendorff Perfusion Buffer containing an Iso-concentration of 100 nM. The flow rate was 3 mL/min for all experiments. To assure easier handling for the WB experiments, the hearts were cut into three parts and were shock frozen with liquid nitrogen. The mouse hearts were stored at -80°C until further use.

2.2.5 FRET Microscopy

Adult mouse CMs were isolated according to the protocol described in section 2.2.3. After recalcification, CMs were plated onto laminin coated round glass coverslides (Ø 25 mm) and incubated at 37°C and 5% CO_2. Measurements were performed 2 - 10 h after cell isolation. A coverslide with adherent cells was mounted into a microscopy cell chamber and was washed with 400 µL of FRET Buffer. Another 400 µL of fresh FRET Buffer were added to the chamber. FRET experiments were performed by using an inverted fluorescent microscope with an oil immersion objective with a 60x magnification. CMs were excited at 440 nm by using a coolLED single-wavelength light emitting diode. The emitted light of the sample was split into individual donor and acceptor channel by a beam-splitter and a Complementary Metal-Oxide-Semiconductor (CMOS) camera (see Figure 2.2).

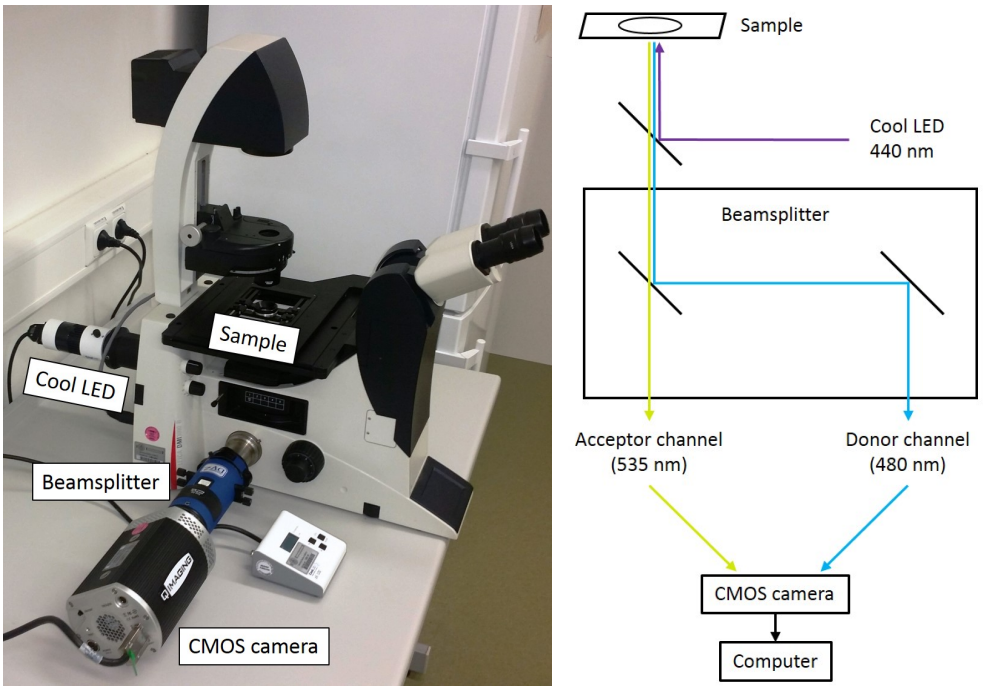

Figure 2.2: FRET Microscope. **Left**, Experimental setup of the Förster Resonance Energy Transfer (FRET) microscope, including a cool LED, beamsplitter and a Complementary Metal-Oxide-Semiconductor (CMOS) camera. **Right**, Schematic representation of the FRET microscope. A sample is excited with a single wavelength light of 440 nm. A beamsplitter splits the image into individual donor (Cyan Fluorescent Protein (CFP), 480 nm) and acceptor channel (Yellow Fluorescent Protein (YFP), 535 nm). Images are taken by a CMOS camera and analysed with a computer.

CMs which express the biosensor homogeneously were selected for FRET experiments. The settings (exposure time and LED intensity) were adjusted to reach a good signal to noise ratio of the cell. Images of the CFP and YFP emission channels were acquired every 5 seconds. The pharmacological compounds of interest were diluted in FRET Buffer. 400 μL of the desired compound solution was pipetted carefully into the measuring chamber. Before adding any compound, it was assured that the FRET ratio reached a stable baseline.

The emission spectrum of the donor and acceptor overlap in the region of the maximum emission of the acceptor, which leads to a detection of the donor fluorescence in the acceptor channel. It is necessary to calculate a spectral bleedthrough factor b to account for this phenomenon. The bleedthrough of the acceptor into the donor channel is negligible. For determination of this correction factor, HEK293a cells were transfected with a plasmid encoding only for the CFP fluorophore. A glass coverslide with adherent HEK293a cells that express the CFP fluorophore were measured as described above to determine the amount of emitted CFP light in the YFP channel.

The recorded images of the CFP and YFP emission channels were split into individual channels. The FRET ratio was determined as described in equation 2.1.

$$FRET = \frac{averaged\,YFP\,intensity}{averaged\,CFP\,intensity} \tag{2.1}$$

According to equation 2.2, the bleedthrough factor was subtracted from the FRET ratio resulting in the corrected FRET ratio ($FRET_{corr}$).

$$FRET_{corr} = \frac{YFP - b * CFP}{CFP} = \frac{YFP}{CFP} - b = FRET - b \tag{2.2}$$

The corrected FRET ratio values were normalized between 0% and 100% for a better comparability of the different experiments.

2.2.6 Single-Cell Contractility Measurements

Adult mouse CMs were isolated according to the protocol described in section 2.2.3. After 10 min of sedimentation after recalcification, the supernatant was discarded and the cell pellet was washed with 7.5 mL of myocyte culture medium. 7.5 mL of fresh myocyte culture medium was added. The cell suspension was incubated for at least 90 min at 37°C and 5% CO_2. After washing with 7.5 mL with IonOptix Buffer, 7.5 mL of fresh IonOptix Buffer was added.
200 μL of cell suspension was added into a measuring chamber. Next, CMs were paced for 4 ms at 0.5 Hz and 15.0 V. Afterwards, contractile responses were evaluated by the optical sarcomere length measurement method (IonOptix). The pharmacological compounds of interest were diluted in IonOptix Buffer. 200 μL of the desired compound solution was pipetted carefully into the measuring chamber. Finally, effects on the arrhythmia susceptibility were determined by quantifying extra beats of paced CMs.

2.2.7 Chemical Cardiomyocyte Detubulation

Osmotic shock-induced detubulation of CMs was performed to remove T-tubules. Adult mouse CMs were isolated according to the protocol described in section 2.2.3. After recalcification, CMs were plated onto laminin coated round glass coverslides (Ø 25 mm) and incubated at 37°C and 5% CO_2 for at least one hour. Then, a coverslide with adherent cells was mounted into a microscopy cell chamber. The coverslide was washed with 400 μL of FRET Buffer to remove dead and non adherent cells. Cells were incubated with 1.5 M formamide solution for 15 min at room temperature and washed twice with FRET Buffer. FRET experiments were performed according to the protocol in section 2.2.5.

2.2.8 Western Blot Analysis

Shock frozen adult mouse hearts were homogenized in Lysis Buffer by a homogenizer. Protein concentrations were quantified with an Bicinchoninic Acid (BCA) assay. Heart lysates were diluted in Lysis Buffer including SDS Stop 3x Buffer. Samples for detection of PDE2A, PDE3A, PDE4A, PDE4B and PDE4D were cooked for 5 min at 95°, whereas samples for PLN and RyR2 detection were not cooked. Proteins were separated according to their size by Sodium Dodecyl Sulfate Polyacrylamide Gel Electrophoresis (SDS-PAGE) with 5-15% acrylamide gels. Separated proteins were transferred onto a nitrocellulose membrane, blocked with 5% non-fat milk solution and analyzed by using specific antibodies.
WB experiments were performed to determine the phosphorylation of PLN and RyR2 after whole heart stimulation with Iso as well as analyzing specific PDE expression. PDE WBs were performed using hearts of PDE4B and PDE4D knockout mice as well as WT animals. The hearts were explanted from sacrificed mice, perfused with ice-cold Phosphate Buffered Saline (PBS) until they were blood free, then snap frozen with liquid nitrogen and stored until further use at -80°C.
In order to detect multiple proteins on one nitrocellulose membrane, it was stripped and reprobed with a different primary antibody. Membranes were washed in H_2O for 4 min, followed by an incubation step with 0.2 M NaOH for 8 min. Before blocking, membranes were washed with H_2O for 4 min.

2.2.9 Immunofluorescence Staining

Adult mouse CMs were isolated according to the protocol described in section 2.2.3. After 10 min of sedimentation after recalcification, the supernatant was discarded and the cell pellet was washed with 10 mL of Stopping Buffer 2 without Fetal Calf Serum (FCS) before 7.5 mL of fresh Stopping Buffer 2 without FCS was added. The CMs were plated onto laminin coated round glass coverslides (Ø 25 mm) and incubated at 37°C and 5% CO_2 for at least two hours. The glass coverslide with adherent cells was washed once with PBS and the cells were fixed by incubation with ice-cold ethanol for 20 min at -20°C. After three washing steps with PBS, CMs were blocked by incubation with Blocking Buffer (see Table 2.38) for 2 h at room temperature in the dark. The cells were incubated with primary antibodies diluted in Blocking Buffer over night at 4°C and washed afterwards three times with PBS. Incubation with secondary antibodies in Blocking Buffer was performed in the dark for 2 h at room temperature and washed three times with PBS. Stained cells were kept at 4°C in PBS until use.

2.2.10 STED Microscopy

STED microscopy was performed in collaboration with the UKE Microscopy Imaging Facility using a Leica TCS SP5 microscope stand. The preparation of the IF staining is described in section 2.2.9. The glass coverslide with adherent stained CMs was mounted at room temperature in the dark over night on a rectangular glass microscope slide using moviol.
STED and corresponding confocal microscopy were carried out in sequential line scanning mode using an Abberior STED microscope. The setup is built on a Nikon Ti-E microscope body with perfect focus system and employed for excitation and detection of the fluorescence signal a 60x (NA 1.4) P-Apo oil immersion objective. Two pulsed lasers were used for excitation at 561 nm and 640 nm and a near-infrared pulsed laser (775 nm) for depletion. The detected fluorescence signal was directed through a variable sized pinhole (set to match 1 airy at 640 nm) and detected by novel state of the art Avalance Photo Diode with appropriate filter settings for Cy3 (595-635 nm) and Cy5 (615-755 nm). Images were recorded with a dwell time of 5 μs with a pixel size of 20x20 nm. The images were taken in 2D-STED mode. The acquisitions were carried out in time gating mode i.e. with a time gating width of 8 ns and a delay of 781 ps for both the red and far red channel.

2.2.11 Enzyme-Linked Immunosorbent Assay (ELISA)

Adult mouse CMs were isolated according to the protocol described in section 2.2.3. After 10 min of sedimentation after recalcification, the supernatant was discarded and the cell pellet was resuspended in FRET Buffer. Cell suspension of 30,000 cells was centrifuged for 2 min at 2000 rpm and 4°C. The pellet was lysed in 240 μL 0.1 M HCl. After 10 min of incubation on ice, the lysate was shock frozen, using liquid nitrogen. ELISA experiment and data evaluation was performed according to the protocol of the used cAMP ELISA kit (see Table 2.5).

2.2.12 Statistical Analysis

All data shown in bar graphs are presented as mean ± Standard Error of Mean (SEM) of n/N cells. n represents the number of measured cells isolated from N mice. Statistical analyses were performed with the Microsoft Excel Professional Plus 2013 and R 3.3.2 software. Differences between the groups were analysed by using mixed ANOVA followed by Wald χ^2-test or Kruskal-Wallis ANOVA. WB and ELISA experiments were analyzed by one-way ANOVA. No sample exclusion was performed. A value of $p<0.05$ was considered significant.

3. Results

3.1 Effect of PDE4B and PDE4D Deletion on PDE Expression

First, it was analyzed whether global deficiency of PDE4B and PDE4D in adult mice causes a CM specific change in expression of the most relevant PDE subfamilies PDE2A, PDE3A, PDE4A, PDEB and PDE4D. Adult hearts of PDE4B-WT, PDE4B-KO, PDE4D-WT and PDE4D-KO mice were harvested and analyzed by WB (see Figure 3.1). No statistical differences could be observed, except for PDE4B in the PDE4B-KO mice and PDE4D in PDE4D-KO mice (see Figure 3.2), which makes the PDE4B and PDE4D deficient mice a suitable model for analyzing the impact of these PDE subfamilies on the cAMP signaling in adult mouse CMs.

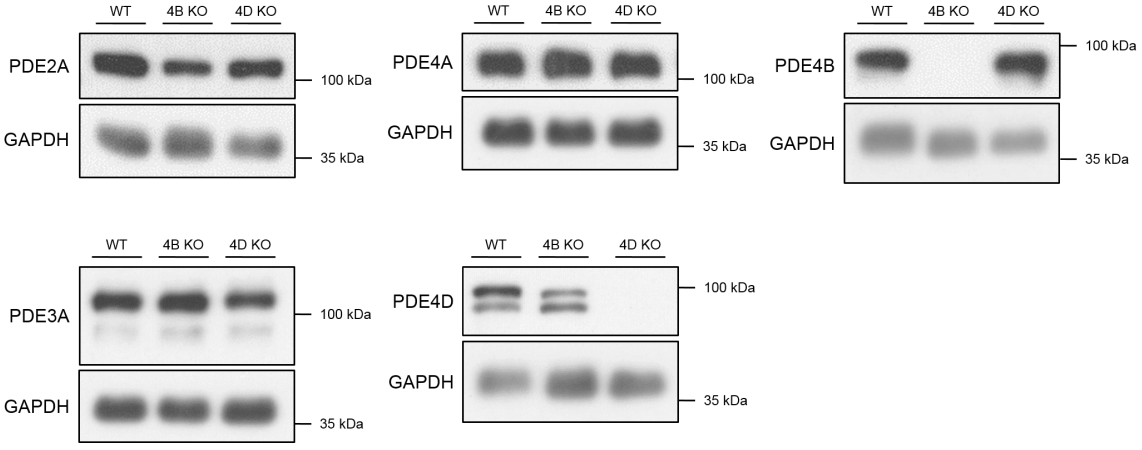

Figure 3.1: Western Blot PDE Expression. Representative WB for the expression of PDE2A, PDE3A, PDE4A, PDE4B and PDE4D performed with 20 μg heart lysates each, isolated from WT, PDE4B-KO and PDE4D-KO adult mice. Glyceraldehyde 3-Phosphate Dehydrogenase (GAPDH) was used as a loading control.

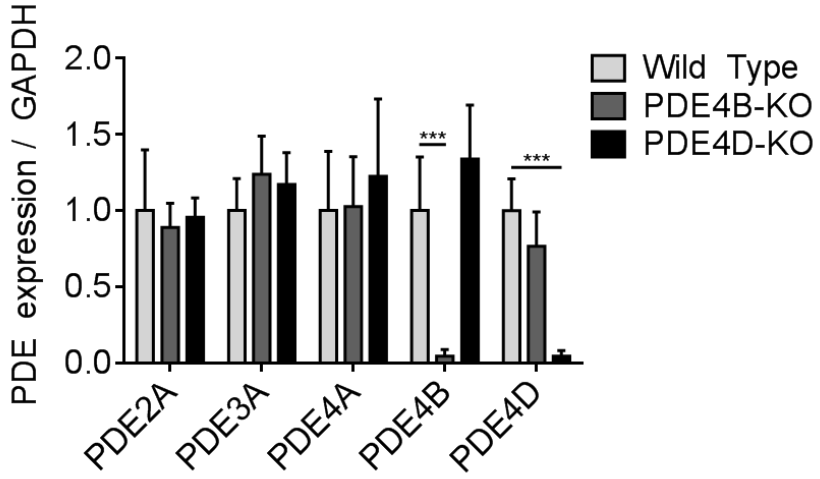

Figure 3.2: Quantification of PDE Expression. Quantification of WB experiments performed to analyze the expression of PDE2A, PDE3A, PDE4A, PDE4B and PDE4D of whole heart lysates isolated from WT as well as PDE4B and PDE4D deficient mice. Data of 5 individual heart lysates is presented as mean ± SEM. *** - significant differences at $p<0.001$.

3.2 Determination of Spectral Bleedthrough Factor

The overlapping emission spectra of donor and acceptor (CFP and YFP) lead to a detection of the donor fluorescence in the acceptor channel. To counteract this phenomenon, it is necessary to calculate the spectral bleedthrough factor b. The bleedthrough of the acceptor into the donor channel is negligible. For determination of b, the amount of detected fluorescence in the acceptor (YFP) channel of excited HEK293a cells, transfected with a plasmid encoding for the donor chromophore (CFP), was detected. This factor is unique for every microscope and allows to compare experiments that were performed at different microscopes. The bleedthrough factor for the microscope used for FRET measurements in this project is shown in equation 3.1.

$$b_{Leica} = 0.892 \tag{3.1}$$

The individual results of 19 independent measurements are listed in the appendix in Table 5.1.

3.3 Impact of PDE4B and PDE4D on the Caveolin-Rich Plasma Membrane Microdomain

To determine the impact of PDE4B and PDE4D on the regulation of the caveolin-rich plasma membrane microdomain, PDE4B-KO and PDE4D-KO mice were crossed with transgenic mice, expressing the highly sensitive pm-Epac1 FRET biosensor specifically in CMs. The CM specificity was achieved by the α-MHC promoter. Isolation of adult mouse CMs and FRET measurements were performed according to sections 2.2.3 and 2.2.5.

The first FRET experiment was performed to figure out whether the genetic ablation of PDE4B and PDE4D causes changes in the accumulation of cAMP within the plasma membrane microdomain. A high dose of Iso, 100 nM, was applied to adult mouse CMs to result in an increased intracellular cAMP level. 100 μM of IBMX as a nonselective PDE inhibitor and 10 μM of Forskolin as an activator of Adenylyl Cyclase (AC) were next added to the cells to reach the maximum concentration of cAMP (see Figure 3.3). The ratio between the Iso-mediated cAMP increase and the maximum cAMP response was significantly increased in the PDE4B-KO CMs, compared to the associated WT cells. Also, this ratio was significantly enhanced in PDE4D-KO CMs, which is an indication that both PDEs are involved in the regulation of the caveolin-rich plasma membrane microdomain (see Figure 3.3).

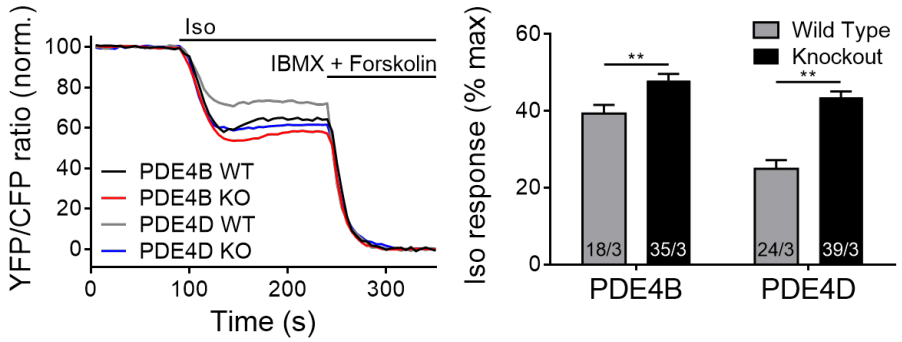

Figure 3.3: FRET Responses Measured in the Plasma Membrane Microdomain. Left, Averaged FRET traces (18/3 for PDE4B WT, 35/3 for PDE4B KO, 24/3 for PDE4D WT and 39/3 for PDE4D KO) of adult mouse CMs, freshly isolated from PDE4B-KO, PDE4B-WT, PDE4D-KO and PDE4D-WT mice, harboring the caveolin-rich plasma membrane specific FRET biosensor, stimulated with 100 nM Isoprenaline (Iso), followed by 100 μM 3-Isobutyl-1-Methylxanthine (IBMX) and 10 μM Forskolin. Error bars are not shown for a clearer presentation. **Right**, Quantification of the FRET response due to changes in cAMP levels. Data of n/N experiments is presented as mean $\pm$ SEM with n, the number of measured cells isolated from N mice. ** - significant differences at $p<0.01$.

The results show an increased cAMP level in PDE4B-KO and PDE4D-KO cells during the steady state after adding Iso, which suggests that there is either a local decrease in cAMP hydrolysis or an increased cAMP synthesis.
To distinguish between these two possibilities, a second FRET experiment was performed to determine the rate of cAMP degradation, which should directly correlate with local microdomain specific PDE activity. To assure that this effect is not based on increased cAMP synthesis of the knockout CMs, Iso-prestimulated CMs were acutely treated with the β-AR antagonist propranolol. After a steady state was reached, this Iso-mediated cAMP synthesis was blocked by adding the β-AR antagonist propranolol at a high saturating concentration of 100 μM. Prestimulation with Iso leads to an accumulation of cAMP within the microdomain, while propranolol treatment leads to an instantaneous inhibition of cAMP production, after which microdomain specific relaxation kinetics can be measured. The half maximum degradation time $\tau_{1/2}$ was analyzed to determine a possible impact of PDE4B and PDE4D on the regulation of the plasma membrane microdomain. $\tau_{1/2}$ was calculated with an exponential decay equation using the Origin 8.5G software. The cAMP decay in the PDE4B-KO CMs was slowed down by ∼30% compared to the associated WT cells. In PDE4D-KO CMs, cAMP degradation time was prolonged by 37% (see Figure 3.4). Those results indicate that the increased cAMP accumulation in the plasma membrane microdomain, shown in Figure 3.3, is based on a decreased PDE activity and not on an increased cAMP synthesis.
Relative basal levels of cAMP were compared by performing the following FRET experiments. By adding IBMX and Forskolin to the CMs, a maximum accumulation of cAMP was reached. Activation of ACs by forskolin, leads to a maximum production rate of cAMP within the CMs, whereas IBMX leads to an inhibition of all PDEs, except of PDE8 and PDE9. In combination, this results in a maximum accumulation of cAMP within the CMs. This concentration is equal in both knockout and WT cells. By normalizing the FRET traces to the FRET ratio of the steady state after adding IBMX and forskolin, statements could be made about the basal levels of cAMP in the caveolin-rich plasma membrane. The results for the basal cAMP concentration in the caveolin-rich plasma membrane are shown in Figure 3.5. Although both PDEs of interest were shown to be active in regulating the caveolin-rich plasma membrane, basal cAMP levels were significantly increased only in PDE4B-KO CMs. PDE4D-KO CMs did not show any altered basal cAMP levels.

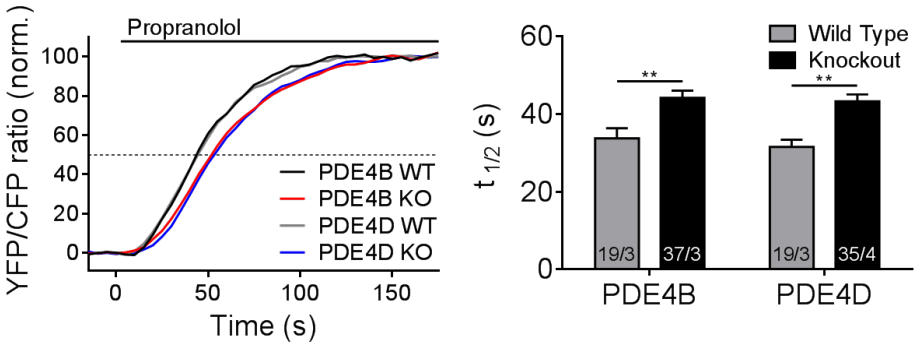

Figure 3.4: FRET Measurement of Local PDE Activity in the Plasma Membrane Microdomain. Left, Averaged FRET traces (19/3 for PDE4B WT, 37/3 for PDE4B KO, 19/3 for PDE4D WT and 35/4 for PDE4D KO) of adult mouse CMs, freshly isolated from PDE4B-KO, PDE4B-WT, PDE4D-KO and PDE4D-WT mice, harboring the caveolin-rich plasma membrane specific FRET biosensor, prestimulated with 100 nM Isoprenaline (Iso), followed by 100 μM propranolol. Decay of cAMP after adding propranolol was determined by calculating the half maximum degradation time $\tau_{1/2}$. Error bars are not shown for a clearer presentation. **Right**, Quantification of $\tau_{1/2}$. Data of n/N experiments is presented as mean ± SEM with n, the number of measured cells isolated from N mice. ** - significant differences at p<0.01.

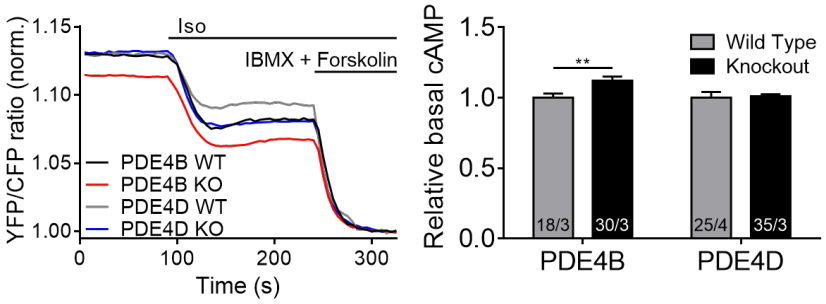

Figure 3.5: Basal cAMP Levels in the Plasma Membrane Microdomain. Left, Averaged FRET traces (18/3 for PDE4B WT, 30/3 for PDE4B KO, 25/4 for PDE4D WT and 35/3 for PDE4D KO) of adult mouse CMs, freshly isolated from PDE4B-KO, PDE4B-WT, PDE4D-KO and PDE4D-WT mice, harboring the caveolin-rich plasma membrane specific FRET biosensor, stimulated with 100 nM Isoprenaline (Iso), followed by 100 μM 3-Isobutyl-1-Methylxanthine (IBMX) and 10 μM Forskolin. FRET traces were normalized to the steady state FRET ratio after adding IBMX and Forskolin. Error bars are not shown for a clearer presentation. **Right**, Quantification of the relative basal cAMP levels. Relative basal cAMP levels were normalized to the respective WT. Data of n/N experiments is presented as mean ± SEM with n, the number of measured cells isolated from N mice. ** - significant differences at p<0.01.

3.4 Role of PDE4B and PDE4D on the SERCA2a Microdomain

3.4.1 FRET Microscopy

Transgenic mice that express the SERCA2a microdomain specific cAMP FRET bio E1-PLN were crossed with PDE4B-KO and PDE4D-KO mice. The SERCA2a specificity was achieved by fusing the Epac1-camps biosensor to PLN, the regulator of SERCA2a. The construct is expressed under the α-MHC promoter. Isolation of adult mouse CMs and FRET measurements were performed as described in sections 2.2.3 and 2.2.5.

To figure out whether PDE4B and PDE4D have an influence on the regulation of the cAMP signaling in the SERCA2a microdomain, freshly isolated adult mouse CMs were treated with 100 mM Iso, followed by 100 μM IBMX and 10 μM Forskolin. The ratio between the Iso mediated cAMP increase and the maximal cAMP response showed a significant impact of PDE4D ablation (see Figure 3.6). After Iso application, cAMP responses were not different in the SERCA2a microdomain of PDE4B-KO CMs, compared to littermate WT cells.

The increased cAMP accumulation could be based either on an increased AC activity or a reduced PDE activity. To figure out the relevant mechanism, CMs were treated with 100 μM of the β-AR antagonist propranolol after prestimulation with 100 nM Iso. Half maximum degradation time of cAMP $\tau_{1/2}$ was determined after adding propranolol (see Figure 3.7). cAMP degradation time was significantly prolonged in the PDE4D-KO CMs, whereas no difference could be detected in the PDE4B-KO cells. Increased cAMP levels, shown in Figure 3.6, are based on reduced PDE activity, which leads to the assumption that PDE4D is a critical regulator of the SERCA2a microdomain.

Although PDE4D was shown to be active in the regulation of signaling events in the SERCA2a microdomain, basal cAMP levels were changed neither in PDE4B-KO nor in PDE4D-KO CMs (see Figure 3.8). Changes in basal cAMP were assessed by performing FRET experiments in which 100 μM of the nonselective PDE inhibitor IBMX and 10 μM of the AC activator Forskolin were added to the CMs. Application of those two pharmacological compounds results in the maximum cAMP response in the SERCA2a microdomain, which should be equal in both knockout and WT CMs.

Normalized FRET traces showed no significant differences in cAMP levels in the SERCA2a microdomain for all genotypes (see Figure 3.8).

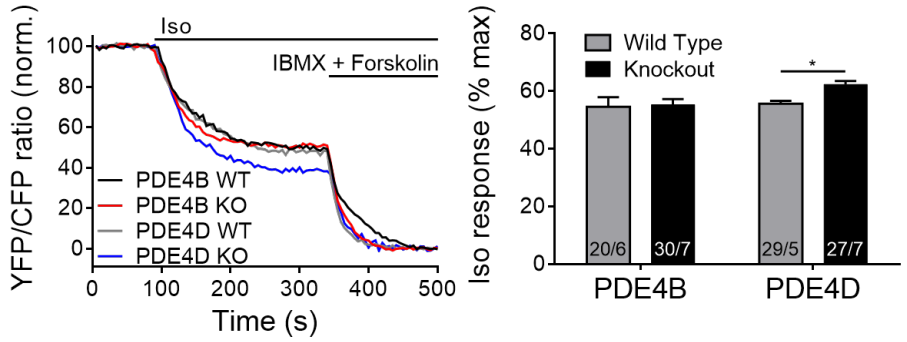

Figure 3.6: FRET Responses Measured in the SERCA2a Microdomain. **Left**, Averaged FRET traces (20/6 for PDE4B WT, 30/7 for PDE4B KO, 29/5 for PDE4D WT and 27/7 for PDE4D KO) of adult mouse CMs, freshly isolated from PDE4B-KO, PDE4B-WT, PDE4D-KO and PDE4D-WT mice, harboring the Sarco/Endoplasmic Reticulum Ca^{2+}-ATPase 2a (SERCA2a) microdomain specific FRET biosensor, stimulated with 100 nM Isoprenaline (Iso), followed by 100 μM 3-Isobutyl-1-Methylxanthine (IBMX) and 10 μM Forskolin. Error bars are not shown for a clearer presentation. **Right**, Quantification of the FRET response due to changes in cAMP levels. Data of n/N experiments is presented as mean ± SEM with n, the number of measured cells isolated from N mice. * - significant differences at p<0.05.

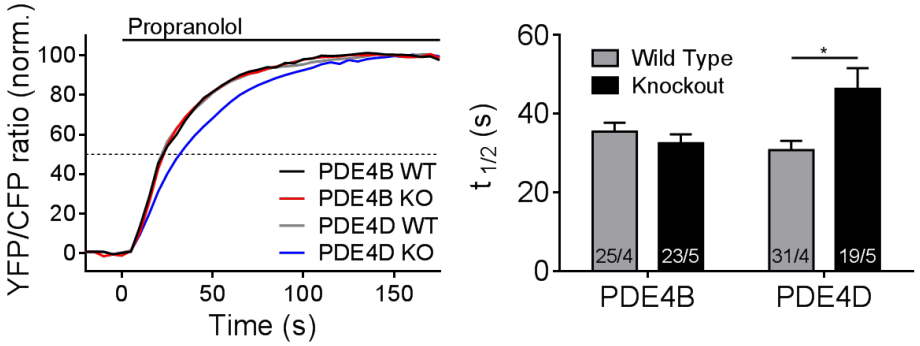

Figure 3.7: FRET Measurement of Local PDE Activity in the SERCA2a Microdomain. **Left**, Averaged FRET traces (25/4 for PDE4B WT, 23/5 for PDE4B KO, 31/4 for PDE4D WT and 19/5 for PDE4D KO) of adult mouse CMs, freshly isolated from PDE4B-KO, PDE4B-WT, PDE4D-KO and PDE4D-WT mice, harboring the SERCA2a microdomain specific FRET biosensor, prestimulated with 100 nM Isoprenaline (Iso), followed by 100 μM propranolol. Decay of cAMP after adding propranolol was determined by calculating the half maximum degradation time $\tau_{1/2}$. Error bars are not shown for a clearer presentation. **Right**, Quantification of $\tau_{1/2}$. Data of n/N experiments is presented as mean ± SEM with n, the number of measured cells isolated from N mice. * - significant differences at p<0.05.

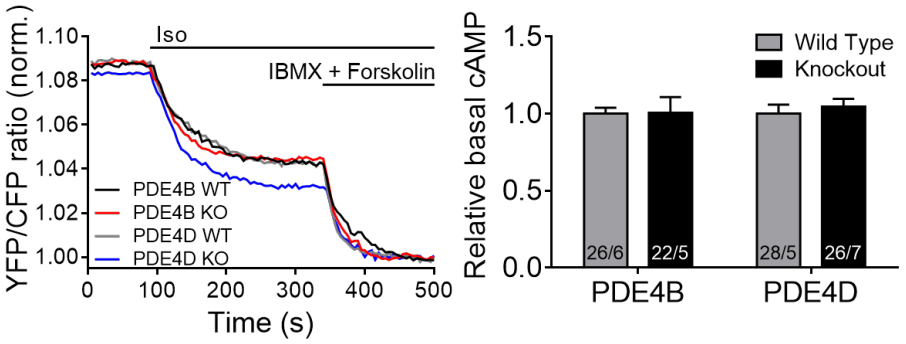

Figure 3.8: FRET SERCA2a Microdomain Basal cAMP. Left, Averaged FRET traces (26/6 for PDE4B WT, 22/5 for PDE4B KO, 28/5 for PDE4D WT and 26/7 for PDE4D KO) of adult mouse CMs, freshly isolated from PDE4B-KO, PDE4B-WT, PDE4D-KO and PDE4D-WT mice, harboring the SERCA2a microdomain specific FRET biosensor, stimulated with 100 nM Isoprenaline (Iso), followed by 100 μM 3-Isobutyl-1-Methylxanthine (IBMX) and 10 μM Forskolin. FRET traces were normalized to the steady state FRET ratio after adding IBMX and Forskolin. Error bars are not shown for a clearer presentation. **Right**, Quantification of the relative basal cAMP levels. Relative basal cAMP levels were normalized to the respective WT. Data of n/N experiments is presented as mean $\pm$ SEM with n, the number of measured cells isolated from N mice. Differences are statistically not significant.

3.4.2 Western Blot

Western Blot (WB) experiments were performed to verify the results obtained by FRET microscopy with a SERCA2a microdomain specific biosensor by analyzing specific PKA substrate phosphorylation. Whole hearts, harvested from adult PDE4B-KO, PDE4D-KO and associated WT mice, were Langendorff perfused according to the protocol in section 2.2.4. Whole hearts were stimulated with 100 nM Iso for 15 min. WB experiments were performed with whole heart lysates. Nitrocellulose membranes were probed for phosphorylated PLN at the phosphorylation site Ser-16, total PLN and GAPDH. PKA dependent phosphorylation of PLN was increased by 3.5 fold in PDE4D-KO hearts (see Figure 3.9). In contrast to hearts of PDE4D-KO mice, no altered phosphorylation levels could be detected in PDE4B-KO hearts. Comparing the PLN phosphorylation to GAPDH, the same result as to total PLN was obtained (see Figure 3.10).

Both FRET and WB experiments indicate that PDE4D is a critical regulator of the SERCA2a microdomain, whereas PDE4B ablation did not show any changes in SERCA2a microdomain specific PDE activity and PKA dependent PLN phosphorylation.

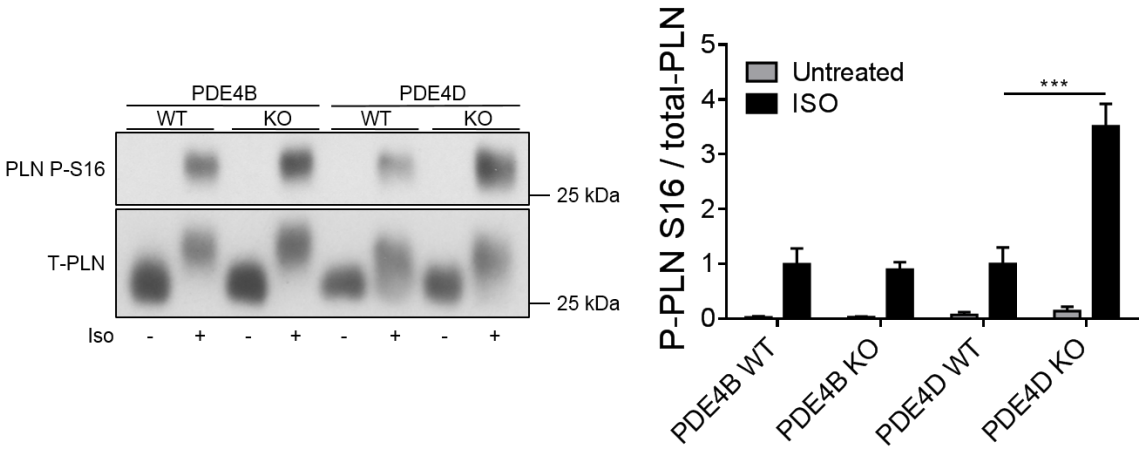

Figure 3.9: Western Blot Analysis of PKA Dependent PLN Phosphorylation in Iso-Stimulated Whole Hearts (PLN Ser-16) Compared to Total PLN. Left, Representative WB of PLN Ser-16 phosphorylation of Langendorff-perfused whole hearts, harvested from PDE4B-KO, PDE4B-WT, PDE4D-KO and PDE4B-WT mice. WB was performed using 20 μg of whole heart lysate per lane. Total Phospholamban (PLN) was used as a loading control after stripping the membrane. **Right**, Quantification of the WB experiments. n=5 samples per group. *** - significant differences at $p<0.001$.

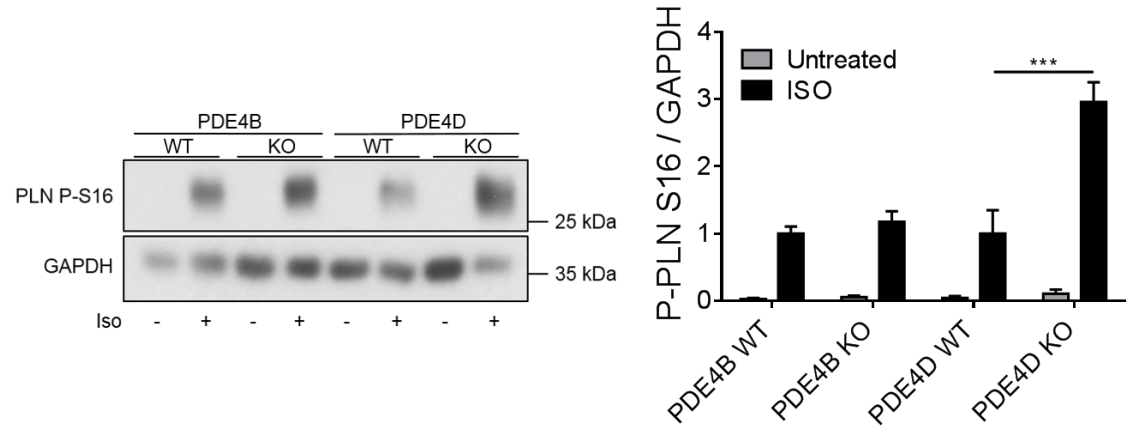

Figure 3.10: Western Blot Analysis of PKA Dependent PLN Phosphorylation in Iso-Stimulated Whole Hearts (PLN Ser-16) Compared to GAPDH. Left, Representative WB of PLN Ser-16 phosphorylation of Langendorff-perfused whole hearts, harvested from PDE4B-KO, PDE4B-WT, PDE4D-KO and PDE4B-WT mice. WB was performed using 20 μg of whole heart lysate per lane. GAPDH was used as a loading control. **Right**, Quantification of the WB experiments. n=5 samples per group. *** - significant differences at $p<0.001$.

3.5 Contribution of PDE4B and PDE4D on the Cardiac RyR2 Microdomain

3.5.1 FRET Microscopy

To investigate the impact of PDE4B and PDE4D on the cAMP dynamics around the cardiac RyR2, PDE4B and PDE4D deficient mice were crossed with mice expressing the highly sensitive cAMP specific FRET biosensor E1-JNC. The CM specific expression of this FRET sensor is achieved by the α-MHC promoter. Isolation of adult mouse CMs and FRET microscopy were performed as described in sections 2.2.3 and 2.2.5.

The influence of PDE4B and PDE4D on the microdomain formed around the intracellular regulator for Ca^{2+} release from the SR was tested by performing FRET microscopy experiments. CMs were pharmacologically stimulated with 100 nM of the β-AR agonist Iso, followed by 100 μM of IBMX and 10 μM Forskolin.

Unexpectedly, PDE4B-KO CMs showed a significantly increased accumulation of cAMP compared to the maximal cAMP response (see Figure 3.11). This increase is based on a reduced PDE activity within the RyR2 microdomain, proved by a significantly prolonged degradation time in propranolol treated PDE4B-KO CMs (see Figure 3.12). An impact on altered cAMP dynamics in PDE4D-KO CMs could be detected in neither of the two experiments.

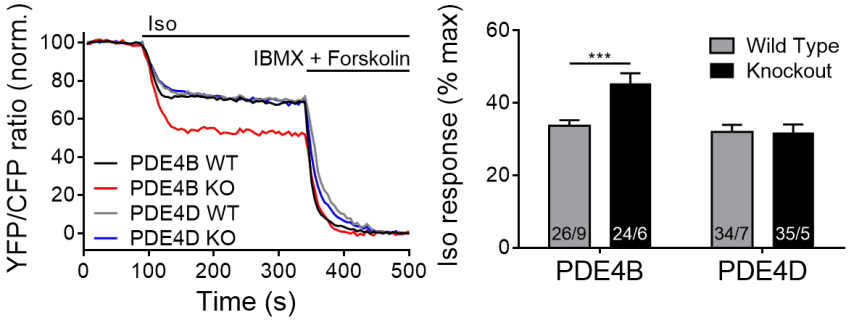

Figure 3.11: FRET Responses Measured in the RyR2 Microdomain. **Left**, Averaged FRET traces (26/9 for PDE4B WT, 24/6 for PDE4B KO, 34/7 for PDE4D WT and 35/5 for PDE4D KO) of adult mouse CMs, freshly isolated from PDE4B-KO, PDE4B-WT, PDE4D-KO and PDE4D-WT mice, harboring the Ryanodine Receptor Type 2 (RyR2) microdomain specific FRET biosensor, stimulated with 100 nM Isoprenaline (Iso), followed by 100 μM 3-Isobutyl-1-Methylxanthine (IBMX) and 10 μM Forskolin. Error bars are not shown for a clearer presentation. **Right**, Quantification of the FRET response due to changes in cAMP levels. Data of n/N experiments is presented as mean $\pm$ SEM with n, the number of measured cells isolated from N mice. *** - significant differences at $p<0.001$.

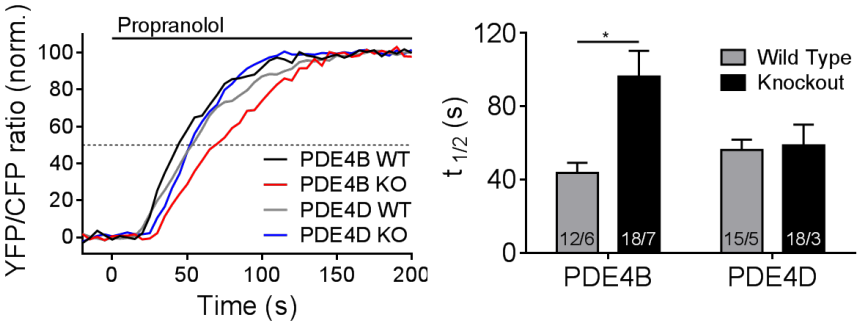

Figure 3.12: FRET Measurement of Local PDE Activity in the RyR2 Microdomain. Left, Averaged FRET traces (12/6 for PDE4B WT, 18/7 for PDE4B KO, 15/5 for PDE4D WT and 18/3 for PDE4D KO) of adult mouse CMs, freshly isolated from PDE4B-KO, PDE4B-WT, PDE4D-KO and PDE4D-WT mice, harboring the RyR2 microdomain specific FRET biosensor, prestimulated with 100 nM Isoprenaline (Iso), followed by 100 μM propranolol. Decay of cAMP after adding propranolol was determined by calculating the half maximum degradation time $\tau_{1/2}$. Error bars are not shown for a clearer presentation. **Right**, Quantification of $\tau_{1/2}$. Data of n/N experiments is presented as mean ± SEM with n, the number of measured cells isolated from N mice. * - significant differences at p<0.05.

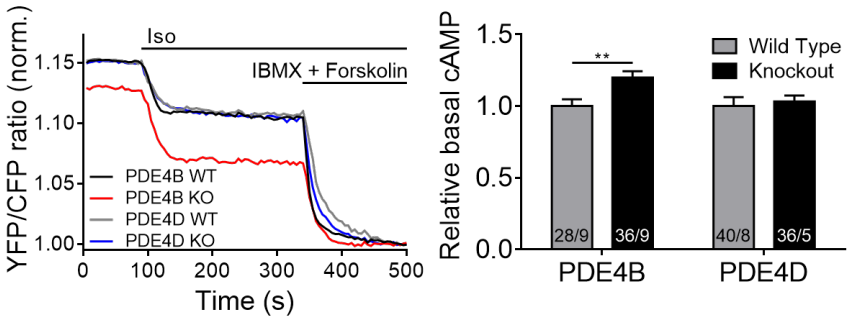

Figure 3.13: Basal cAMP Levels in the RyR2 Microdomain. Left, Averaged FRET traces (28/9 for PDE4B WT, 36/9 for PDE4B KO, 40/8 for PDE4D WT and 36/5 for PDE4D KO) of adult mouse CMs, freshly isolated from PDE4B-KO, PDE4B-WT, PDE4D-KO and PDE4D-WT mice, harboring the RyR2 microdomain specific FRET biosensor, stimulated with 100 nM Isoprenaline (Iso), followed by 100 μM 3-Isobutyl-1-Methylxanthine (IBMX) and 10 μM Forskolin. FRET traces were normalized to the steady state FRET ratio after adding IBMX and Forskolin. Error bars are not shown for a clearer presentation. **Right**, Quantification of the relative basal cAMP levels. Relative basal cAMP levels were normalized to the respective WT. Data of n/N experiments is presented as mean ± SEM with n, the number of measured cells isolated from N mice. ** - significant differences at p<0.01.

Relative basal levels of cAMP in the RyR2 microdomain were determined by normalizing the FRET traces to the steady state after adding IBMX and Forskolin. Increased levels of cAMP could be detected in PDE4B-KO CMs, whereas PDE4D-KO cells did not show any altered cAMP concentrations at a basal state (see Figure 3.13).

3.5.2 FRET with Detubulated Adult Mouse Cardiomyocytes

The FRET experiments shown in section 3.5.1 indicate an interaction between PDE4B with the cardiac RyR2. To determine whether PDE4B is directly or indirectly involved in the RyR2 microdomain regulation, FRET experiments were performed with freshly isolated adult mouse CMs after artificially formamide-induced detubulation. An indirect regulation of the RyR2 microdomain could be based on the size of the junctional gap of approximately 15 nm, which results in a detection of the LTCC-associated PDE4B in the RyR2 complex.
The FRET experiments shown in Figure 3.14 were performed after osmotic shock induced detubulation with 1.5 M formamide. Similar to non formamide treated cells (see Figure 3.11) ratio between the Iso-induced cAMP accumulation to the maximum cAMP response was significantly increased in PDE4B-KO CMs, whereas no alterations in cAMP levels could be detected in PDE4D deficient CMs.

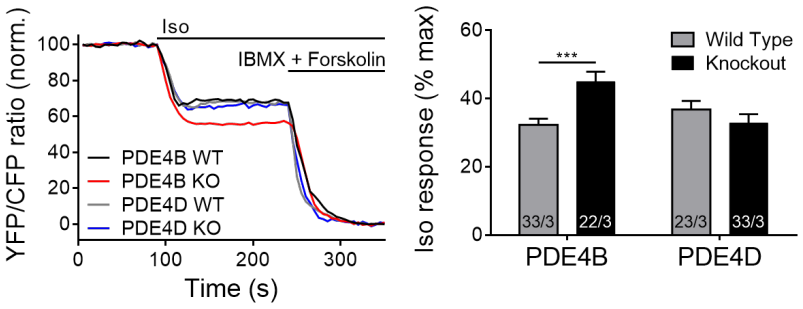

Figure 3.14: FRET Responses Measured in the RyR2 Microdomain in Detubulated Cardiomyocytes. **Left**, Averaged FRET traces (33/3 for PDE4B WT, 22/3 for PDE4B KO, 18/2 for PDE4D WT and 33/3 for PDE4D KO) of adult mouse CMs, freshly isolated from PDE4B-KO, PDE4B-WT, PDE4D-KO and PDE4D-WT mice, harboring the Ryanodine Receptor Type 2 (RyR2) microdomain specific FRET biosensor, stimulated with 100 nM Isoprenaline (Iso), followed by 100 μM 3-Isobutyl-1-Methylxanthine (IBMX) and 10 μM Forskolin. Cardiomyocytes were chemically detubulated by incubation with 1.5 M formamide for 15 min. Error bars are not shown for a clearer presentation. **Right**, Quantification of the FRET response due to changes in cAMP levels. Data of n/N experiments is presented as mean ± SEM with n, the number of measured cells isolated from N mice. *** - significant differences at p<0.001.

Determination of the PDE activity in the RyR2 microdomain of detubulated CMs showed a significantly decreased local PDE effect in PDE4B-KO CMs. PDE4D-KO CMs, however, showed no alterations in PDE activity as compared to the respective WT CMs (see Figure 3.15).

In conclusion, the results shown in sections 3.5.1 and 3.5.2 suggest a T-tubule independent regulation of the cAMP signaling in the RyR2 microdomain. This could be a hint for a direct interaction between PDE4B and the cardiac RyR2 complex.

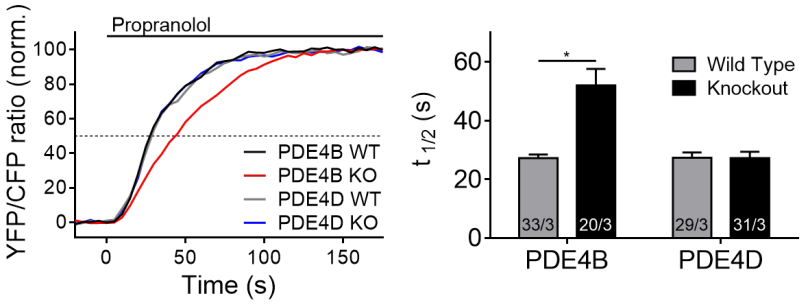

Figure 3.15: FRET Measurement of Local PDE Activity in the RyR2 Microdomain in Detubulated Cardiomyocytes. Left, Averaged FRET traces (30/2 for PDE4B WT, 20/3 for PDE4B KO, 29/3 for PDE4D WT and 29/2 for PDE4D KO) of adult mouse CMs, freshly isolated from PDE4B-KO, PDE4B-WT, PDE4D-KO and PDE4D-WT mice, harboring the RyR2 microdomain specific FRET biosensor, prestimulated with 100 nM Isoprenaline (Iso), followed by 100 μM propranolol. Decay of cAMP after adding propranolol was determined by calculating the half maxiumum degradation time $\tau_{1/2}$. Cardiomyocytes were chemically detubulated by incubation with 1.5 M formamide for 15 min. Error bars are not shown for a clearer presentation. **Right**, Quantification of $\tau_{1/2}$. Data of n/N experiments is presented as mean $\pm$ SEM with n, the number of measured cells isolated from N mice. * - significant differences at $p<0.05$.

3.5.3 Western Blot

WB experiments were performed to gain a deeper insight into the involvement of PDE4B and PDE4D in the regulation of the RyR2 microdomain. Whole hearts, harvested from adult PDE4B-KO, PDE4D-KO and associated WT mice, were Langendorff perfused according to the protocol in section 2.2.4 and were stimulated with 100 nM Iso for 15 min. WB experiments were performed with whole heart lysates. Nitrocellulose membranes were probed for phosphorylated RyR2 (at the phosphorylation site Ser-2808) and for total RyR2.
Langendorff-perfused PDE4B-KO whole mouse hearts stimulated with Iso showed a significantly increased RyR2 phosphorylation at Ser-2808, compared the the PDE4B-WT hearts (see Figure 3.16).
No statistical differences could be detected in the samples from PDE4D deficient mice.

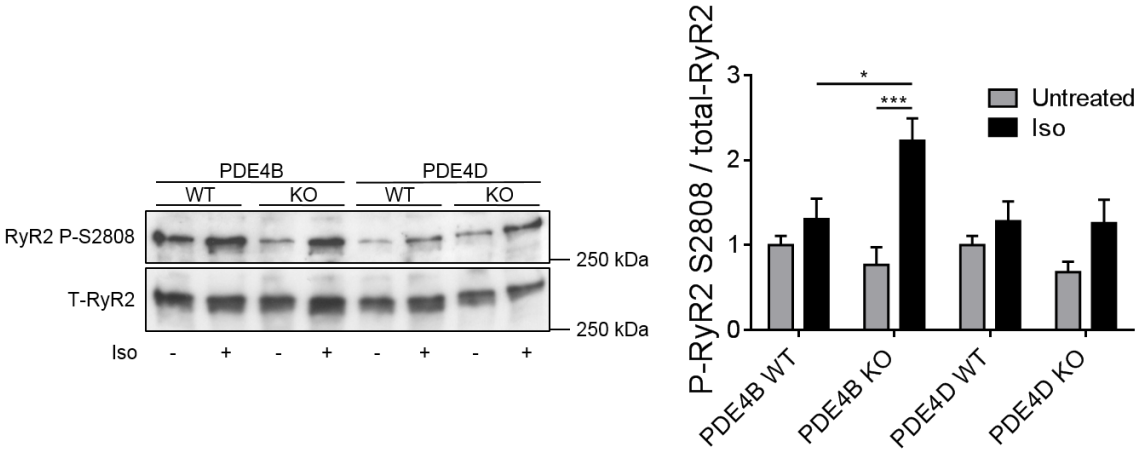

Figure 3.16: Western Blot Analysis of Iso-Stimulated Whole Hearts (RyR2 Ser-2808). Left, Representative WB of RyR2 Ser-2808 phosphorylation of Langendorff-perfused whole hearts harvested from PDE4B-KO, PDE4B-WT, PDE4D-KO and PDE4B-WT mice. WB was performed using 45 μg of whole heart lysate. Total Ryanodine Receptor Type 2 (RyR2) was used as a loading control after stripping the membrane. **Right**, Quantification of the WB experiments. n=5 samples per group. *, *** - significant differences at $p<0.05$, $p<0.001$.

3.5.4 Single Cell Contractility Measurements

Effects of PDE4B and PDE4D on the arrhythmia susceptibility were determined by quantifying extra beats of paced single CMs at 0.5 Hz. Isolated CMs from PDE4B and PDE4D deficient mice as well as the respective WT littermates were stimulated with 100 nM Iso. Extra beats were counted during a period of 60 s right after the maximum change of the sarcomeric length was reached. Representative traces for

the contractility measurements are shown in Figure 3.18 and Figure 3.19.
Almost every electrically triggered contraction was followed by an additional spontaneous contraction in PDE4B-KO CMs after stimulation with 100 nM Iso (see Figure 3.17), producing significantly more extra beats compared to Iso-stimulated PDE4B-WT CMs and untreated PDE4B-KO CMs. PDE4D-KO CM showed significantly less extra beats after Iso stimulation compared to PDE4B-KO CMs, but significantly more compared to Iso treated PDE4D-WT CMs and untreated PDE4D-KO CMs.
All extra beats occurred only after the sarcomeric length of the CMs reached the baseline. Therefore, it was reminiscent of DADs, suggesting a possible involvement of intracellular Ca^{2+} release through the RyR2.

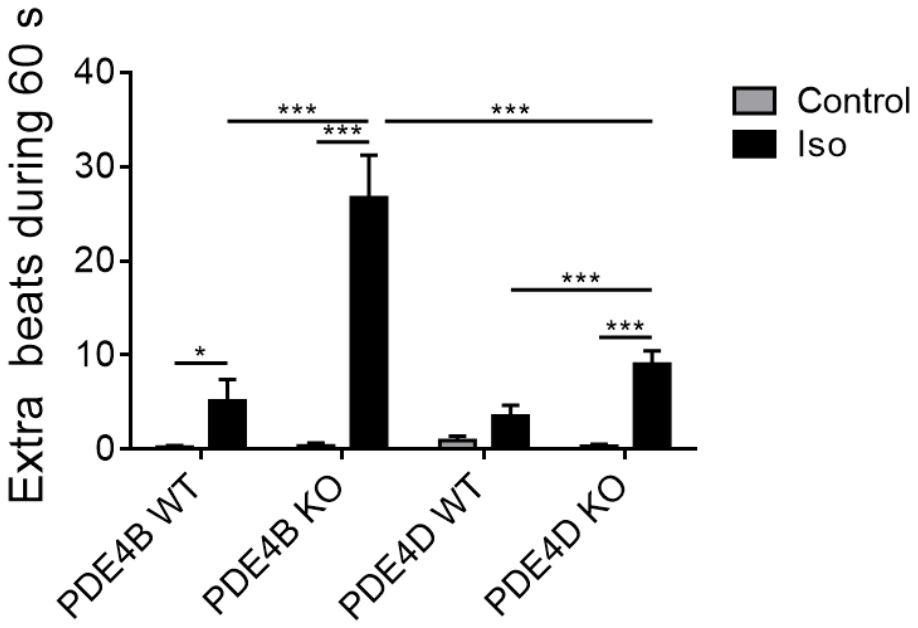

Figure 3.17: Arrhythmia Susceptibility in Iso stimulated WT and PDE4B and PDE4D Deficient Cardiomyocytes. Evaluation of extra beats during 60 s of contractility measurements of untreated and Iso-stimulated (100 nM) CMs isolated from PDE4B-WT, PDE4B-KO, PDE4D-WT and PDE4D-KO CMs. Data of 20-35 CMs isolated from 3-4 mice are presented as mean ± SEM. *, *** - significant differences at $p<0.05$ and $p<0.001$, respectively.

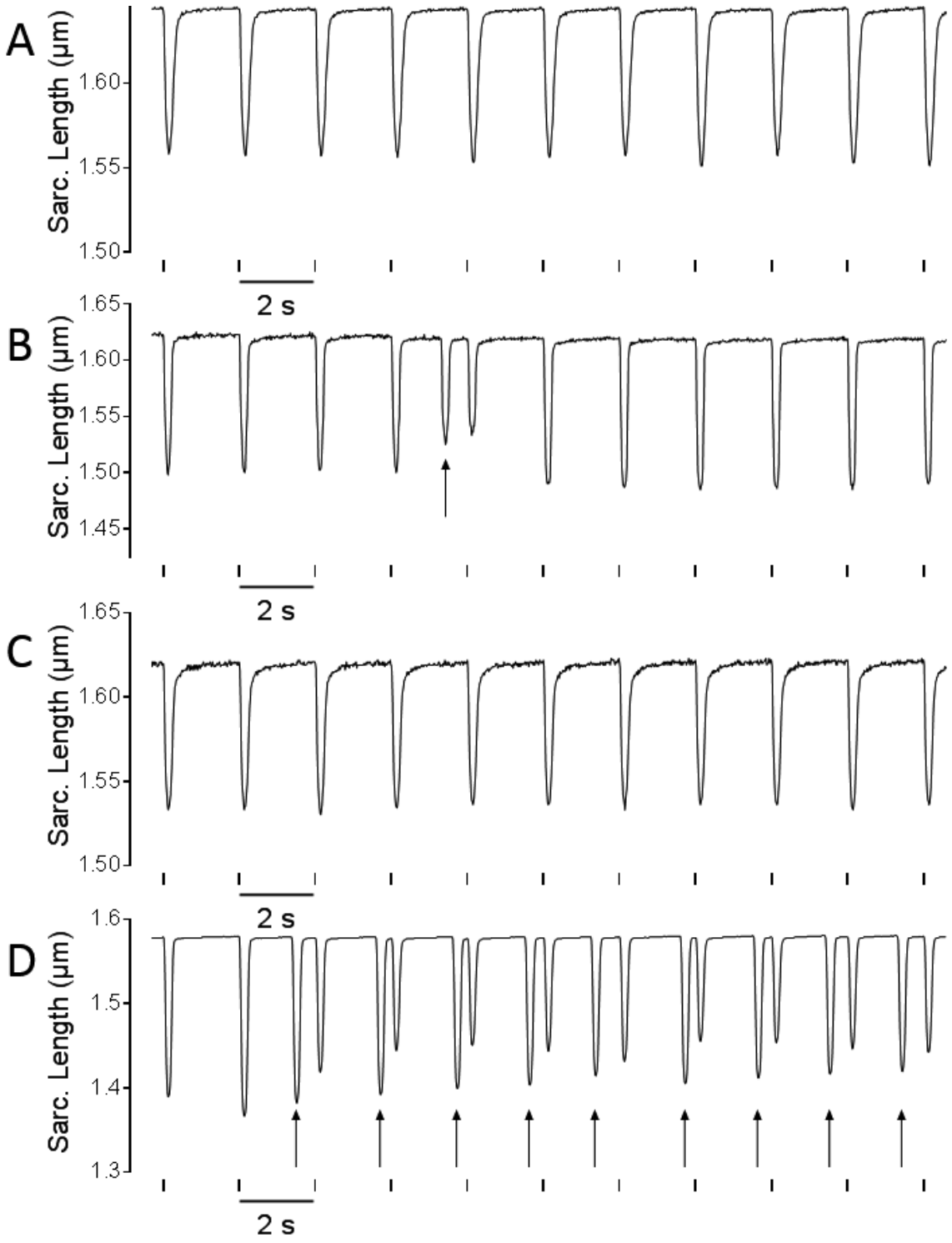

Figure 3.18: Contractility Measurements of PDE4B-WT and PDE4B-KO Cardiomyocytes Representative traces of contractility measurements of untreated and Iso-stimulated (100 nM) CMs of PDE4B-WT and PDE4B-KO CMs. Single CMs were paced for 4 ms at 0.5 Hz and 15.0 V. Extra beats are marked with an arrow. **A** Untreated PDE4B-WT CM, **B** Iso treated PDE4B-WT CM, **C** untreated PDE4B-KO CM and **D** Iso treated PDE4B-KO CM.

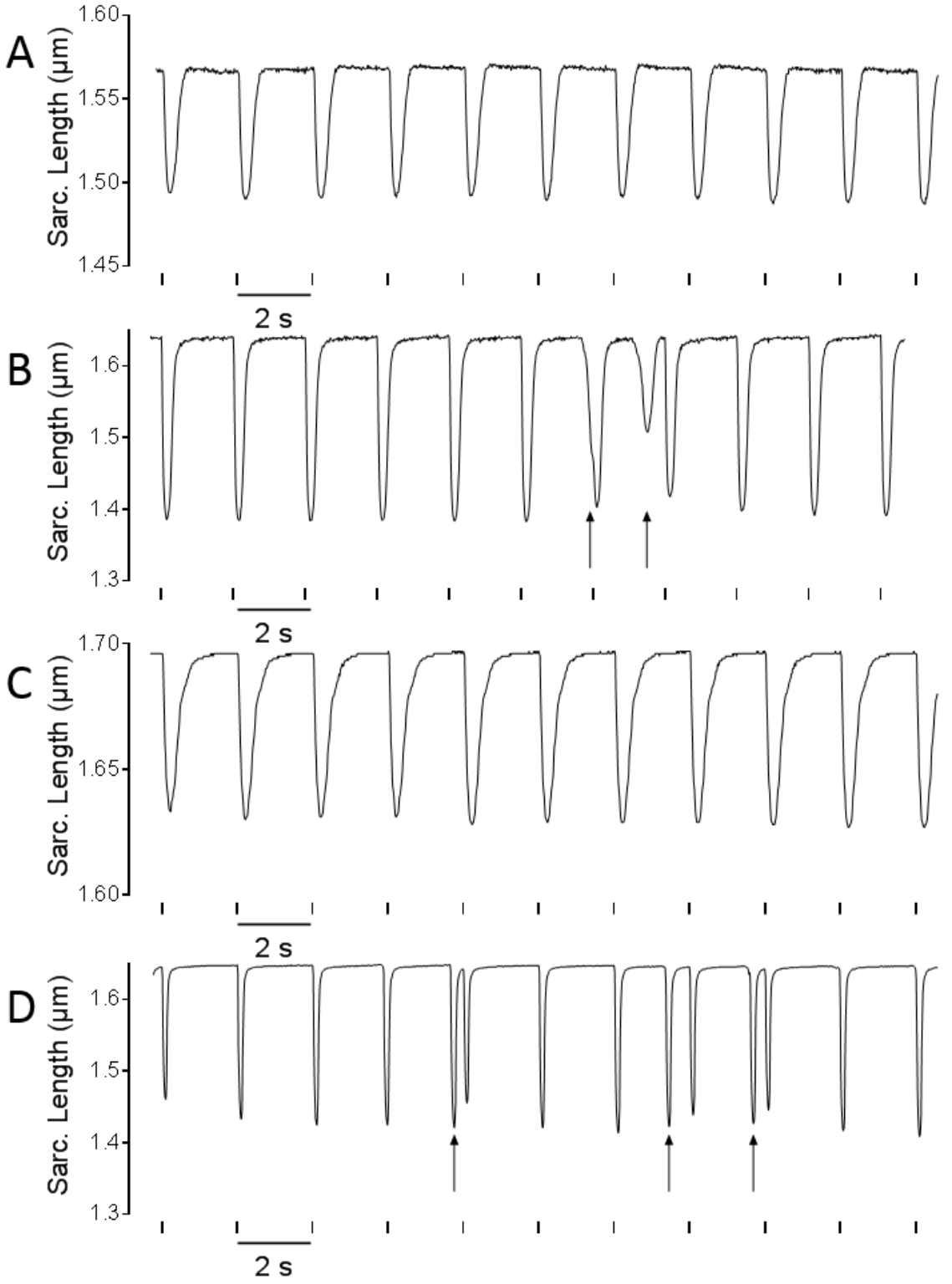

Figure 3.19: Contractility Measurements of PDE4D-WT and PDE4D-KO Cardiomyocytes Representative traces of contractility measurements of untreated and Iso-stimulated (100 nM) CMs of PDE4D-WT and PDE4D-KO CMs. Single CMs were paced for 4 ms at 0.5 Hz and 15.0 V. Extra beats are marked with an arrow. **A** Untreated PDE4D-WT CM, **B** Iso treated PDE4B-WT CM, **C** untreated PDE4D-KO CM and **D** Iso treated PDE4D-KO CM.

3.5.5 STED Microscopy

Stimulated Emission Depletion (STED) microscopy was performed to determine the subcellular localization of PDE4B by specific immunofluorescence staining. It was examined by STED microscopy whether or not PDE4B and RyR2 colocalize in adult mouse CMs. Confocal and STED microscopy images of PDE4B and RyR2 stained CMs are shown in Figure 3.21. The evaluation of the colocalization was limited to the pixel size of the recorded STED images. One pixel represents 20 nm, which is approximately the distance between the LTCC and the RyR2, which makes it impossible to distinguish between the LTCC-associated PDE4B and the PDE4B that might be attached to the RyR2 complex as two separate peaks.
The colocalization was analyzed along the z-lines and the distribution between direct overlapping and shifted overlapping by 20-60 nm was quantified (see Figure 3.20). 84 z-lines of 11 individual cells were analyzed. 48.8% of the analyzed z-lines showed a direct overlap between the fluorescence peak of PDE4B and RyR2, 51.2% of the analyzed peaks showed a shift in fluorescence peak by 1 or two pixels. The distribution of almost 50% to 50% suggests that PDE4B could be present in both LTCC and RyR2 microdomains.

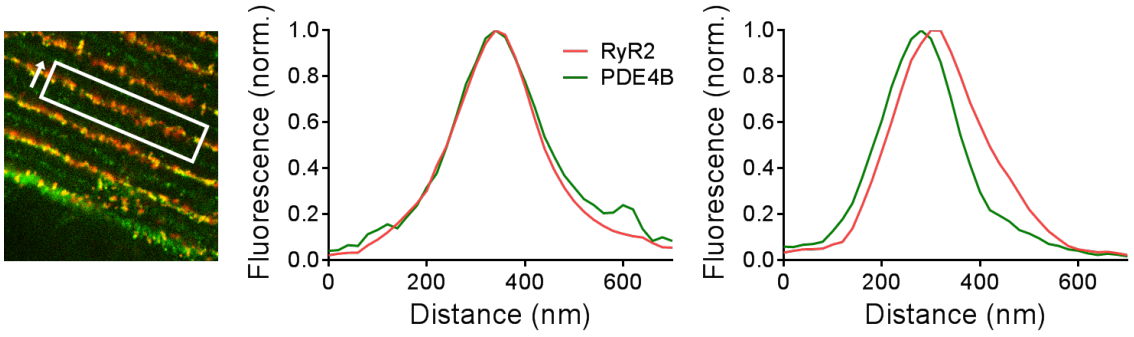

Figure 3.20: Evaluation of Co-localization of PDE4B and RyR2. Left, representative region of interest for calculating the fluorescence intensity including the direction of measurement. **Middle**, Representative trace of direct colocalization of PDE4B and RyR2. **Right**, Representative trace of slightly shifted distribution of PDE4B and RyR2.

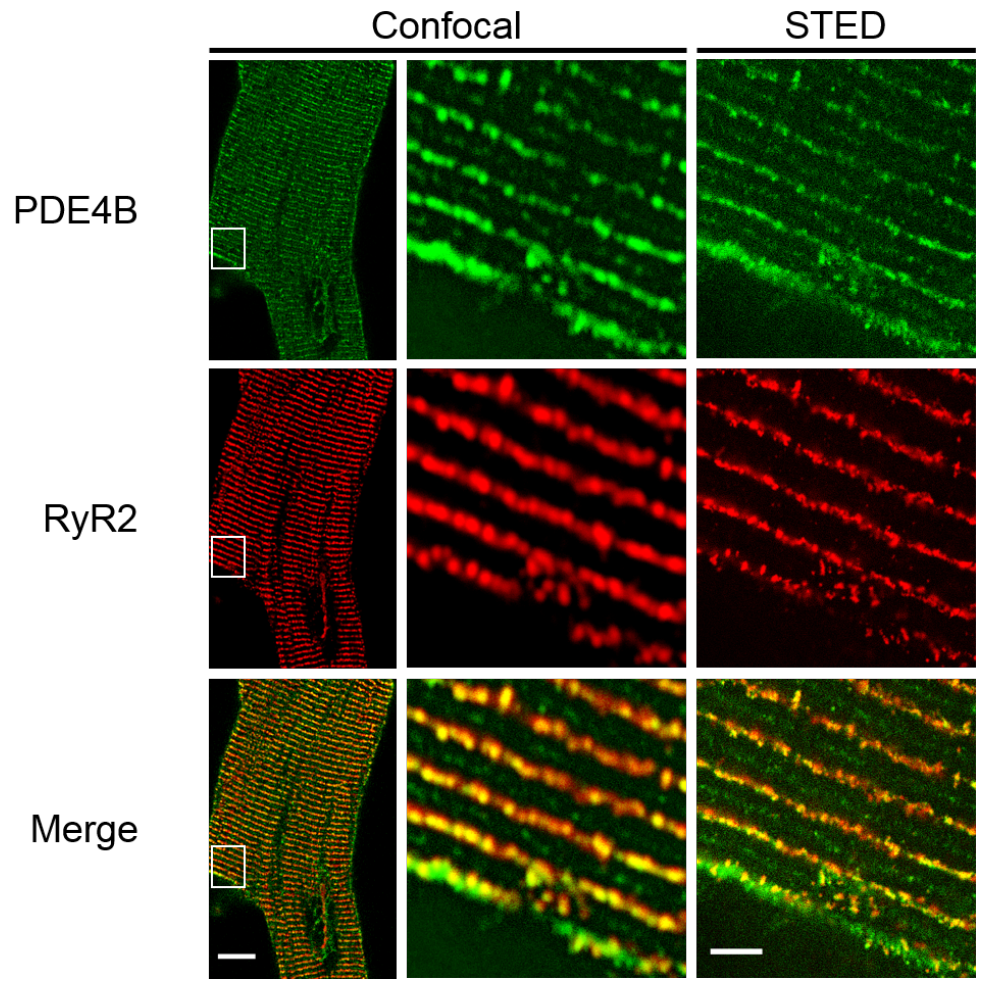

Figure 3.21: Localization of PDE4B and RyR2 in Adult Mouse Cardiomyocytes. Confocal- and Stimulated Emission Depletion (STED)- microscopy images of a Cardiomyocyte (CM) isolated from an adult WT mouse stained with anti-PDE4B and anti-RyR2 antibody. Scale bar: 10 μm for whole cell image, 2 μm for STED image.

3.6 cAMP Measurements by ELISA

As described in sections 3.3 and 3.5.1, the genetic ablation of PDE4B was associated with an increased concentration of basal cAMP within the caveolin-rich plasma membrane and RyR2 microdomain. To distinguish whether this increase is microdomain specific, ELISA experiments were performed to measure whole cell cAMP concentrations at a basal state. Global cAMP concentration in CMs isolated of adult WT mice as well as PDE4B and PDE4D deficient mice were not significantly altered (see Figure 3.22).

Those results indicate that the increased basal cAMP levels in PDE4B deficient mice detected by FRET experiments are most likely based on an altered microdomain regulation and not on a global cell cAMP content.

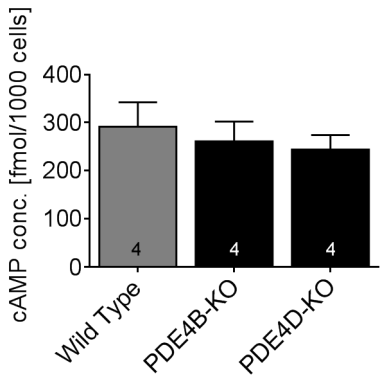

Figure 3.22: Quantification of Basal Whole Cell cAMP Concentrations. Quantification of basal cAMP concentrations of WT, PDE4B-KO and PDE4D-KO adult mouse CMs by ELISA. Total cAMP levels were determined by using 30,000 CMs. WT cAMP concentrations were quantified from two PDE4B-WT and two PDE4D-WT mice. Data of 4 individual animals is presented as mean ± SEM. No statistical differences were detected between the individual groups.

4. Discussion

The present study aimed to uncover the involvement of PDE4B and PDE4D in the regulation of cAMP signaling events in Ca^{2+} handling microdomains of adult mouse CMs.

Alterations in the regulation of CM specific microdomains have been shown to be associated with several heart diseases like arrhythmia and heart failure, especially regarding PDE expression and localization. To gain a deeper insight in the regulation of microdomains, it is necessary to have powerful tools to uncover molecular mechanisms that regulate the compartmentation of the ubiquitous second messenger cAMP. Classical biochemical techniques require thousands of cells to analyze a limited number of time points without any spatial resolution at a cellular level. FRET microscopy can overcome this limitation by enabling real-time monitoring of signaling events in living cells and tissues with a high temporal resolution.

The development of targeted versions of FRET biosensors led to a better understanding of the regulation of microdomains by enabling a high spatial resolution. Many studies that use targeted FRET biosensors were performed with virus transduced HEK293A cells, neonatal CMs or adult rat CMs [245]. Transgenic mouse models expressing targeted FRET biosensors have the great advantage that cAMP dynamics can be determined in adult CMs without the need of a long term cultivation. Further, FRET microscopy enables the use of an intact living system, such as living CMs or even whole hearts [285].

In mice, PDE4D deficiency was associated with growth retardation, reduced viability and reduced female fertility, which demonstrates a critical role of this enzyme family in the regulation of cell homeostasis [279]. Regarding altered cardio related parameters, PDE4D-KO mice are associated with a hyperphosphorylated RyR2, an increased sensitivity to exercise-induced arrhythmia and development of a late-onset dilated cardiomyopathy [142]. By sacrificing mice at the age of 8-20 weeks in the present work, age dependent cardiomyopathy was not yet pronounced.

PDE4B-KO mice appeared normal and exhibited no overt morphological abnormalities [278].

Reported cardiac specific phenotypes in PDE4D deficient mice could neither not be confirmed in mice that have been used for this work nor are they related with altered cAMP signaling events in the RyR2 microdomain. Thus, PDE4B and PDE4D

deficient mice seem to be a suitable animal model to investigate the specific impact of PDE4B and PDE4D on the regulation of cAMP signaling in Ca^{2+} microdomains. To rule out possible influences of fluctuations in the genetic background, results of knockout animals were always compared to associated WT littermates.

4.1 Maintained PDE Expression

It might be assumed that PDE4B and PDE4D deficiency would result in an altered expression of other major cAMP specific PDEs like PDE2A, PDE3A, PDE4A or PDE4B, which explains the maintained cAMP concentrations in PDE4D-KO CMs. However, WB experiments using specific antibodies showed unaltered expression of the mentioned PDEs (see Figure 3.2).
The conserved expression of PDE2A, PDE3A, PDE4A, PDE4B and PDE4D as well as the maintained whole cell basal cAMP levels make mice with a global deficiency of PDE4B and PDE4D a suitable model for analyzing the impact of those PDE4 subfamilies on the cAMP signaling in adult mouse CMs.

4.2 Effect of PDE4B and PDE4D on the Caveolin-Rich Plasma Membrane Microdomain

PDE4B and PDE4D deficient mice were crossed with mice expressing the highly sensitive pm-Epac1 FRET biosensor targeted to the caveolin-rich plasma membrane. Although not directly localized in the LTCC microdomain, this sensor is a suitable model to uncover cAMP dynamics in the LTCC complex due to the close proximity to the Ca^{2+} channels in the caveolin-rich plasma membrane [160].
cAMP responses after Iso treatment were significantly increased compared to the maximum cAMP responses in both PDE4B and PDE4D deficient mice. IBMX was used as a non selective PDE inhibitor, although it was shown to be insensitive to the cAMP degrading PDE8 [113]. Western Blot experiments showed no alterations in PDE8A expression in PDE4B-KO and PDE4D-KO mice (data not shown). Thus, IBMX can be used without any restrictions.
To figure out whether the increased cAMP accumulation was based on a decreased PDE activity or an increased cAMP synthesis, Iso-prestimulated CMs were treated with 100 μM propranolol, a non selective β-AR antagonist. Iso prestimulation leads to an accumulation of cAMP within the microdomain. Propranolol prevents cAMP synthesis, resulting in a PDE dependent hydrolysis of cAMP. cAMP diffusion out of the microdomain into the cytoplasm is negligible since the rate of diffusion is expected to be equal in both WT and knockout CMs. Nevertheless, absolute $\tau_{1/2}$ values, obtained with different localized FRET biosensors, cannot be compared since

the rate of spatial biosensor inhibition differs between individual microdomains of interest.
Prolonged cAMP degradation time in both knockouts of interest lead to the conclusion that the increased cAMP accumulation is based on a decrease in PDE activity. Obtained results by FRET microscopy go along with the previous finding, that both PDE4B and PDE4D are associated with the LTCC. PDE4B was already shown to be associated within the cardiac LTCC complex by regulating Ca^{2+} current und thus being protective against ventricular arrhythmia [147]. PDE4D is as well part of the LTCC, whereas it does not seem to have any impact on the regulation of the Ca^{2+} current [148]. It is suggested that PDE4B and PDE4D regulate cardiac ECC by different mechanisms. Although PDE4D is not involved in regulating the LTCC-associated Ca^{2+} current, the results suggest an equal influence of PDE4B and PDE4D on the regulation of the cAMP dynamics in this compartment.
Experiments performed in neonatal PDE4B-KO mouse CMs which express a plasma membrane specific FRET based biosensor revealed in the same results as in adult mouse CMs, as shown in this work [147]. This is remarkable since T-tubules are absent in neonatal CMs [286]. Thus, a relocalization upon T-tubule formation does not seem to affect the impact of PDEs on the LTCC complex regulation. This suggests that CM maturation goes along with a relocalization of the LTCC complex, whereas the regulation seems to be maintained.

4.3 Impact of PDE4B and PDE4D on the SERCA2a Microdomain

4.3.1 FRET Microscopy

FRET experiments performed with PDE4B-KO and PDE4D-KO CMs expressing the highly cAMP specific Epac1-camps biosensor fused to PLN, the negatively regulator of SERCA2a, showed no altered signaling events in PDE4B deficient adult mouse CMs. This goes along with previous knowledge of the SERCA2a microdomain regulation. Even in the absence of PDE4D, cAMP levels keep decreasing after propranolol was added to Iso-prestimulated CMs. This is most likely based on the impact of PDE3A on the regulation of the SERCA2a microdomain. Further, cAMP is partially diffusing out of the microdomain. Iso-induced cAMP accumulation in the SERCA2a microdomain was significantly increased in PDE4D deficient mice. FRET experiments with the non-selective beta blocker propranolol uncovered that this accumulation is based on a reduced PDE activity in this complex.
To figure out the amount of diffusing cAMP compared to PDE degraded cAMP, CMs could be treated with Iso and IBMX, to inhibit the activity of all PDEs except

of PDE8 and PDE9 and then apply propranolol. In this case, the decay of cAMP should be based only on diffusion.
These data indicate that in the SERCA2a microdomain, PDE4D but not PDE4B is responsible for suppressing the cAMP effects on PKA dependent Ca^{2+} cycling [198, 287].

4.3.2 Western Blot

According to FRET experiments with a SERCA2a microdomain specific FRET biosensor, showed a significant impact of PDE4D on the cAMP signaling could be postulated. WB experiments were performed to determine whether PDE4D is also affecting downstream events in the SERCA2a complex. This was analyzed by looking at the PLN Ser-16 phosphorylation in Iso-stimulated Langendorff-perfused whole mouse hearts. As expected, Iso-stimulated whole hearts showed a significantly increased PLN phosphorylation.
Widely used primary antibodies for WB application that detect total PLN correspond to a region within amino acids 9-19, including Ser-16 and Thr-17. Thus, an increased PLN phosphorylation goes along with a reduced signal for total PLN. This problem has been bypassed by using a total PLN antibody, specific for amino acids 1-11, which detects a phosphorylation independently of total PLN. Comparing Ser-16 phosphorylation of PLN either to total PLN or GAPDH led to the same results. Hence, the primary antibody used for total PLN detection by WB delivers trustworthy results.
Collectively all findings of this work go along with the fact that PDE4D is responsible for the regulation of PLN phosphorylation [198, 199].

4.4 Impact of PDE4B and PDE4D on the RyR2 Microdomain

4.4.1 FRET Microscopy

cAMP dynamics in the RyR2 complex were analyzed by utilizing the highly sensitive cAMP FRET biosensor E1-JNC. This sensor was generated by fusing Epac1-camps to JNC, a protein which directly interacts with the RyR2.
A previous study mentioned that the only PDE isoform present in the RyR2 microdomain belongs to the PDE4D family, namely PDE4D3 [142]. Surprisingly, FRET experiments did not show any altered cAMP signaling in PDE4D deficient CMs. However, PDE4B-KO CMs showed an increased Iso-induced cAMP accumulation in the RyR2 microdomain that was based on a reduced PDE activity. cAMP levels kept on decreasing after propranolol application, even in the absence of PDE4B.

This indicates a cAMP diffusion out of the microdomain or an involvement of other PDEs on the cAMP dynamics in the RyR2 complex.
The PDE4B effect, measured in the RyR2 microdomain, could be based either on a direct or indirect interaction. An indirect interaction could be du to a close proximity of the LTCC and the RyR2 of ∼15 nm. Thus, the detected impact of PDE4B could be based on the LTCC-associated PDE4B overcoming the junctional gap.

4.4.2 FRET with Detubulated Adult Mouse Cardiomyocytes

To figure out whether PDE4B is directly attached to the RyR2 complex or not, FRET experiments were performed with detubulated CMs. This was achieved by a 1.5 M formamide-induced osmotic shock. The detubulation process occurs during formamide washout and the T-tubules appear to reseal within the cell. It was shown that formamide-induced detubulation had no direct effects on cell proteins that might alter cell functions [288]. For this reason, this procedure is a suitable way to analyze T-tubule independent signaling events in adult mouse CMs as shown by previous publications [289, 290].
FRET experiments performed with detubulated CMs resulted in the same findings as with regular CMs.
Regular CMs showed a significantly increased $\tau_{1/2}$ of ∼100% compared to detubulated CMs. This is an indication for spatial changes within the microdomain. Absent T-tubules leave a gap resulting in a reduced spatial inhibition. This is why cAMP could be able to diffuse easier out of the RyR2 microdomain of detubulated CMs, which is also an indication for a successful detubulation.
PDE4D deficient mice did not show any changes in cAMP signaling compared to WT littermates. PDE4B-KO mice with absent T-tubules accumulated significantly more cAMP compared to WTs. This increasement could be shown to be based on a reduced PDE activity by applying propranolol to Iso-prestimulated CMs. Degradation time of CMs was significantly prolonged in PDE4B-KO cells.
This leads to the conclusion that PDE4B might be directly associated with the RyR2 since a possible effect of the LTCC-associated PDE4B could be ruled out by performing FRET experiments with detubulated CMs.
Detubulated CMs also showed a cAMP decay in PDE4B deficient CMs, indicating that in addition to diffusion of cAMP, other PDEs could be present. A possible PDE subfamily involved in the RyR2 microdomain regulation could be PDE8A. It was reported that PDE8A deficient CMs showed a 'leaky' RyR2 phenotype [112].

4.4.3 Western Blot

Downstream events of β-AR signaling on the RyR2 microdomain regulation were detected by analyzing Ser-2808 phosphorylation of the RyR2. Phosphorylation was

assessed in whole heart lysates of Langendorff-perfused whole mouse hearts stimulated with Iso. A previous study reported a hyperphosphorylation at Ser-2808 of the RyR2 in PDE4D deficient mice [142].
Surprisingly, the results of this work could not confirm this observation. Even a slight but non-significant reduction (p=0.1) of RyR2 phosphorylation in PDE4D deficient mice was shown. This could be based on a different genetic background of the used animals. In contrast to C57/BL6 mice, animals with a mixed background of FVB/N1 and C57/BL6 were used for the experiments performed for this project. This goes along with a study that analyzed the impact of PDE4D on cardiac contractility [150]. They reported a significantly reduced Ser-2808 phosphorylation of the RyR2.
In Iso-stimulated whole hearts, deficiency of PDE4B resulted in an increased Ser-2808 phosphorylation compared to Iso-stimulated WT hearts and unstimulated PDE4B-KO hearts. This supports the hypothesis of the direct interaction between PDE4B and RyR2.

4.4.4 Single Cell Contractility Measurements

A direct impact of PDE4B and PDE4D deficiency on the arrhythmia susceptibility in adult mouse CMs was analyzed by performing contractility measurements of single CMs at a basal level and upon β-AR stimulation. PDE4B-KO CMs showed significantly more extra beats under β-AR stress. Almost every electrically forced contraction was followed by a spontaneous extra beat. PDE4D deficient CMs also showed increased spontaneous extra beats upon Iso stimulation compared to littermate WTs but approximately 3 times less compared to Iso-stimulated PDE4B-KO CMs.
All extra beats occurred at the earliest after 500 ms after the cell was electrically stimulated. It is reminiscent of DADs triggered due to an intracellular Ca^{2+} release from the SR through the RyR2.
A previous study that analyzed the impact of PDE4B on the LTCC Ca^{2+} current showed increased numbers of extra beats in both PDE4B and PDE4D deficient mice [148]. However, the amount of spontaneous beats in PDE4B-KO CM in experiments performed for this project were increased by $\sim$100%, compared to the previous study. Extra beats in PDE4D-KO CMs were on a comparable level. The differences might be due to the experimental setup which was slightly changed compared to the previously described experiments. In contrast to continuous Iso stimulation, CMs in the mentioned study were pulse stimulated with 100 nM Iso for 15 seconds. Short-term exposure of Iso is affected slightly by PDE4B and PDE4D ablation, whereas in a long term exposure effects, mimicking physiological processes better than short term exposure, effects of PDE4B are much more pronounced compared to PDE4D.

Influence of PDE4D ablation could be based on an altered regulation of the LTCC complex, which leads to an increased amount of released Ca^{2+} in the junctional gap and thus leading to a 'leaky' RyR2.
Collectively, PDE4B ablation was shown to alter the regulation of the RyR2 on a functional level by spontaneously releasing Ca^{2+} from the SR resulting in cardiac arrhythmia. This is a clear indication of the functional relevance of PDE4B on the regulation of the RyR2 microdomain regulation.

4.4.5 STED Microscopy

All experiments discussed in the previous sections led to the conclusion that PDE4B is functionally involved in the regulation of the RyR2 microdomain. FRET experiments with detubulated CMs even suggest a spatial association between PDE4B and the RyR2. However, it cannot be completely ruled out that the effect of the LTCC-associated PDE4B is strong enough to overcome the gap between the LTCC and RyR2 and thus all effects of PDE4B ablation on the regulation of the RyR2 microdomain are based on the PDE4B located in the T-tubules.
Immuno Fluorescence staining combined with STED microscopy was performed to fill the gap of knowledge of the structural distribution of PDE4B within adult mouse CMs. The benefit of super resolution microscopy such as STED microscopy, compared to conventional confocal microscopy, is the improved spatial resolution by up to 12 fold.
The evaluation of the STED microscopy images was limited due to the pixel size of 20 nm. The colocalization of PDE4B and the RyR2 resulted in a directly overlapping fluorescence signal in almost 50% of analyzed z-lines. All remaining z-lines showed a shifted fluorescence signal of PDE4B and RyR2 by 20-60 nm. As mentioned previously, the junctional gap has a size of ∼15 nm, which is why STED microscopy does not enable to directly distinguish between RyR2 and LTCC-associated PDE4B.
However, the balanced distribution between direct and shifted overlap of fluorescence signals of PDE4B and RyR2 suggests that PDE4B might be present not only in proximity to the LTCC but also in the RyR2 microdomain.
It would have been beneficial to strengthen the results obtained by STED microscopy and FRET microscopy with detubulated CMs using another method to dissolve the structural distribution of PDE4B such as Co-Immunoprecipitation (Co-IP). However, we did not succeed in co-immunoprecipitating PDEs with the RyR2.

4.5 Altered Basal cAMP Levels

The performed experiments to determine basal cAMP levels did not allow to make statements about exact concentrations. All data on basal cAMP levels obtained by

FRET microscopy are compared to WT CMs.
Surprisingly, PDE4D deficient CMs did not show any altered basal cAMP levels in the caveolin-rich plasma membrane microdomain, whereas cAMP levels in PDE4B-KO CMs were significantly increased. The same phenomenon occurred in the RyR2 and SERCA2a microdomain.
The altered behavior of PDE4B and PDE4D ablation on basal cAMP levels could be based on the structure of the PDE4 family (see Figure 1.1). PDE4 isoforms can be classified according to the size of their N-terminal regions, dependent on the presence and size of the Upstream Conserved Regions (UCRs) UCR1 and UCR2. UCR1 harbors a PKA phosphorylation site, leading to an increased activity upon PKA presence up to 250%. Long PDE4 forms are harboring both UCRs, whereas UCR1 lacks in PDE4 short forms.
The most represented PDE4D isoforms in mouse CMs are PDE4D3, PDE4D5 and PDE4D9: all three classified as PDE4 long forms [134]. Harboring UCR1 and thus a PKA phosphorylation site, they show a relatively low activity at a basal state. This explains the maintained cAMP levels in microdomains that are controlled by PDE4D.
Although PDE4B3, a PDE4 long form, was shown to be the major PDE4B isoform expressed in neonatal and adult mouse CMs [123], a possible explanation for the altered basal cAMP levels in PDE4B deficient mice could be based on an the presence of PDE4B2, the only PDE4B short form. In this case, PDE4B2 would lack UCR1 and accordingly the PKA phosphorylation site, which would result in a high PDE4B activity at a basal state that would be lost upon PDE4B ablation. To verify this hypothesis, it would be necessary to perform WB experiments with specific PDEB2 antibodies or real-time PCR.
Microdomain specific increased basal concentrations of cAMP in PDE4B-KO CMs could be based on globally increased cAMP levels. This hypothesis could be excluded by performed ELISA experiments, showing an equal basal cAMP concentration in WT and knockout CMs (see Figure 3.22).
The possibility of compensatory changes in the pattern of PDE expression were analyzed by WB experiments.

4.6 Conclusion

FRET experiments to uncover the impact of PDE4B and PDE4D on the cAMP dynamics in the caveolin-rich plasma membrane proved the existence of PDE4B and PDE4D in the caveolin-rich plasma membrane microdomain with an equally strong effect on the regulation of cAMP signal transduction (see Figure 4.1).
SERCA2a microdomain is preferentially controlled by the PDE4 subfamily 4D as shown by FRET and WB analysis of PLN phosphorylation.

The presence of functional PDE4D in the RyR2 microdomain could not be confirmed by experiments performed for this work. Instead, a direct impact of PDE4B on the regulation of the RyR2 microdomain could be shown. FRET microscopy with CMs, which express a RyR2 microdomain specific biosensor, WB experiments and single CM contractility measurements led to the conclusion that PDE4B is functionally involved in the RyR2 microdomain regulation. FRET microscopy with osmotic shock-induced detubulated CMs showed a T-tubule independent impact of PDE4B on the RyR2 complex regulation and thus a direct interaction between PDE4B and RyR2. Further, STED microscopy suggests a structural connection between PDE4B and the RyR2. Unfortunately, due to experimental limitation this finding could not be confirmed by Co-IP experiments.

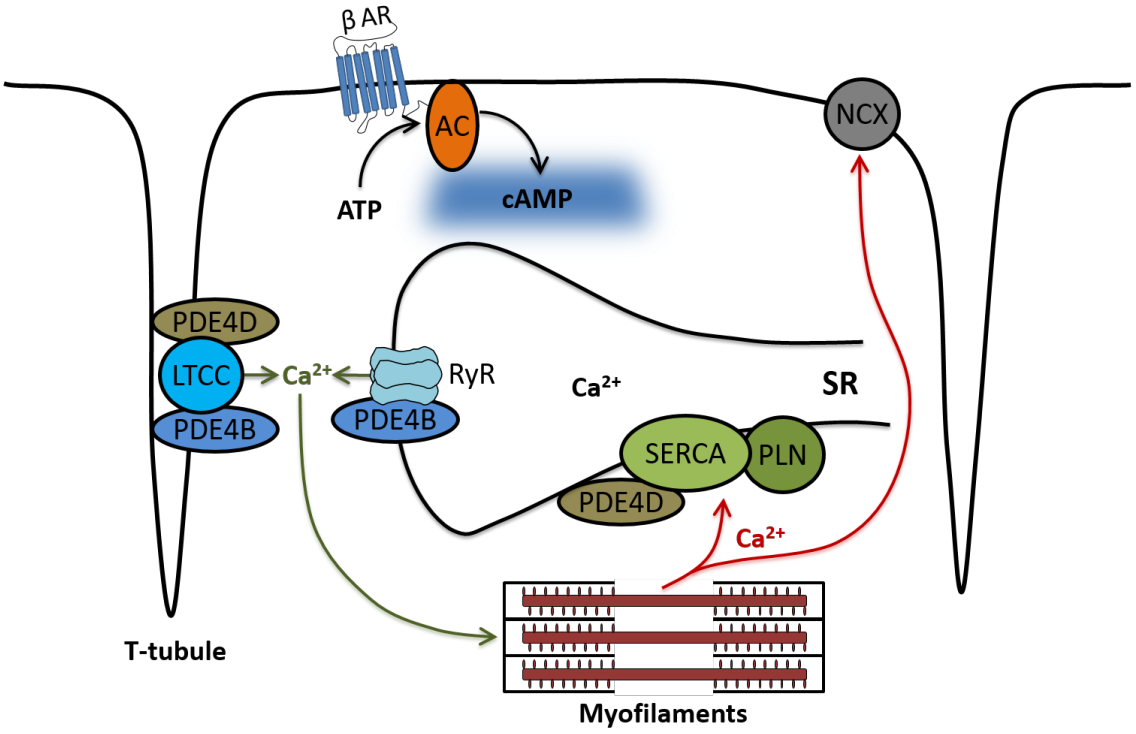

Figure 4.1: Schematic Representation of the Functional Distribution Phosphodiesterase 4B and 4D Revealed in this Study. Ca^{2+} cycling is crucial for a proper Excitation-Contraction Coupling (ECC) of a Cardiomyocyte (CM). Ca^{2+} influx through the L-Type Calcium Channel (LTCC), which is under control of PDE4B and PDE4D, causes a Ca^{2+}-induced Ca^{2+}-release from the Sarcoplasmic Reticulum (SR) through the PDE4B controlled Ryanodine Receptor Type 2 (RyR2) which activates the myofilaments resulting in CM contraction. Ca^{2+} is either transferred into the SR by Sarco/Endoplasmic Reticulum Ca^{2+}-ATPase 2a (SERCA2a), regulated by PDE4D and negatively regulated by Phospholamban (PLN), or excluded from the CM via Sodium-Calcium Exchanger (NCX).

Alterations in the distribution of PDEs in CMs are critically associated with heart diseases as arrhythmia and heart failure. This work led to a better understanding of the complex structure of these Ca^{2+} handling microdomains, which could be the key for the development of improved therapies for these life threatening diseases.

4.7 Outlook

In rodent CMs, PDE4 is the predominant cAMP degrading PDE family whereas PDE3 is the most represented PDE family in human ventricular CMs. Nevertheless, isoforms belonging to the PDE4 family have a major impact on human cardiac pathology since they are associated with heart diseases as arrhythmia and heart failure. As a follow up study it would be beneficial to analyze the impact of PDE3A on the regulation of cAMP dynamics in Ca^{2+} handling microdomains of adult mouse CMs. Addressing the unsolved question of the altered basal cAMP levels in PDE4B deficient mice could be of great interest regarding the future treatment of patients with cardiac diseases. In this case, the responsible PDE4B isoform would have to be identified, for example by WB or real-time PCR.
Studying a possible altered PDE4 associated redistribution of cAMP signaling in diseased CMs would be another very important step. This could be analyzed by performing experiments with CMs, isolated from Transverse Aortic Constriction (TAC) operated mice which leads to a pressure-overload-induce heart failure.
Finally, it would be desirable to analyze microdomain specific impact of PDE4B and PDE4D in human ventricular CMs, to investigate to what extent the results found in this work can be transferred to human CMs.
After the mechanisms by which PDE4B and PDE4D are involved in compartmentalized cAMP signal transduction in CMs are totally resolved, gene therapy approaches with a targeted overexpression of specific PDE4 isoforms could be the key for an improved medication of human cardiac diseases.

Bibliography

[1] Kristie McCormick and George S Baillie. Compartmentalisation of second messenger signalling pathways. *Current Opinion in Genetics & Development*, 27:20–25, 2014.

[2] Makoto Endo. Calcium Ion as a Second Messenger With Special Reference to Excitation-Contraction Coupling. *Journal of Pharmacological Sciences*, 100(5):519–524, 2006.

[3] Kazuki Kato, Hiroki Omura, Ryuichiro Ishitani, and Osamu Nureki. Cyclic GMP AMP as an Endogenous Second Messenger in Innate Immune Signaling by Cytosolic DNA. *Annual Review of Biochemistry*, 86(1):541–566, 2017.

[4] T W Rall and Earl W Sutherland. Fractionation and characterization of a cyclic adenine ribonucleotide formed by tissue particles. *The Journal Of Biological Chemistry*, 134(4):635–646, 1957.

[5] T W Rall and Earl W Sutherland. Formation of a cyclic adenine ribonucleotide by tissue particles. *The Journal Of Biological Chemistry*, Vol. 232(2):1065—-1076., 1958.

[6] Alexander Y Kots, Emil Martin, Iraida G Sharina, and Ferid Murad. *A Short History of cGMP, Guanylyl Cyclases, and cGMP-Dependent Protein Kinases*, pages 1–14. Springer Berlin Heidelberg, Berlin, Heidelberg, 2009.

[7] D F Ashman, R Lipton, M M Melicow, and T D Price. Isolation of adenosine 3,5-monophosphate and guanosine 3,5-monophosphate from rat urine. *Biochemical and Biophysical Research Communications*, 11(4):330–334, 1963.

[8] Jason L Larabee, Salika M Shakir, Soumitra Barua, and Jimmy D Ballard. Increased cAMP in Monocytes Augments Notch Signaling Mechanisms by Elevating RBP-J and Transducin-like Enhancer of Split (TLE). *Journal of Biological Chemistry*, 288(30):21526–21536, 2013.

[9] A D Ado and M M Goldshtein. The responsiveness of mice B-lymphocytes to neuromediators during an immune reaction. *Brain, Behavior, and Immunity*, 2(1):79–85, 1988.

[10] H Frerichs. Insulin secretion. *Diabetologia Croatica*, 4(2-3):147–156, 1975.

[11] M Nenquin and J.-C. Henquin. Sulphonylurea receptor-1, sulphonylureas and amplification of insulin secretion by Epac activation in β cells. *Diabetes, Obesity and Metabolism*, 18(7):698–701, 2015.

[12] Elisa Canepa, Cinzia Domenicotti, Barbara Marengo, Mario Passalacqua, Umberto M Marinari, Maria A Pronzato, Ernesto Fedele, and Roberta Ricciarelli. Cyclic adenosine monophosphate as an endogenous modulator of the amyloid-β precursor protein metabolism. *IUBMB Life*, 65(2):127–133, 2013.

[13] Shengbiao Wang, Jiexiong Chen, Katherine T Au, and Michael G Ross. Expression of aquaporin 8 and its up-regulation by cyclic adenosine monophosphate in human WISH cells. *American Journal of Obstetrics and Gynecology*, 188(4):997–1001, 2003.

[14] Shailesh R Agarwal, Jackson Gratwohl, Mia Cozad, Pei-Chi Yang, Colleen E Clancy, and Robert D Harvey. Compartmentalized cAMP Signaling Associated With Lipid Raft and Non-raft Membrane Domains in Adult Ventricular Myocytes. *Frontiers in Pharmacology*, 9:332, 2018.

[15] G A Robinson, R W Butcher, and E W Sutherland. Cyclic AMP. *Annual Review of Biochemistry*, 37(1):149–174, 1968.

[16] Juana M Gancedo. Biological roles of cAMP: variations on a theme in the different kingdoms of life. *Biological Reviews*, 88(3):645–668, 2013.

[17] Nicholas J Batty, Keith K Fenrich, and Karim Fouad. The role of cAMP and its downstream targets in neurite growth in the adult nervous system. *Neuroscience Letters*, 652:56–63, 2017.

[18] Jin-Hee Han, Steven A Kushner, Adelaide P Yiu, Christy J Cole, Anna Matynia, Robert A Brown, Rachael L Neve, John F Guzowski, Alcino J Silva, and Sheena A Josselyn. Neuronal Competition and Selection During Memory Formation. *Science*, 316(5823):457 LP – 460, 2007.

[19] Roberta Ricciarelli, Daniela Puzzo, Olga Bruno, Elisa Canepa, Elena Gardella, Daniela Rivera, Lucia Privitera, Cinzia Domenicotti, Barbara Marengo, Umberto Maria Marinari, Agostino Palmeri, Maria Adelaide Pronzato, Ottavio Arancio, and Ernesto Fedele. A novel mechanism for cyclic adenosine monophosphate mediated memory formation: Role of amyloid beta. *Annals of Neurology*, 75(4):602–607, 2014.

[20] Takayuki Fujita, Masanari Umemura, Utako Yokoyama, Satoshi Okumura, and Yoshihiro Ishikawa. The role of Epac in the heart. *Cellular and Molecular Life Sciences*, 74(4):591–606, 2017.

[21] Marianne Freyss-Beguin, Geneviève Griffaton, Paul Lechat, Douglas Picken, Marie Claude Quennedey, Bruno Rouot, and Jean Schwartz. Comparison of the chronotropic effect and the cyclic AMP accumulation induced by β2-agonists in rat heart cell culture. *British Journal of Pharmacology*, 78(4):717–723, 1983.

[22] Pierre Bobin, Milia Belacel-Ouari, Ibrahim Bedioune, Liang Zhang, Jérôme Leroy, Véronique Leblais, Rodolphe Fischmeister, and Grégoire Vandecasteele. Cyclic nucleotide phosphodiesterases in heart and vessels: A therapeutic perspective. *Archives of Cardiovascular Diseases*, 109(6):431–443, 2016.

[23] Hideki Chusho, Naohisa Tamura, Yoshihiro Ogawa, Akihiro Yasoda, Michio Suda, Takashi Miyazawa, Kenji Nakamura, Kazuki Nakao, Tatsuya Kurihara, Yasato Komatsu, Hiroshi Itoh, Kiyoshi Tanaka, Yoshihiko Saito, Motoya Katsuki, and Kazuwa Nakao. Dwarfism and early death in mice lacking C-type natriuretic peptide. *Proceedings of the National Academy of Sciences*, 98(7):4016–4021, 2001.

[24] A Geiselhöringer, M Gaisa, F Hofmann, and J Schlossmann. Distribution of IRAG and cGKI-isoforms in murine tissues. *FEBS Letters*, 575(1-3):19–22, 2004.

[25] Vadim Y Arshavsky, Trevor D Lamb, and Edward N Pugh. G Proteins and Phototransduction. *Annual Review of Physiology*, 64(1):153–187, 2002.

[26] Katarina Persson, Raj Kumar Pandita, Attila Aszòdi, Marianne Ahmad, Alexander Pfeifer, Reinhard Fässler, and Karl-Erik Andersson. Functional characteristics of urinary tract smooth muscles in mice lacking cGMP protein kinase type I. *American Journal of Physiology-Regulatory, Integrative and Comparative Physiology*, 279(3):R1112–R1120, 2000.

[27] G A Spinas, R Laffranchi, I Francoys, I David, C Richter, and M Reinecke. The early phase of glucose-stimulated insulin secretion requires nitric oxide. *Diabetologia*, 41(3):292–299, 1998.

[28] Bodo Haas, Peter Mayer, Katja Jennissen, Daniela Scholz, Mauricio Berriel Diaz, Wilhelm Bloch, Stephan Herzig, Reinhard Fässler, and Alexander Pfeifer. Protein Kinase G Controls Brown Fat Cell Differentiation and Mitochondrial Biogenesis. *Science Signaling*, 2(99):ra78—-ra78, 2009.

[29] Steffen Massberg, Matthias Sausbier, Peter Klatt, Markus Bauer, Alexander Pfeifer, Wolfgang Siess, Reinhard Fässler, Peter Ruth, Fritz Krombach, and Franz Hofmann. Increased Adhesion and Aggregation of Platelets Lacking Cyclic Guanosine 3',5'-Monophosphate Kinase I. *Journal of Experimental Medicine*, 189(8):1255–1264, 1999.

[30] S W John, A T Veress, U Honrath, C K Chong, L Peng, O Smithies, and H Sonnenberg. Blood pressure and fluid-electrolyte balance in mice with reduced or absent ANP. *American Journal of Physiology-Regulatory, Integrative and Comparative Physiology*, 271(1):R109–R114, 1996.

[31] Kai C. Wollert, Sevdalina Yurukova, Ana Kilic, Frank Begrow, Beate Fiedler, Stepan Gambaryan, Ulrich Walter, Suzanne M. Lohmann, and Michaela Kuhn. Increased effects of C-type natriuretic peptide on contractility and calcium regulation in murine hearts overexpressing cyclic GMP-dependent protein kinase I. *British Journal of Pharmacology*, 140(7):1227–1236, 2003.

[32] Eiki Takimoto, Hunter C Champion, Manxiang Li, Diego Belardi, Shuxun Ren, E Rene Rodriguez, Djahida Bedja, Kathleen L Gabrielson, Yibin Wang, and David A Kass. Chronic inhibition of cyclic GMP phosphodiesterase 5A prevents and reverses cardiac hypertrophy. *Nature Medicine*, 11:214, 2005.

[33] I F Ghalayini. Nitric oxide cyclic GMP pathway with some emphasis on cavernosal contractility. *International Journal Of Impotence Research*, 16:459, 2004.

[34] Franz Hofmann and Jörg W Wegener. *cGMP-Dependent Protein Kinases (cGK)*, pages 17–50. Humana Press, Totowa, NJ, 2013.

[35] Aziz Guellich, Hind Mehel, and Rodolphe Fischmeister. Cyclic AMP synthesis and hydrolysis in the normal and failing heart. *Pfluegers Archiv - European Journal of Physiology*, 466(6):1163–1175, 2014.

[36] Daniel M Johnson and Gudrun Antoons. Arrhythmogenic Mechanisms in Heart Failure: Linking β-Adrenergic Stimulation, Stretch, and Calcium. *Frontiers in Physiology*, 9:1453, 2018.

[37] Zheng Maggie Huang, Jessica I Hold, and Walter J Koch. G protein-coupled receptor kinases in normal and failing myocardium. *Frontiers in Bioscience*, 16(1):3057, 2011.

[38] Jeffrey J Goldberger, Robert O Bonow, Michael Cuffe, Lei Liu, Yves Rosenberg, Prediman K Shah, Sidney C Smith, and Haris Subačius. Effect of Beta-Blocker Dose on Survival After Acute Myocardial Infarction. *Journal of the American College of Cardiology*, 66(13):1431–1441, 2015.

[39] Thomas J Monaco and Nicola A Hanania. Emerging inhaled long-acting beta-2 adrenoceptor agonists for the treatment of COPD. *Expert Opinion on Emerging Drugs*, 22(3):285–299, 2017.

[40] Isabelle Van Liefde, Anne van Witzenburg, and Georges Vauquelin. Isopro-

terenol and selective agonists stimulate similar atypical β-adrenoceptors in rat adipocytes. *Biochemical Pharmacology*, 45(4):974–977, 1993.

[41] Taraknath Taraphdhar and Sreekanth Reddy Basireddy. Isoprenaline in complete heart block patients during ambulance transport. *International Journal of Emergency Medicine*, 8(S1):P3, 2015.

[42] Takeshi Ebihara, Masanori Morita, Masahiro Kawada, Koji Amano, Fumitaka Kato, and Yasuki Nakata. Efficacy of isoproterenol for treating amlodipine overdose resulting in bradycardia. *Acute Medicine & Surgery*, 4(3):353–357, 2017.

[43] Beth Drolet. Initiation and Use of Propranolol for Infantile Hemangioma : Report of a Consensus Conference abstract. *Pediatrics*, 2015.

[44] R. K. Perera and V. O. Nikolaev. Compartmentation of cAMP signalling in cardiomyocytes in health and disease. *Acta Physiologica*, 207(4):650–662, 2013.

[45] Regina Celia Spadari, Claudia Cavadas, Ana Elisa T Saturi de Carvalho, Daniela Ortolani, Andre Luiz de Moura, and Paula Frizera Vassalo. Role of Beta-adrenergic Receptors and Sirtuin Signaling in the Heart During Aging, Heart Failure, and Adaptation to Stress. *Cellular and Molecular Neurobiology*, 38(1):109–120, 2018.

[46] T Frielle, S Collins, K W Daniel, M G Caron, R J Lefkowitz, and B K Kobilka. Cloning of the cDNA for the human beta 1-adrenergic receptor. *Proceedings of the National Academy of Sciences*, 84(22):7920–7924, 1987.

[47] Florian Brueckner, Chayne L Piscitelli, Ching-Ju Tsai, Jörg Standfuss, Xavier Deupi, and Gebhard F X Schertler. Chapter Six - Structure of β-Adrenergic Receptors. In P Michael Conn, editor, *G Protein Coupled Receptors*, volume 520 of *Methods in Enzymology*, pages 117–151. Academic Press, 2013.

[48] L J Emorine, S Marullo, M M Briend-Sutren, G Patey, K Tate, C Delavier-Klutchko, and A D Strosberg. Molecular characterization of the human beta 3-adrenergic receptor. *Science*, 245(4922):1118–1121, 1989.

[49] B K Kobilka, R A Dixon, T Frielle, H G Dohlman, M A Bolanowski, I S Sigal, T L Yang-Feng, U Francke, M G Caron, and R J Lefkowitz. cDNA for the human beta 2-adrenergic receptor: a protein with multiple membrane-spanning domains and encoded by a gene whose chromosomal location is shared with that of the receptor for platelet-derived growth factor. *Proceedings of the National Academy of Sciences*, 84(1):46–50, 1987.

[50] Juan P Aragón, Marah E Condit, Shashi Bhushan, Benjamin L Predmore, Sandeep S Patel, D Bennett Grinsfelder, Susheel Gundewar, Saurabh Jha,

John W Calvert, Lili A Barouch, Madhav Lavu, Harold M Wright, and David J Lefer. Beta3-Adrenoreceptor Stimulation Ameliorates Myocardial Ischemia-Reperfusion Injury Via Endothelial Nitric Oxide Synthase and Neuronal Nitric Oxide Synthase Activation. *Journal of the American College of Cardiology*, 58(25):2683–2691, 2011.

[51] Michael R Bristow, Patti Larrabee, Wayne Minobe, Robert Roden, Lisa Skerl, Jana Klein, David Handwerger, David J Port, and B Müller-Beckmann. Receptor Pharmacology of Carvedilol in the Human Heart. *Journal of Cardiovascular Pharmacology*, 19, 1992.

[52] Verónica García-Morales, María Luaces-Regueira, and Manuel Campos-Toimil. The cAMP effectors PKA and Epac activate endothelial NO synthase through PI3K/Akt pathway in human endothelial cells. *Biochemical Pharmacology*, 145:94–101, 2017.

[53] Ornella Lucchesi, María C Ruete, Matías A Bustos, María F Quevedo, and Claudia N Tomes. The signaling module cAMP/Epac/Rap1/PLCϵ/IP3 mobilizes acrosomal calcium during sperm exocytosis. *Biochimica et Biophysica Acta (BBA) - Molecular Cell Research*, 1863(4):544–561, 2016.

[54] Xiaodong Cheng, Zhenyu Ji, Tamara Tsalkova, and Fang Mei. Epac and PKA: A tale of two intracellular cAMP receptors. *Acta Biochimica et Biophysica Sinica*, 40(7):651–662, 2008.

[55] Matthias Schäfer, Karen Frischkopf, Gerhild Taimor, Hans Michael Piper, and Klaus-Dieter Schlüter. Hypertrophic effect of selective β1-adrenoceptor stimulation on ventricular cardiomyocytes from adult rat. *American Journal of Physiology-Cell Physiology*, 279(2):C495–C503, 2000.

[56] Chengjun Cao, Mei Wu, Jian Bing, Li Tao, Xuefen Ding, Xiaoyun Liu, and Guanghua Huang. Global regulatory roles of the cAMP/PKA pathway revealed by phenotypic, transcriptomic and phosphoproteomic analyses in a null mutant of the PKA catalytic subunit in Candida albicans. *Molecular Microbiology*, 105(1):46–64, 2017.

[57] Sabrina Manni, Joseph H. Mauban, Christopher W. Ward, and Meredith Bond. Phosphorylation of the cAMP-dependent protein kinase (PKA) regulatory subunit modulates PKA-AKAP interaction, substrate phosphorylation, and calcium signaling in cardiac cells. *Journal of Biological Chemistry*, 283(35):24145–24154, 2008.

[58] Alessandro Cannavo, Daniela Liccardo, and Walter Koch. Targeting cardiac β-adrenergic signaling via GRK2 inhibition for heart failure therapy. *Frontiers in Physiology*, 4:264, 2013.

[59] Martin J Lohse, Stefan Engelhardt, and Thomas Eschenhagen. What Is the Role of beta-Adrenergic Signaling in Heart Failure? *Circulation Research*, 93(10):896–906, 2003.

[60] Catherine Communal, Krishna Singh, Douglas Brian Sawyer, and Wilson Steven Colucci. Opposing effects of beta(1)- and beta(2)-adrenergic receptors on cardiac myocyte apoptosis : role of a pertussis toxin-sensitive G protein. *Circulation*, 100 22:2210–2212, 1999.

[61] Julia Gorelik, Peter T. Wright, Alexander R. Lyon, and Sian E. Harding. Spatial control of the βaR system in heart failure: The transverse tubule and beyond. *Cardiovascular Research*, 98(2):216–224, 2013.

[62] Viacheslav O Nikolaev, Moritz Bünemann, Eva Schmitteckert, Martin J Lohse, and Stefan Engelhardt. Cyclic AMP Imaging in Adult Cardiac Myocytes Reveals Far Reaching β1 Adrenergic but Locally Confined β2 Adrenergic Receptor Mediated Signaling. *Circulation Research*, 99(10):1084–1091, 2006.

[63] Alexander Froese and Viacheslav O. Nikolaev. Imaging alterations of cardiomyocyte cAMP microdomains in disease. *Frontiers in Pharmacology*, 6(August):3–7, 2015.

[64] Joseph A Hill and Eric N Olson. Cardiac Plasticity. *New England Journal of Medicine*, 358(13):1370–1380, 2008.

[65] Yow Keat Tham, Bianca C Bernardo, Jenny Y Y Ooi, Kate L Weeks, and Julie R McMullen. Pathophysiology of cardiac hypertrophy and heart failure: signaling pathways and novel therapeutic targets. *Archives of Toxicology*, 89(9):1401–1438, 2015.

[66] I L Buxton and L L Brunton. Compartments of cyclic AMP and protein kinase in mammalian cardiomyocytes. *Journal of Biological Chemistry*, 258(17):10233–10239, 1983.

[67] Susan F Steinberg and Laurence L Brunton. Compartmentation of G Protein-Coupled Signaling Pathways in Cardiac Myocytes. *Annual Review of Pharmacology and Toxicology*, 41(1):751–773, 2001.

[68] S L Keely. Activation of cAMP-dependent protein kinase without a corresponding increase in phosphorylase activity. *Research communications in chemical pathology and pharmacology*, 18:283–290, 1977.

[69] S J Singer and Garth L Nicolson. The Fluid Mosaic Model of the Structure of Cell Membranes. *Science*, 175(4023):720–731, 1972.

[70] Aviva M Tolkovsky and Alexander Levitzki. Mode of coupling between the β-adrenergic receptor and adenylate cyclase in turkey erythrocytes. *Biochemistry*, 17(18):3795–3810, 1978.

[71] Ioanna Bethani, Sigrid S Skanland, Ivan Dikic, and Amparo Acker-Palmer. Spatial organization of transmembrane receptor signalling. *The EMBO Journal*, 29(16):2677–2688, 2010.

[72] Jessica L Esseltine and John D Scott. AKAP signaling complexes: pointing towards the next generation of therapeutic targets? *Trends in Pharmacological Sciences*, 34(12):648–655, 2013.

[73] Alessia Perino, Alessandra Ghigo, John D Scott, and Emilio Hirsch. Anchoring Proteins as Regulators of Signaling Pathways. *Circulation Research*, 111(4):482–492, 2012.

[74] Davide Calebiro and Isabella Maiellaro. cAMP signaling microdomains and their observation by optical methods. *Frontiers in Cellular Neuroscience*, 8:350, 2014.

[75] Andreas Horner, Frank Goetz, Robert Tamp, Enno Klussmann, and Peter Pohl. Mechanism for Targeting the A-kinase Anchoring Protein AKAP18d to the Membrane. *Journal of Biological Chemistry*, 287(51):42495–42501, 2012.

[76] Carmen W Dessauer. Adenylyl Cyclase A-kinase Anchoring Protein Complexes: The Next Dimension in cAMP Signaling. *Molecular Pharmacology*, 76(5):935–941, 2009.

[77] Paolo Di Benedetto, Cristina Delneri, Emanuele Biasutti, Luisa Monti Bragadin, and Tullio Giorgini. Vesicourethral dysfunction in multiple sclerosis. Initial assessment based on lower urinary tract symptoms and their pathophysiology. *Neurological Sciences*, 29(4):348–351, 2008.

[78] Dong I Lee, Guangshuo Zhu, Takashi Sasaki, Gun-Sik Cho, Nazha Hamdani, Ronald Holewinski, Su-Hyun Jo, Thomas Danner, Manling Zhang, Peter P Rainer, Djahida Bedja, Jonathan A Kirk, Mark J Ranek, Wolfgang R Dostmann, Chulan Kwon, Kenneth B Margulies, Jennifer E Van Eyk, Walter J Paulus, Eiki Takimoto, and David A Kass. Phosphodiesterase 9A controls nitric-oxide-independent cGMP and hypertrophic heart disease. *Nature*, 519:472, 2015.

[79] Dario Diviani, Kimberly L. Dodge-Kafka, Jinliang Li, and Michael S. Kapiloff. A-kinase anchoring proteins: scaffolding proteins in the heart. *American Journal of Physiology-Heart and Circulatory Physiology*, 301(5):H1742–H1753, 2011.

[80] Cecile Terrenoire, Miles D Houslay, George S Baillie, and Robert S Kass. The Cardiac IKs Potassium Channel Macromolecular Complex Includes the Phosphodiesterase PDE4D3. *Journal of Biological Chemistry*, 284(14):9140–9146, 2009.

[81] Iain D C Fraser, Steven J Tavalin, Linda B Lester, Lorene K Langeberg, Ann M Westphal, Rebecca A Dean, Neil V Marrion, and John D Scott. A novel lipid-anchored A-kinase Anchoring Protein facilitates cAMP-responsive membrane events. *The EMBO Journal*, 17(8):2261–2272, 1998.

[82] Tianyan Gao, Atsuko Yatani, Mark L Dell'Acqua, Hidenori Sako, Stuart A Green, Nathan Dascal, John D Scott, and M.Marlene Hosey. cAMP-Dependent Regulation of Cardiac L-Type Ca2+ Channels Requires Membrane Targeting of PKA and Phosphorylation of Channel Subunits. *Neuron*, 19(1):185–196, 1997.

[83] A. Singh, J. M. Redden, M. S. Kapiloff, and K. L. Dodge-Kafka. The Large Isoforms of A-Kinase Anchoring Protein 18 Mediate the Phosphorylation of Inhibitor-1 by Protein Kinase A and the Inhibition of Protein Phosphatase 1 Activity. *Molecular Pharmacology*, 79(3):533–540, 2011.

[84] Miles D Houslay and David R Adams. PDE4 cAMP phosphodiesterases: modular enzymes that orchestrate signalling cross-talk, desensitization and compartmentalization. *The Biochemical journal*, 370(Pt 1):1–18, 2003.

[85] Robert J Lefkowitz and Sudha K Shenoy. Transduction of Receptor Signals by beta - Arrestins. *Science*, 308(5721):512–517, 2005.

[86] Louis M Luttrell and Robert J Lefkowitz. The role of β-arrestins in the termination and transduction of G-protein-coupled receptor signals. *Journal of Cell Science*, 115(3):455–465, 2002.

[87] George S Baillie and Miles D Houslay. Arrestin times for compartmentalised cAMP signalling and phosphodiesterase-4 enzymes. *Current Opinion in Cell Biology*, 17(2):129–134, 2005.

[88] Wito Richter, Peter Day, Rani Agrawal, Matthew D Bruss, Sébastien Granier, Yvonne L Wang, Søren G F Rasmussen, Kathleen Horner, Ping Wang, Tao Lei, Andrew J Patterson, Brian Kobilka, and Marco Conti. Signaling from β1- and β2-adrenergic receptors is defined by differential interactions with PDE4. *The EMBO Journal*, 27(2):384–393, 2008.

[89] Marco Mongillo, Theresa McSorley, Sandrine Evellin, Arvind Sood, Valentina Lissandron, Anna Terrin, Elaine Huston, Annette Hannawacker, Martin J. Lohse, Tullio Pozzan, Miles D. Houslay, and Manuela Zaccolo. Fluorescence

resonance energy transfer-based analysis of cAMP dynamics in live neonatal rat cardiac myocytes reveals distinct functions of compartmentalized phosphodiesterases. *Circulation Research*, 95(1):67–75, 2004.

[90] Marco Conti and Joseph Beavo. Biochemistry and physiology of cyclic nucleotide phosphodiesterases: essential components in cyclic nucleotide signaling. *Annual review of biochemistry*, 76:481–511, 2007.

[91] Sharron H Francis, Mitsi A Blount, and Jackie D Corbin. Mammalian Cyclic Nucleotide Phosphodiesterases: Molecular Mechanisms and Physiological Functions. *Physiological Reviews*, 91(2):651–690, 2011.

[92] Bracy A Fertig and George S Baillie. PDE4-Mediated cAMP Signalling. *Journal of Cardiovascular Development and Disease*, 5(1):8, 2018.

[93] Manuela Zaccolo and Matthew A Movsesian. cAMP and cGMP signaling crosstalk: Role of phosphodiesterases and implications for cardiac pathophysiology. *Circulation Research*, 100(11):1569–1578, 2007.

[94] Oleg E Osadchii. Myocardial Phosphodiesterases and Regulation of Cardiac Contractility in Health and Cardiac Disease. *Cardiovascular Drugs and Therapy*, 21(3):171–194, 2007.

[95] Xiefan Fang, Jourdon Robinson, John Wang-Hu, Lingli Jiang, Daniel A Freeman, Scott A Rivkees, and Christopher C Wendler. cAMP induces hypertrophy and alters DNA methylation in HL-1 cardiomyocytes. *American Journal of Physiology-Cell Physiology*, 309(6):C425–C436, 2015.

[96] Miles D. Houslay, George S. Baillie, and Donald H. Maurice. cAMP-specific phosphodiesterase-4 enzymes in the cardiovascular system: A molecular toolbox for generating compartmentalized cAMP signaling. *Circulation Research*, 100(7):950–966, 2007.

[97] Clint L Miller and Chen Yan. Targeting Cyclic Nucleotide Phosphodiesterase in the Heart: Therapeutic Implications. *Journal of Cardiovascular Translational Research*, 3(5):507–515, 2010.

[98] W K Sonnenburg, D Seger, and J A Beavo. Molecular cloning of a cDNA encoding the "61-kDa" calmodulin-stimulated cyclic nucleotide phosphodiesterase. Tissue-specific expression of structurally related isoforms. *Journal of Biological Chemistry*, 268(1):645–652, 1993.

[99] Clint L Miller, Masayoshi Oikawa, Yujun Cai, Andrew P Wojtovich, David J Nagel, Xiangbin Xu, Haodong Xu, Vince Florio, Sergei D Rybalkin, Joseph A Beavo, Yiu-Fai Chen, Jian-Dong Li, Burns C Blaxall, Jun-ichi Abe, and Chen

Yan. Role of Ca2+ Calmodulin-Stimulated Cyclic Nucleotide Phosphodiesterase 1 in Mediating Cardiomyocyte Hypertrophy. *Circulation Research*, 105(10):956–964, 2009.

[100] Torsten R Dunkern and Armin Hatzelmann. Characterization of inhibitors of phosphodiesterase 1C on a human cellular system. *The FEBS Journal*, 274(18):4812–4824, 2007.

[101] Marco Mongillo, Carlo G Tocchetti, Anna Terrin, Valentina Lissandron, York-Fong Cheung, Wolfgang R Dostmann, Tullio Pozzan, David A Kass, Nazareno Paolocci, Miles D Houslay, and Manuela Zaccolo. Compartmentalized Phosphodiesterase-2 Activity Blunts beta Adrenergic Cardiac Inotropy via an NO/cGMP-Dependent Pathway. *Circulation Research*, 98(2):226–234, 2006.

[102] Sergio E Martinez, Albert Y Wu, Natalie A Glavas, Xiao-Bo Tang, Stewart Turley, Wim G J Hol, and Joseph A Beavo. The two GAF domains in phosphodiesterase 2A have distinct roles in dimerization and in cGMP binding. *Proceedings of the National Academy of Sciences*, 99(20):13260–13265, 2002.

[103] Silvio Weber, Miriam Zeller, Kaomei Guan, Frank Wunder, Michael Wagner, and Ali El-Armouche. PDE2 at the crossway between cAMP and cGMP signalling in the heart. *Cellular Signalling*, 38:76–84, 2017.

[104] Liliana R V Castro, Ignacio Verde, Dermot M F Cooper, and Rodolphe Fischmeister. Cyclic Guanosine Monophosphate Compartmentation in Rat Cardiac Myocytes. *Circulation*, 113(18):2221–2228, 2006.

[105] Stefania Monterisi, Miguel J Lobo, Craig Livie, John C Castle, Michael Weinberger, George Baillie, Nicoletta C Surdo, Nshunge Musheshe, Alessandra Stangherlin, Eyal Gottlieb, Rory Maizels, Mario Bortolozzi, Massimo Micaroni, and Manuela Zaccolo. PDE2A2 regulates mitochondria morphology and apoptotic cell death via local modulation of cAMP/PKA signalling. *eLife*, 6:e21374, 2017.

[106] Lin Yang, Zhiguang Zhou, Tao Du, Shaozhen Tan, Yi Zhnag, and Ping Jin. Detection of carboxypeptidase H specific T cells in peripheral blood of latent autoimmune diabetic patients with carboxypeptidase antibody positivity by ELISPOT assay. *Journal of Central South University (Medical Sciences)*, 34(10):1011–1016, 2009.

[107] Aniella Abi-Gerges, Wito Richter, Florence Lefebvre, Philippe Mateo, Audrey Varin, Christophe Heymes, Jane-Lise Samuel, Claire Lugnier, Marco Conti, Rodolphe Fischmeister, and Grégoire Vandecasteele. Decreased Expression

and Activity of cAMP Phosphodiesterases in Cardiac Hypertrophy and Its Impact on beta Adrenergic cAMP Signals. *Circulation Research*, 105(8):784–792, 2009.

[108] Ryan Hambleton, Judith Krall, Eliso Tikishvili, Matthew Honeggar, Faiyaz Ahmad, Vincent C Manganiello, and Matthew A Movsesian. Isoforms of Cyclic Nucleotide Phosphodiesterase PDE3 and Their Contribution to cAMP Hydrolytic Activity in Subcellular Fractions of Human Myocardium. *Journal of Biological Chemistry*, 280(47):39168–39174, 2005.

[109] Ronald E Weishaar, Dianne C Kobylarz-Singer, and Harvey R Kaplan. Subclasses of cyclic AMP phosphodiesterase in cardiac muscle. *Journal of Molecular and Cellular Cardiology*, 19(10):1025–1036, 1987.

[110] Youn Wook Chung, Claudia Lagranha, Yong Chen, Junhui Sun, Guang Tong, Steven C Hockman, Faiyaz Ahmad, Shervin G Esfahani, Dahae H Bae, Nazari Polidovitch, Jian Wu, Dong Keun Rhee, Beom Seob Lee, Marjan Gucek, Mathew P Daniels, Christine A Brantner, Peter H Backx, Elizabeth Murphy, and Vincent C Manganiello. Targeted disruption of PDE3B, but not PDE3A, protects murine heart from ischemia/reperfusion injury. *Proceedings of the National Academy of Sciences*, 112(17):E2253—-E2262, 2015.

[111] S H Soderling, S J Bayuga, and J A Beavo. Cloning and characterization of a cAMP-specific cyclic nucleotide phosphodiesterase. *Proceedings of the National Academy of Sciences*, 95(15):8991–8996, 1998.

[112] Enrico Patrucco, Masami Shimizu Albergine, Luis F Santana, and Joseph A Beavo. Phosphodiesterase 8A (PDE8A) regulates excitation contraction coupling in ventricular myocytes. *Journal of Molecular and Cellular Cardiology*, 49(2):330–333, 2010.

[113] Thérèse Keravis and Claire Lugnier. Cyclic nucleotide phosphodiesterase (PDE) isozymes as targets of the intracellular signalling network: Benefits of PDE inhibitors in various diseases and perspectives for future therapeutic developments. *British Journal of Pharmacology*, 165(5):1288–1305, 2012.

[114] David M.G. Halpin. ABCD of the phosphodiesterase family: Interaction and differential activity in COPD. *International Journal of COPD*, 3(4):543–561, 2008.

[115] A. T. Bender. Cyclic Nucleotide Phosphodiesterases: Molecular Regulation to Clinical Use. *Pharmacological Reviews*, 58(3):488–520, 2006.

[116] Thomas Eschenhagen. PDE4 in the human heart major player or little helper? *British Journal of Pharmacology*, 169(3):524–527, 2013.

[117] Graeme B Bolger. Molecular biology of the cyclic AMP-specific cyclic nucleotide phosphodiesterases: A diverse family of regulatory enzymes. *Cellular Signalling*, 6(8):851–859, 1994.

[118] Simon J MacKenzie, George S Baillie, Ian McPhee, Carolynn MacKenzie, Rachael Seamons, Theresa McSorley, Jenni Millen, Matthew B Beard, Gino Heeke, and Miles D Houslay. Long PDE4 cAMP specific phosphodiesterases are activated by protein kinase A-mediated phosphorylation of a single serine residue in Upstream Conserved Region 1 (UCR1). *British Journal of Pharmacology*, 136(3):421–433, 2009.

[119] Andrew T. Bender and Joseph A. Beavo. Cyclic nucleotide phosphodiesterases: molecular regulation to clinical use. *Pharmacological reviews*, 58(3):488–520, 2006.

[120] Miles D. Houslay and David R. Adams. PDE4 cAMP phosphodiesterases: modular enzymes that orchestrate signalling cross-talk, desensitization and compartmentalization. *Biochemical Journal*, 370(1):1–18, 2003.

[121] M D Houslay and G S Baillie. The role of ERK2 docking and phosphorylation of PDE4 cAMP phosphodiesterase isoforms in mediating cross-talk between the cAMP and ERK signalling pathways. *Biochemical Society Transactions*, 31(6):1186–1190, 2003.

[122] Claudio Sette, Marco Conti, and M J Biol Chem. Phosphorylation and Activation of a cAMP-specific Phosphodiesterase by the cAMP-dependent Protein Kinase vated in rat thyroid cells by TSH through a cAMP-de-. 271(28):16526–16534, 1996.

[123] Marco Conti, Wito Richter, Celine Mehats, Gabriel Livera, Jy-Young Park, and Catherine Jin. Cyclic AMP-specific PDE4 Phosphodiesterases as Critical Components of Cyclic AMP Signaling. *Journal of Biological Chemistry*, 278(8):5493–5496, 2003.

[124] Marco Conti and Joseph Beavo. Biochemistry and Physiology of Cyclic Nucleotide Phosphodiesterases: Essential Components in Cyclic Nucleotide Signaling. *Annual Review of Biochemistry*, 76(1):481–511, 2007.

[125] Alex B Burgin, Olafur T Magnusson, Jasbir Singh, Pam Witte, Bart L Staker, Jon M Bjornsson, Margret Thorsteinsdottir, Sigrun Hrafnsdottir, Timothy Hagen, Alex S Kiselyov, Lance J Stewart, and Mark E Gurney. Design of phosphodiesterase 4D (PDE4D) allosteric modulators for enhancing cognition with improved safety. *Nature Biotechnology*, 28:63, 2009.

[126] F Ahmad, T Murata, K Shimizu, E Degerman, D Maurice, and V Manganiello. Cyclic Nucleotide Phosphodiesterases: important signaling modulators and therapeutic targets. *Oral Diseases*, 21(1):e25–e50, 2014.

[127] Elaine Huston, Irene Gall, Thomas M Houslay, and Miles D Houslay. Helix-1 of the cAMP-specific phosphodiesterase PDE4A1 regulates its phospholipase-D-dependent redistribution in response to release of Ca2+. *Journal of Cell Science*, 119(18):3799–3810, 2006.

[128] Kirsty F. Houslay, Frank Christian, Ruth MacLeod, David R. Adams, Miles D. Houslay, and George S. Baillie. Identification of a multifunctional docking site on the catalytic unit of phosphodiesterase-4 (PDE4) that is utilised by multiple interaction partners. *Biochemical Journal*, 474(4):597–609, 2017.

[129] Claire Y Zhao, Joseph L Greenstein, and Raimond L Winslow. Interaction between phosphodiesterases in the regulation of the cardiac β-adrenergic pathway. *Journal of Molecular and Cellular Cardiology*, 88:29–38, 2015.

[130] Stephan E Lehnart and Andrew R Marks. Phosphodiesterase 4D and heart failure: a cautionary tale. *Expert Opinion on Therapeutic Targets*, 10(5):677–688, 2006.

[131] Milton Packer, Joseph R Carver, Richard J Rodeheffer, Russell J Ivanhoe, Robert DiBianco, Steven M Zeldis, Grady H Hendrix, William J Bommer, Uri Elkayam, Marrick L Kukin, George I Mallis, Josephine A Sollano, James Shannon, P K Tandon, and David L DeMets. Effect of Oral Milrinone on Mortality in Severe Chronic Heart Failure. *New England Journal of Medicine*, 325(21):1468–1475, 1991.

[132] George S. Baillie, David R. Adams, Narinder Bhari, Thomas M. Houslay, Suryakiran Vadrevu, Dong Meng, Xiang Li, Allan Dunlop, Graeme Milligan, Graeme B. Bolger, Enno Klussmann, and Miles D. Houslay. Mapping binding sites for the PDE4D5 cAMP-specific phosphodiesterase to the N- and C-domains of β-arrestin using spot-immobilized peptide arrays. *Biochemical Journal*, 404(1):71–80, 2007.

[133] Yehia Daaka, Louis M Luttrell, and Robert J Lefkowitz. Switching of the coupling of the β2-adrenergic receptor to different G proteins by protein kinase A. *Nature*, 390:88, 1997.

[134] George S Baillie, Arvind Sood, Ian McPhee, Irene Gall, Stephen J Perry, Robert J Lefkowitz, and Miles D Houslay. β-Arrestin-mediated PDE4 cAMP phosphodiesterase recruitment regulates β-adrenoceptor switching from Gs to Gi. *Proceedings of the National Academy of Sciences*, 100(3):940–945, 2003.

[135] Martin J Lynch, George S Baillie, Ahmed Mohamed, Xiang Li, Charlotte Maisonneuve, Enno Klussmann, Gino van Heeke, and Miles D Houslay. RNA Silencing Identifies PDE4D5 as the Functionally Relevant cAMP Phosphodiesterase Interacting with beta-Arrestin to Control the Protein Kinase A/AKAP79-mediated Switching of the beta2-Adrenergic Receptor to Activation of ERK in HEK293B2 Cells. *Journal of Biological Chemistry*, 280(39):33178–33189, 2005.

[136] Xiaohong Wang, Haitao Gu, Wei Huang, Jiangtong Peng, Yutian Li, Liwang Yang, Dongze Qin, Kobina Essandoh, Yigang Wang, Tianqing Peng, and Guo-Chang Fan. Hsp20-Mediated Activation of Exosome Biogenesis in Cardiomyocytes Improves Cardiac Function and Angiogenesis in Diabetic Mice. *Diabetes*, 65(10):3111–3128, 2016.

[137] Persoulla Nicolaou, Ralph Knöll, Kobra Haghighi, Guo-Chang Fan, Gerald W Dorn, Gerd Hasenfuss, and Evangelia G Kranias. Human Mutation in the Anti-apoptotic Heat Shock Protein 20 Abrogates Its Cardioprotective Effects. *Journal of Biological Chemistry*, 283(48):33465–33471, 2008.

[138] Deron J Tessier, Padmini Komalavilas, Alyssa Panitch, Lokesh Joshi, and Colleen M Brophy. The small heat shock protein (HSP) 20 is dynamically associated with the actin cross-linking protein actinin11This paper was presented at the annual meeting of the Association for Academic Surgery, Boston, MA, November 7,9, 2002. *Journal of Surgical Research*, 111(1):152–157, 2003.

[139] Guo-Chang Fan, Xiaoyang Zhou, Xiaohong Wang, Guojie Song, Jiang Qian, Persoulla Nicolaou, Guoli Chen, Xiaoping Ren, and Evangelia G Kranias. Heat Shock Protein 20 Interacting With Phosphorylated Akt Reduces Doxorubicin-Triggered Oxidative Stress and Cardiotoxicity. *Circulation Research*, 103(11):1270–1279, 2008.

[140] Helen V. Edwards, John D. Scott, and George S. Baillie. PKA phosphorylation of the small heat-shock protein Hsp20 enhances its cardioprotective effects. *Biochemical Society Transactions*, 40(1):210–214, 2012.

[141] Tamara P Martin, Maria P Hortigon-Vinagre, Jane E Findlay, Christina Elliott, Susan Currie, and George S Baillie. Targeted disruption of the heat shock protein 20 phosphodiesterase 4D (PDE4D) interaction protects against pathological cardiac remodelling in a mouse model of hypertrophy. *FEBS Open Bio*, 4(1):923–927, 2014.

[142] Stephan E. Lehnart, Xander H T Wehrens, Steven Reiken, Sunita Warrier, Andriy E. Belevych, Robert D. Harvey, Wito Richter, S. L Catherine Jin, Marco Conti, and Andrew R. Marks. Phosphodiesterase 4D deficiency in the

ryanodine-receptor complex promotes heart failure and arrhythmias. *Cell*, 123(1):25–35, 2005.

[143] Xander H T Wehrens, Stephan E Lehnart, Fannie Huang, John A Vest, Steven R Reiken, Peter J Mohler, Jie Sun, Silvia Guatimosim, Long-Sheng Song, Nora Rosemblit, Jeanine M D'Armiento, Carlo Napolitano, Mirella Memmi, Silvia G Priori, W J Lederer, and Andrew R Marks. FKBP12.6 Deficiency and Defective Calcium Release Channel (Ryanodine Receptor) Function Linked to Exercise-Induced Sudden Cardiac Death. *Cell*, 113(7):829–840, 2003.

[144] Wei Wu and Michael C Sanguinetti. Molecular Basis of Cardiac Delayed Rectifier Potassium Channel Function and Pharmacology. *Cardiac Electrophysiology Clinics*, 8(2):275–284, 2016.

[145] Andrew R Tapper and Jr. George. Location and orientation of minK within the IKs potassium channel complex. *Journal of Biological Chemistry*, 2001.

[146] Anna Terrin, Stefania Monterisi, Alessandra Stangherlin, Anna Zoccarato, Andreas Koschinski, Nicoletta C Surdo, Marco Mongillo, Akira Sawa, Niove E Jordanides, Joanne C Mountford, and Manuela Zaccolo. PKA and PDE4D3 anchoring to AKAP9 provides distinct regulation of cAMP signals at the centrosome. *The Journal of Cell Biology*, 198(4):607–621, 2012.

[147] Delphine Mika, Wito Richter, Ruth E Westenbroek, William a Catterall, and Marco Conti. PDE4B mediates local feedback regulation of β1-adrenergic cAMP signaling in a sarcolemmal compartment of cardiac myocytes. *Journal of cell science*, 127(Pt 5):1033–42, 2014.

[148] Jérôme Leroy, Wito Richter, Delphine Mika, Liliana R V Castro, Aniella Abi-gerges, Moses Xie, Colleen Scheitrum, Florence Lefebvre, Julia Schittl, Philippe Mateo, Ruth Westenbroek, William a Catterall, Flavien Charpentier, Marco Conti, Rodolphe Fischmeister, and Grégoire Vandecasteele. Phosphodiesterase 4B in the cardiac L-type Ca 2 + channel complex regulates Ca 2 + current and protects against ventricular arrhythmias in mice. 121(7):2651–2661, 2011.

[149] Tatiana M Vinogradova, Syevda Sirenko, Yevgeniya O Lukyanenko, Dongmei Yang, Kirill V Tarasov, Alexey E Lyashkov, Nevin J Varghese, Yue Li, Khalid Chakir, Bruce Ziman, and Edward G Lakatta. Basal Spontaneous Firing of Rabbit Sinoatrial Node Cells Is Regulated by Dual Activation of PDEs (Phosphodiesterases) 3 and 4. *Circulation: Arrhythmia and Electrophysiology*, 11(6):e005896, 2018.

[150] Sanja Beca, Peter B. Helli, Jeremy a. Simpson, Dongling Zhao, Gerrie P. Farman, Peter P. Jones, Xixi Tian, Lindsay S. Wilson, Faiyaz Ahmad, S. R Wayne

Chen, Matthew a. Movsesian, Vincent Manganiello, Donald H. Maurice, Marco Conti, and Peter H. Backx. Phosphodiesterase 4D regulates baseline sarcoplasmic reticulum Ca 2+ release and cardiac contractility, independently of L-type Ca 2+ current. *Circulation Research*, 109(9):1024–1030, 2011.

[151] Sanja Beca, Faiyaz Ahmad, Weixing Shen, Jie Liu, Samy Makary, Nazari Polidovitch, Junhui Sun, Steven Hockman, Youn Wook Chung, Matthew Movsesian, Elizabeth Murphy, Vincent Manganiello, and Peter H. Backx. Phosphodiesterase type 3A regulates basal myocardial contractility through interacting with sarcoplasmic reticulum calcium atpase type 2a Signaling complexes in mouse heart. *Circulation Research*, 112(2):289–297, 2013.

[152] David A Eisner, Jessica L Caldwell, Kornél Kistamás, and Andrew W Trafford. Calcium and Excitation-Contraction Coupling in the Heart. *Circulation research*, 121(2):181–195, jul 2017.

[153] Donald M Bers. Cardiac excitation contraction coupling. *Nature*, 415:198, 2002.

[154] Randi J Parks, Oleg Bogachev, Martin Mackasey, Gibanananda Ray, Robert A Rose, and Susan E Howlett. The impact of ovariectomy on cardiac excitation-contraction coupling is mediated through cAMP/PKA-dependent mechanisms. *Journal of Molecular and Cellular Cardiology*, 111:51–60, 2017.

[155] A Fabiato. Calcium-induced release of calcium from the cardiac sarcoplasmic reticulum. *American Journal of Physiology-Cell Physiology*, 245(1):C1–C14, 1983.

[156] Matthew A. Nystoriak, Madeline Nieves-Cintrón, and Manuel F. Navedo. Capturing single L-type Ca2+channel function with optics. *Biochimica et Biophysica Acta - Molecular Cell Research*, 1833(7):1657–1664, 2013.

[157] Jörg Striessnig, Alexandra Pinggera, Gurjot Kaur, Gabriella Bock, and Petronel Tuluc. L-type Ca2+channels in heart and brain. *Wiley Interdisciplinary Reviews: Membrane Transport and Signaling*, 3(2):15–38, 2014.

[158] Alexey V Glukhov, Anamika Bhargava, and Julia Gorelik. *Distribution and Regulation of L-Type Ca2+ Channels in Cardiomyocyte Microdomains*, pages 293–319. Springer International Publishing, Cham, 2017.

[159] Diane Lipscombe, Thomas D Helton, and Weifeng Xu. L-Type Calcium Channels: The Low Down. *Journal of Neurophysiology*, 92(5):2633–2641, 2004.

[160] Robert D Harvey and Johannes W Hell. CaV1.2 signaling complexes in the heart. *Journal of Molecular and Cellular Cardiology*, 58:143–152, 2013.

[161] A Melton, E Martin, and Eds Winston. Voltage-Gated Calcium Channels. (October):101–106, 2010.

[162] Francesca Rusconi, Paola Ceriotti, Michele Miragoli, Pierluigi Carullo, Nicolò Salvarani, Marcella Rocchetti, Elisa Di Pasquale, Stefano Rossi, Maddalena Tessari, Silvia Caprari, Magali Cazade, Paolo Kunderfranco, Jean Chemin, Marie Louise Bang, Fabio Polticelli, Antonio Zaza, Giuseppe Faggian, Gianluigi Condorelli, and Daniele Catalucci. Peptidomimetic Targeting of Cavβ2 Overcomes Dysregulation of the L-Type Calcium Channel Density and Recovers Cardiac Function. *Circulation*, 134(7):534–546, 2016.

[163] Kirsten Krahnstoever Davison and Leann L Birch. Auto-regulation of Cardiac L-type Calcium Channels. 64(12):2391–2404, 2008.

[164] Ravi C Balijepalli, Jason D Foell, Duane D Hall, Johannes W Hell, and Timothy J Kamp. Localization of cardiac L-type Ca2+ channels to a caveolar macromolecular signaling complex is required for β2-adrenergic regulation. *Proceedings of the National Academy of Sciences*, 103(19):7500–7505, 2006.

[165] Davit Hakobyan and Andreas Heuer. Key Molecular Requirements for Raft Formation in Lipid/Cholesterol Membranes. *PLOS ONE*, 9(2):1–11, 2014.

[166] Olaf S Andersen and Roger E Koeppe. Bilayer Thickness and Membrane Protein Function: An Energetic Perspective. *Annual Review of Biophysics and Biomolecular Structure*, 36(1):107–130, 2007.

[167] M Simionescu, N Simionescu, and G E Palade. Segmental differentiations of cell junctions in the vascular endothelium. The microvasculature. *The Journal of Cell Biology*, 67(3):863–885, 1975.

[168] Hemal H Patel, Fiona Murray, and Paul A Insel. Caveolae as Organizers of Pharmacologically Relevant Signal Transduction Molecules. *Annual Review of Pharmacology and Toxicology*, 48(1):359–391, 2008.

[169] Babak Razani, Scott E Woodman, and Michael P Lisanti. Caveolae: From Cell Biology to Animal Physiology. *Pharmacological Reviews*, 54(3):431–467, 2002.

[170] Marissa I Boulware, Holly Kordasiewicz, and Paul G Mermelstein. Caveolin Proteins Are Essential for Distinct Effects of Membrane Estrogen Receptors in Neurons. *Journal of Neuroscience*, 27(37):9941–9950, 2007.

[171] Amy Cavalli, Mansoureh Eghbali, Tamara Y Minosyan, Enrico Stefani, and Kenneth D Philipson. Localization of sarcolemmal proteins to lipid rafts in the myocardium. *Cell Calcium*, 42(3):313–322, 2007.

[172] Peter C Gray, John D Scott, and William A Catterall. Regulation of ion channels by cAMP-dependent protein kinase and A-kinase anchoring proteins. *Current Opinion in Neurobiology*, 8(3):330–334, 1998.

[173] Joanne T Hulme, Misol Ahn, Stephen D Hauschka, Todd Scheuer, and William A Catterall. A Novel Leucine Zipper Targets AKAP15 and Cyclic AMP-dependent Protein Kinase to the C Terminus of the Skeletal Muscle Ca2+ Channel and Modulates Its Function. *Journal of Biological Chemistry*, 277(6):4079–4087, 2002.

[174] Joanne T Hulme, Teddy W.-C. Lin, Ruth E Westenbroek, Todd Scheuer, and William A Catterall. β-Adrenergic regulation requires direct anchoring of PKA to cardiac CaV1.2 channels via a leucine zipper interaction with A kinase-anchoring protein 15. *Proceedings of the National Academy of Sciences*, 100(22):13093–13098, 2003.

[175] C Blake Nichols, Charles F Rossow, Manuel F Navedo, Ruth E Westenbroek, William A Catterall, Luis F Santana, and G Stanley McKnight. Sympathetic Stimulation of Adult Cardiomyocytes Requires Association of AKAP5 With a Subpopulation of L-Type Calcium Channels. *Circulation Research*, 107(6):747–756, 2010.

[176] Manuel F Navedo, Madeline Nieves-Cintrón, Gregory C Amberg, Can Yuan, V Scott Votaw, W Jonathan Lederer, G Stanley McKnight, and Luis F Santana. AKAP150 Is Required for Stuttering Persistent Ca2+ Sparklets and Angiotensin II Induced Hypertension. *Circulation Research*, 102(2):e1–e11, 2008.

[177] Muthu Periasamy and Anuradha Kalyanasundaram. SERCA pump isoforms: Their role in calcium transport and disease. *Muscle & Nerve*, 35(4):430–442, 2007.

[178] Richard R. Zwaal, Kurt Van Baelen, José T.M. Groenen, Anton Van Geel, Veerle Rottiers, Titus Kaletta, Leonard Dode, Luc Raeymaekers, Frank Wuytack, and Thierry Bogaert. The Sarco-Endoplasmic Reticulum Ca2+ATPase Is Required for Development and Muscle Function in Caenorhabditis elegans. *Journal of Biological Chemistry*, 276(47):43557–43563, 2001.

[179] Douglas M Anderson, Catherine A Makarewich, Kelly M Anderson, John M Shelton, Svetlana Bezprozvannaya, Rhonda Bassel-Duby, and Eric N Olson. Widespread control of calcium signaling by a family of SERCA-inhibiting micropeptides. *Science Signaling*, 9(457):ra119—-ra119, 2016.

[180] Przemek A Gorski, Delaine K Ceholski, and Howard S Young. *Structure-Function Relationship of the SERCA Pump and Its Regulation by Phospholam-*

ban and Sarcolipin, pages 77–119. Springer International Publishing, Cham, 2017.

[181] Alexander R. Lyon, Mark L. Bannister, Tom Collins, Emma Pearce, Amir H. Sepehripour, Sukhpreet S. Dubb, Edwin Garcia, Peter O'Gara, Lifan Liang, Erik Kohlbrenner, Roger J. Hajjar, Nicholas S. Peters, Philip A. Poole-Wilson, Ken T. Macleod, and Sian E. Harding. SERCA2a gene transfer decreases sarcoplasmic reticulum calcium leak and reduces ventricular arrhythmias in a model of chronic heart failure. *Circulation: Arrhythmia and Electrophysiology*, 4(3):362–372, 2011.

[182] Anne-Marie Lompré, Marielle Anger, and Dmitri Levitsky. Sarco(endo)plasmic Reticulum Calcium Pumps in the Cardiovascular System: Function and Gene Expression. *Journal of Molecular and Cellular Cardiology*, 26(9):1109–1121, 1994.

[183] D H MacLennan. Purification and properties of an adenosine triphosphatase from sarcoplasmic reticulum. *Journal of Biological Chemistry*, 245(17):4508:4518, 1970.

[184] Ian Curtis Smith, Eric Bombardier, Chris Vigna, and A Russell Tupling. ATP Consumption by Sarcoplasmic Reticulum Ca2+ Pumps Accounts for 40-50% of Resting Metabolic Rate in Mouse Fast and Slow Twitch Skeletal Muscle. *PLOS ONE*, 8(7), 2013.

[185] Eleri Hughes, Jonathan C Clayton, and David A Middleton. Cytoplasmic residues of phospholamban interact with membrane surfaces in the presence of SERCA: A new role for phospholipids in the regulation of cardiac calcium cycling? *Biochimica et Biophysica Acta (BBA) - Biomembranes*, 1788(2):559–566, 2009.

[186] Sana A Shaikh, Sanjaya K Sahoo, and Muthu Periasamy. Phospholamban and sarcolipin: Are they functionally redundant or distinct regulators of the Sarco(Endo)Plasmic Reticulum Calcium ATPase? *Journal of Molecular and Cellular Cardiology*, 91:81–91, 2016.

[187] Michio Asahi, Hiroyuki Nakayama, Michihiko Tada, and Kinya Otsu. Regulation of Sarco(endo)plasmic Reticulum Ca2+ Adenosine Triphosphatase by Phospholamban and Sarcolipin: Implication for Cardiac Hypertrophy and Failure. *Trends in Cardiovascular Medicine*, 13(4):152–157, 2003.

[188] P James, M Inui, M Tada, M Chiesi, and E Carafoli. Nature and site of phospholamban regulation of the Ca2+ pump of sarcoplasmic reticulum. *Nature*, 342:90, 1989.

[189] Michio Asahi, Edward McKenna, Kazimierz Kurzydlowski, Michihiko Tada, and David H MacLennan. Physical interactions between phospholamban and sarco(endo)plasmic reticulum Ca2+-ATPases are dissociated by elevated Ca2+, but not by phospholamban phosphorylation, vanadate, or thapsigargin, and are enhanced by ATP. *Journal of Biological Chemistry*, 275(20):15034–15038, 2000.

[190] Martin Gustavsson, Raffaello Verardi, Daniel G Mullen, Kaustubh R Mote, Nathaniel J Traaseth, T Gopinath, and Gianluigi Veglia. Allosteric regulation of SERCA by phosphorylation-mediated conformational shift of phospholamban. *Proceedings of the National Academy of Sciences*, 110(43):17338–17343, 2013.

[191] Tatsuya Sasaki, Makoto Inui, Yoshihiro Kimura, Tsunehiko Kuzuya, and Michihiko Tada. Molecular mechanism of regulation of Ca2+ pump ATPase by phospholamban in cardiac sarcoplasmic reticulum: Effects of synthetic phospholamban peptides on Ca2+ pump ATPase. *Journal of Biological Chemistry*, 267(3):1674–1679, 1992.

[192] N J Traaseth, D D Thomas, and G Veglia. Effects of Ser16 Phosphorylation on the Allosteric Transitions of Phospholamban/Ca2+-ATPase Complex. *Journal of Molecular Biology*, 358(4):1041–1050, 2006.

[193] Hongtao Shi, Qinghua Han, Jianrong Xu, Wenyuan Liu, Tingting Chu, and Li Zhao. Urotensin II induction of neonatal cardiomyocyte hypertrophy involves the CaMKII/PLN/SERCA 2a signaling pathway. *Gene*, 583(1):8–14, 2016.

[194] Mariano N Di Carlo, Matilde Said, Haiyun Ling, Carlos A Valverde, Verónica C De Giusti, Leandro Sommese, Julieta Palomeque, Ernesto A Aiello, Darlene G Skapura, Gustavo Rinaldi, Jonathan L Respress, Joan Heller Brown, Xander H T Wehrens, Margarita A Salas, and Alicia Mattiazzi. CaMKII-dependent phosphorylation of cardiac ryanodine receptors regulates cell death in cardiac ischemia/reperfusion injury. *Journal of Molecular and Cellular Cardiology*, 74:274–283, 2014.

[195] Meike Kuschel, Peter Karczewski, Petra Hempel, Wolfgang-peter Schlegel, Ernst-georg Krause, Sabine Bartel, Katherine A Sheehan, Yunbo Ke, Beata M Wolska, R John Solaro, James G Ryall, Jonathan D Schertzer, Kate T Murphy, Andrew M Allen, Gordon S Lynch, Sanda Despa, Amy L Tucker, Donald M Bers, Minkyung Kim, Grant W Hennig, Terence K Smith, Brian A Perrino, and Gastrointest Liver. Ser 16 prevails over Thr 17 phospholamban phosphorylation in the β -adrenergic regulation of cardiac relaxation Ser 16 prevails

over Thr 17 phospholamban phosphorylation in the beta adrenergic regulation of cardiac relaxation. *Proteins*, pages 1625–1633, 2011.

[196] Cecilia Mundiña-Weilenmann, Leticia Vittone, Manuel Ortale, Gladys Chiappe De Cingolani, and Alicia Mattiazzi. Immunodetection of phosphorylation sites gives new insights into the mechanisms underlying phospholamban phosphorylation in the intact heart. *Journal of Biological Chemistry*, 271(52):33561–33567, 1996.

[197] Guoxiang Chu, Gregory F. Egnaczyk, Wen Zhao, Su Hyun Jo, Guo Chang Fan, John E. Maggio, Rui Ping Xiao, and Evangelia G. Kranias. Phosphoproteome Analysis of Cardiomyocytes Subjected to β-Adrenergic Stimulation: Identification and Characterization of a Cardiac Heat Shock Protein p20. *Circulation Research*, 94(2):184–193, 2004.

[198] Sanja Beca, Peter B. Helli, Jeremy A. Simpson, Dongling Zhao, Gerrie P. Farman, Peter P. Jones, Xixi Tian, Lindsay S. Wilson, Faiyaz Ahmad, S. R Wayne Chen, Matthew A. Movsesian, Vincent Manganiello, Donald H. Maurice, Marco Conti, and Peter H. Backx. Phosphodiesterase 4D regulates baseline sarcoplasmic reticulum Ca 2+ release and cardiac contractility, independently of L-type Ca 2+ current. *Circulation Research*, 109(9):1024–1030, 2011.

[199] Sanja Beca, Faiyaz Ahmad, Weixing Shen, Jie Liu, Samy Makary, Nazari Polidovitch, Junhui Sun, Steven Hockman, Youn Wook Chung, Matthew Movsesian, Elizabeth Murphy, Vincent Manganiello, and Peter H Backx. Phosphodiesterase type 3A regulates basal myocardial contractility through interacting with sarcoplasmic reticulum calcium atpase type 2a Signaling complexes in mouse heart. *Circulation Research*, 112(2):289–297, 2013.

[200] James G Ryall, Jonathan D Schertzer, Kate T Murphy, Andrew M Allen, and Gordon S Lynch. Chronic β2-adrenoceptor stimulation impairs cardiac relaxation via reduced SR Ca2+-ATPase protein and activity. *American Journal of Physiology-Heart and Circulatory Physiology*, 294(6):H2587–H2595, 2008.

[201] Volker Henn, Bayram Edemir, Eduard Stefan, Burkhard Wiesner, Dorothea Lorenz, Franziska Theilig, Roland Schmitt, Lutz Vossebein, Grazia Tamma, Michael Beyermann, Eberhard Krause, Friedrich W Herberg, Giovana Valenti, Sebastian Bachmann, Walter Rosenthal, and Enno Klussmann. Identification of a Novel A-kinase Anchoring Protein 18 Isoform and Evidence for Its Role in the Vasopressin-induced Aquaporin-2 Shuttle in Renal Principal Cells. *Journal of Biological Chemistry*, 279(25):26654–26665, 2004.

[202] Birgitte Lygren, Cathrine Rein Carlson, Katja Santamaria, Valentina Lissandron, Theresa McSorley, Jessica Litzenberg, Dorothea Lorenz, Burkhard Wies-

ner, Walter Rosenthal, Manuela Zaccolo, Kjetil Taskén, and Enno Klussmann. AKAP complex regulates Ca2+ re-uptake into heart sarcoplasmic reticulum. *EMBO reports*, 8(11):1061–1067, 2007.

[203] Carlos Wilson, Ernesto Muñoz-Palma, Daniel R Henríquez, Ilaria Palmisano, M Tulio Núñez, Simone Di Giovanni, and Christian González-Billault. A Feed-Forward Mechanism Involving the NOX Complex and RyR-Mediated Ca2+ Release During Axonal Specification. *Journal of Neuroscience*, 36(43):11107–11119, 2016.

[204] Robyn T Rebbeck, Yamuna Karunasekara, Philip G Board, Nicole A Beard, Marco G Casarotto, and Angela F Dulhunty. Skeletal muscle excitation contraction coupling: Who are the dancing partners? *The International Journal of Biochemistry & Cell Biology*, 48:28–38, 2014.

[205] Matthew W Conklin, Chris A Ahern, Paola Vallejo, Vincenzo Sorrentino, Hiroshi Takeshima, and Roberto Coronado. Comparison of Ca2+ Sparks Produced Independently by Two Ryanodine Receptor Isoforms (Type 1 or Type 3). *Biophysical Journal*, 78(4):1777–1785, 2000.

[206] Angela F Dulhunty, Lan Wei-LaPierre, Marco G Casarotto, and Nicole A Beard. Core skeletal muscle ryanodine receptor calcium release complex. *Clinical and Experimental Pharmacology and Physiology*, 44(1):3–12, 2016.

[207] Andrea Faltinová and Alexandra Zahradníková. Modification of cardiac RYR2 gating by a peptide from the central domain of the RYR2. *Central European Journal of Biology*, 8(12):1164–1171, 2013.

[208] Masafumi Yano, Takeshi Yamamoto, Yasuhiro Ikeda, and Masunori Matsuzaki. Mechanisms of Disease: ryanodine receptor defects in heart failure and fatal arrhythmia. *Nature Clinical Practice Cardiovascular Medicine*, 3:43, 2006.

[209] Li Zhu, Xiaowei Zhong, S R.Wayne Chen, Nilesh Banavali, and Zheng Liu. Modeling a ryanodine receptor N-terminal domain connecting the central vestibule and the corner clamp region. *Journal of Biological Chemistry*, 288(2):903–914, 2013.

[210] Manjunatha B. Bhat, Jiying Zhao, Hiroshi Takeshima, and Jianjie Ma. Functional calcium release channel formed by the carboxyl-terminal portion of ryanodine receptor. *Biophysical Journal*, 73(3):1329–1336, 1997.

[211] Gerhard Meissner. The structural basis of ryanodine receptor ion channel function. *The Journal of General Physiology*, 149(12):1065–1089, 2017.

[212] L Zhang, C Franzini-Armstrong, V Ramesh, and L R Jones. Structural Alterations in Cardiac Calcium Release Units Resulting from Overexpression of Junctin. *Journal of Molecular and Cellular Cardiology*, 33(2):233–247, 2001.

[213] Guo-Chang Fan, Qunying Yuan, and Evangelia G Kranias. Regulatory Roles of Junctin in Sarcoplasmic Reticulum Calcium Cycling and Myocardial Function. *Trends in Cardiovascular Medicine*, 18(1):1–5, 2008.

[214] Kimberly L Dodge, Samone Khouangsathiene, Michael S Kapiloff, Robert Mouton, Elaine V Hill, Miles D Houslay, Lorene K Langeberg, and John D Scott. mAKAP assembles a protein kinase A/PDE4 phosphodiesterase cAMP signaling module. *The EMBO Journal*, 20(8):1921–1930, 2001.

[215] Steven O Marx, Steven Reiken, Yuji Hisamatsu, Thotalla Jayaraman, Daniel Burkhoff, Nora Rosemblit, and Andrew R Marks. PKA Phosphorylation Dissociates FKBP12.6 from the Calcium Release Channel (Ryanodine Receptor): Defective Regulation in Failing Hearts. *Cell*, 101(4):365–376, 2000.

[216] Sabine Huke and Donald M Bers. Ryanodine receptor phosphorylation at Serine 2030, 2808 and 2814 in rat cardiomyocytes. *Biochemical and Biophysical Research Communications*, 376(1):80–85, 2008.

[217] D R Witcher, R J Kovacs, H Schulman, D C Cefali, and L R Jones. Unique phosphorylation site on the cardiac ryanodine receptor regulates calcium channel activity. *Journal of Biological Chemistry*, 266(17):11144–11152, 1991.

[218] Patricia Rodriguez, Moninder S Bhogal, and John Colyer. Stoichiometric Phosphorylation of Cardiac Ryanodine Receptor on Serine 2809 by Calmodulin-dependent Kinase II and Protein Kinase A. *Journal of Biological Chemistry*, 278(40):38593–38600, 2003.

[219] X H T Wehrens. Ca2+/Calmodulin-Dependent Protein Kinase II Phosphorylation Regulates the Cardiac Ryanodine Receptor. *Circulation Research*, 94(6):e61—-e70, 2004.

[220] Bailong Xiao, Guofeng Zhong, Masakazu Obayashi, Dongmei Yang, Keyun Chen, Michael P. Walsh, Yakhin Shimoni, Heping Cheng, Henk Ter Keurs, and S. R. Wayne Chen. Ser-2030, but not Ser-2808, is the major phosphorylation site in cardiac ryanodine receptors responding to protein kinase A activation upon β-adrenergic stimulation in normal and failing hearts. *Biochemical Journal*, 396(1):7–16, 2006.

[221] Dariush Mozaffarian, Stefan D. Anker, Inder Anand, David T. Linker, Mark D. Sullivan, John G.F. Cleland, Peter E. Carson, Aldo P. Maggioni, Douglas L. Mann, Bertram Pitt, Philip A. Poole-Wilson, and Wayne C. Levy. Prediction

of mode of death in heart failure: The Seattle Heart Failure Model. *Circulation*, 116(4):392–398, 2007.

[222] Belal A. Mohamed, Nico Hartmann, Petros Tirilomis, Karolina Sekeres, Wener Li, Stefan Neef, Claudia Richter, Elisabeth M. Zeisberg, Lars Kattner, Michael Didié, Kaomei Guan, Jan D. Schmitto, Stephan E. Lehnart, Stefan Luther, Niels Voigt, Tim Seidler, Samuel Sossalla, Gerd Hasenfuss, and Karl Toischer. Sarcoplasmic reticulum calcium leak contributes to arrhythmia but not to heart failure progression. *Science Translational Medicine*, 10(458):1–12, 2018.

[223] Jian Shan, Matthew J Betzenhauser, Alexander Kushnir, Steven Reiken, Albano C Meli, Anetta Wronska, Miroslav Dura, Bi-Xing Chen, and Andrew R Marks. Role of chronic ryanodine receptor phosphorylation in heart failure and β-adrenergic receptor blockade in mice. *The Journal of Clinical Investigation*, 120(12):4375–4387, 2010.

[224] Stephan E Lehnart, Cecile Terrenoire, Steven Reiken, Xander H T Wehrens, Long-Sheng Song, Erik J Tillman, Salvatore Mancarella, James Coromilas, W J Lederer, Robert S Kass, and Andrew R Marks. Stabilization of cardiac ryanodine receptor prevents intracellular calcium leak and arrhythmias. *Proceedings of the National Academy of Sciences*, 103(20):7906–7910, 2006.

[225] Stephan E Lehnart, Marco Mongillo, Andrew Bellinger, Nicolas Lindegger, Bi-Xing Chen, William Hsueh, Steven Reiken, Anetta Wronska, Liam J Drew, Chris W Ward, W J Lederer, Robert S Kass, Gregory Morley, and Andrew R Marks. Leaky Ca2+ release channel/ryanodine receptor 2 causes seizures and sudden cardiac death in mice. *The Journal of Clinical Investigation*, 118(6):2230–2245, 2008.

[226] Steven O Marx and Andrew R Marks. Dysfunctional ryanodine receptors in the heart: New insights into complex cardiovascular diseases. *Journal of Molecular and Cellular Cardiology*, 58:225–231, 2013.

[227] Ling Dai, Yunliang Zang, Dingchang Zheng, Ling Xia, and Yinglan Gong. Role of CaMKII and PKA in Early Afterdepolarization of Human Ventricular Myocardium Cell: A Computational Model Study. *Computational and Mathematical Methods in Medicine*, 2016, 2016.

[228] Shih-Lin Chang, Yao-Chang Chen, Yung-Hsin Yeh, Yu-Jun Lai, Hung-I Yeh, Cheng-I Lin, Yung-Kuo Lin, Yenn-Jiang Lin, Tsu-Juey Wu, Yi-Kung Huang, Shih-Ann Chen, and Yi-Jen Chen. Heart failure enhances arrhythmogenesis in pulmonary veins. *Clinical and Experimental Pharmacology and Physiology*, 38(10):666–674, 2011.

[229] Min-Hung Chen, Po-Yuan Chen, and Ching-Hsing Luo. Quadratic adaptive algorithm for solving cardiac action potential models. *Computers in Biology and Medicine*, 77:261–273, 2016.

[230] Péter P Nánási, János Magyar, András Varró, and Balázs Ördög. Beat-to-beat variability of cardiac action potential duration: underlying mechanism and clinical implications. *Canadian Journal of Physiology and Pharmacology*, 95(10):1230–1235, 2017.

[231] Darby I Cairns, Flavio H Fenton, and E M Cherry. Efficient parameterization of cardiac action potential models using a genetic algorithm. *Chaos: An Interdisciplinary Journal of Nonlinear Science*, 27(9):93922, 2017.

[232] Danny Jans, Geert Callewaert, Olga Krylychkina, Luis Hoffman, Francesco Gullo, Dimiter Prodanov, and Dries Braeken. Action potential-based MEA platform for in vitro screening of drug-induced cardiotoxicity using human iPSCs and rat neonatal myocytes. *Journal of Pharmacological and Toxicological Methods*, 87:48–52, 2017.

[233] Lois Choy, Jie Ming Yeo, Vivian Tse, Shing Po Chan, and Gary Tse. Cardiac disease and arrhythmogenesis: Mechanistic insights from mouse models. *IJC Heart and Vasculature*, 12(May):1–10, 2016.

[234] Mitsunori Maruyama, Tomohiko Ai, Su-Kiat Chua, Hyung-Wook Park, Young-Soo Lee, Mark J Shen, Po-Cheng Chang, Shien-Fong Lin, and Peng-Sheng Chen. Hypokalemia promotes late phase 3 early afterdepolarization and recurrent ventricular fibrillation during isoproterenol infusion in Langendorff perfused rabbit ventricles. *Heart Rhythm*, 11(4):697–706, 2014.

[235] Hai Huang, Michael Pugsley, Bernard Fermini, Michael Curtis, John Koerner, Michael Accardi, and Simon Authier. Cardiac voltage-gated ion channels in safety pharmacology: Review of the landscape leading to the CiPA initiative. *Journal of Pharmacological and Toxicological Methods*, 87, 2017.

[236] Michael B Liu, Christopher Y Ko, Zhen Song, Alan Garfinkel, James N Weiss, and Zhilin Qu. A Dynamical Threshold for Cardiac Delayed Afterdepolarization-Mediated Triggered Activity. *Biophysical Journal*, 111(11):2523–2533, 2016.

[237] T. Förster. Zwischenmolekulare Energiewanderung und Fluoreszenz. *Annalen der Physik*, 437(112):55–75, 1948.

[238] Ferguson Roberg. Donor and Acceptor Overlap (https://www.researchgate.net/ profile/Robert{_}Ferguson23/publication/320870943/ figure/fig1.png), Oct. 27 2018.

[239] Viacheslav O Nikolaev and Martin J Lohse. Monitoring of cAMP Synthesis and Degradation in Living Cells. *Physiology*, 21(2):86–92, 2006.

[240] Jia Yu Liao, Yang Song, and Yan Liu. A new trend to determine biochemical parameters by quantitative FRET assays. *Acta Pharmacologica Sinica*, 36(12):1408–1415, 2015.

[241] Dilip Shrestha, Attila Jenei, Péter Nagy, György Vereb, and János Szoelloesi. *Understanding FRET as a research tool for cellular studies*, volume 16. 2015.

[242] László Bene, Miklós Bagdány, Tamás Ungvári, and László Damjanovich. Dual-Laser Tetra-Polarization FRET (4polFRET) for Site-Selective Control of Homo-FRET in Hetero-FRET Systems on the Cell Surface: The Homo-FRET Gate. *Analytical Chemistry*, 90(17):10159–10170, 2018.

[243] S Melih, Johan Strümpfer, Jen Hsin, Danielle Chandler, Simon Scheuring, Neil Hunter, and Klaus Schulten. Förster energy transfer theory as reflected in the structures of photosynthetic light harvesting systems. 12(3):518–531, 2012.

[244] Sebastian Börner, Frank Schwede, Angela Schlipp, Filip Berisha, Davide Calebiro, Martin J Lohse, and Viacheslav O Nikolaev. FRET measurements of intracellular cAMP concentrations and cAMP analog permeability in intact cells. *Nature protocols*, 6(4):427–438, 2011.

[245] Julia U. Sprenger and Viacheslav O. Nikolaev. Biophysical techniques for detection of cAMP and cGMP in living cells. *International Journal of Molecular Sciences*, 14(4):8025–8046, 2013.

[246] Viacheslav O. Nikolaev, Moritz Bünemann, Eva Schmitteckert, Martin J. Lohse, and Stefan Engelhardt. Cyclic AMP imaging in adult cardiac myocytes reveals far reaching β1 adrenergic but locally confined β2 adrenergic receptor mediated signaling. *Circulation Research*, 99(10):1084–1091, 2006.

[247] Joachim Goedhart, Laura van Weeren, Merel J W Adjobo-Hermans, Ies Elzenaar, Mark A Hink, and Theodorus W J Gadella Jr. Quantitative Co-Expression of Proteins at the Single Cell Level Application to a Multimeric FRET Sensor. *PLOS ONE*, 6(11):1–8, 2011.

[248] Jun He, Tao Yu, Jingying Pan, and He Li. Visualisation and Identification of the Interaction between STIM1s in Resting Cells. *PLOS ONE*, 7(3):1–8, 2012.

[249] Julia U. Sprenger, Ruwan K. Perera, Julia H. Steinbrecher, Stephan E. Lehnart, Lars S. Maier, Gerd Hasenfuss, and Viacheslav O. Nikolaev. In vivo model with targeted cAMP biosensor reveals changes in receptor microdomain communication in cardiac disease. *Nature Communications*, 6:6965, 2015.

[250] Yang Hsiang Chan, Changfeng Wu, Fangmao Ye, Yuhui Jin, Polina B. Smith, and Daniel T. Chiu. Development of ultrabright semiconducting polymer dots for ratiometric pH sensing. *Analytical Chemistry*, 83(4):1448–1455, 2011.

[251] Stephanie Hornig, Christoph Biskup, Anja Gräfe, Jana Wotschadlo, Tim Liebert, Gerhard J Mohr, and Thomas Heinze. Biocompatible fluorescent nanoparticles for pH-sensoring. *Soft Matter*, 4(6):1169–1172, 2008.

[252] Tristan Doussineau, Monique Smaïhi, and Gerhard J Mohr. Two-Dye Core/Shell Zeolite Nanoparticles: A New Tool for Ratiometric pH Measurements. *Advanced Functional Materials*, 19(1):117–122, 2008.

[253] R Madelaine Paredes, Julie C Etzler, Lora Talley Watts, Wei Zheng, and James D Lechleiter. Chemical calcium indicators. *Methods*, 46(3):143–151, 2008.

[254] Jung-Hwa Cho, Carter J Swanson, Jeannie Chen, Ang Li, Lisa G Lippert, Shannon E Boye, Kasey Rose, Sivaraj Sivaramakrishnan, Cheng-Ming Chuong, and Robert H Chow. The GCaMP-R Family of Genetically Encoded Ratiometric Calcium Indicators. *ACS Chemical Biology*, 12(4):1066–1074, 2017.

[255] Thomas Thestrup, Julia Litzlbauer, Ingo Bartholomäus, Marsilius Mues, Luigi Russo, Hod Dana, Yuri Kovalchuk, Yajie Liang, Georgios Kalamakis, Yvonne Laukat, Stefan Becker, Gregor Witte, Anselm Geiger, Taylor Allen, Lawrence C Rome, Tsai-Wen Chen, Douglas S Kim, Olga Garaschuk, Christian Griesinger, and Oliver Griesbeck. Optimized ratiometric calcium sensors for functional in vivo imaging of neurons and T lymphocytes. *Nature Methods*, 11:175, 2014.

[256] Hiromi Imamura, Kim P Huynh Nhat, Hiroko Togawa, Kenta Saito, Ryota Iino, Yasuyuki Kato-Yamada, Takeharu Nagai, and Hiroyuki Noji. Visualization of ATP levels inside single living cells with fluorescence resonance energy transfer-based genetically encoded indicators. *Proceedings of the National Academy of Sciences*, 106(37):15651–15656, 2009.

[257] C. Busch, T. Schroter, M. Grabolle, M. Wenzel, H. Kempe, W. a. Kaiser, U. Resch-Genger, and I. Hilger. An In Vivo Spectral Multiplexing Approach for the Cooperative Imaging of Different Disease-Related Biomarkers with Near-Infrared Fluorescent Forster Resonance Energy Transfer Probes. *Journal of Nuclear Medicine*, 53(4):638–646, 2012.

[258] Nadja I. Bork and Viacheslav O. Nikolaev. cGMP signaling in the cardiovascular system the role of compartmentation and its live cell imaging. *International Journal of Molecular Sciences*, 19(3):21–24, 2018.

[259] R K Perera, J Sprenger, J H Steinbrecher, D Hubscher, S E Lehnart, M Abesser, K Schuh, A El-Armouche, and V O Nikolaev. Microdomain Switch of cGMP-Regulated Phosphodiesterases Leads to ANP-Induced Augmentation of beta -Adrenoceptor-Stimulated Contractility in Early Cardiac Hypertrophy. *Circulation Research*, 2015.

[260] Julia U. Sprenger, Ruwan K. Perera, Konrad R. Götz, and Viacheslav O. Nikolaev. FRET Microscopy for Real-time Monitoring of Signaling Events in Live Cells Using Unimolecular Biosensors. *Journal of Visualized Experiments*, (66):1–7, 2012.

[261] Delphine Mika, Wito Richter, and Marco Conti. A CaMKII/PDE4D negative feedback regulates cAMP signaling. *Proceedings of the National Academy of Sciences*, 2015:201419992, 2015.

[262] Stephen R Adams, Alec T Harootunian, Ying Ji Buechler, Susan S Taylor, and Roger Y Tsien. Fluorescence ratio imaging of cyclic AMP in single cells. *Nature*, 349:694, 1991.

[263] Katie J. Herbst, Qiang Ni, and Jin Zhang. Dynamic visualization of signal transduction in living cells: From second messengers to kinases. *IUBMB Life*, 61(9):902–908, 2009.

[264] Manuela Zaccolo. Use of Chimeric Fluorescent Proteins and Fluorescence Resonance Energy Transfer to Monitor Cellular Responses. *Circulation Research*, 94(7):866–873, 2004.

[265] Lisa M DiPilato, Xiaodong Cheng, and Jin Zhang. Fluorescent indicators of cAMP and Epac activation reveal differential dynamics of cAMP signaling within discrete subcellular compartments. *Proceedings of the National Academy of Sciences*, 101(47):16513–16518, 2004.

[266] Viacheslav O Nikolaev, Moritz Buenemann, Lutz Hein, Annette Hannawacker, and Martin J Lohse. Novel Single Chain cAMP Sensors for Receptor-induced Signal Propagation. *Journal of Biological Chemistry*, 279(36):37215–37218, 2004.

[267] Bas Ponsioen, Jun Zhao, Jurgen Riedl, Fried Zwartkruis, Gerard van der Krogt, Manuela Zaccolo, Wouter H Moolenaar, Johannes L Bos, and Kees Jalink. Detecting cAMP-induced Epac activation by fluorescence resonance energy transfer: Epac as a novel cAMP indicator. *EMBO reports*, 5(12):1176–1180, 2004.

[268] R K Perera, J U Sprenger, J H Steinbrecher, D Hubscher, S E Lehnart, M Abesser, K Schuh, A El-Armouche, and V O Nikolaev. Microdomain Switch

of cGMP-Regulated Phosphodiesterases Leads to ANP-Induced Augmentation of Adrenoceptor-Stimulated Contractility in Early Cardiac Hypertrophy. *Circulation Research*, 116(8):1304–1311, 2015.

[269] Julia U Sprenger, Ruwan K Perera, Julia H Steinbrecher, Stephan E Lehnart, Lars S Maier, Gerd Hasenfuss, and Viacheslav O Nikolaev. In vivo model with targeted cAMP biosensor reveals changes in receptor microdomain communication in cardiac disease. *Nature Communications*, 6:6965, 2015.

[270] Konrad Götz. Real time visualization of cGMP and cAMP dynamics in intact adult cardiomyocytes using new transgenic mice. *"Doctoral Thesis"*, pages 1–121, 2014.

[271] Jörn Heine, Matthias Reuss, Benjamin Harke, Elisa Este, Steffen J Sahl, and Stefan W Hell. Adaptive-illumination STED nanoscopy. *Proceedings of the National Academy of Sciences*, 114(37):9797–9802, 2017.

[272] Ernst Abbe. Beitraege zur Theorie des Mikroskops und der mikroskopischen Wahrnehmung. *Archiv für mikroskopische Anatomie*, 9(1):413–418, 1873.

[273] Ernst Abbe. The Relation of Aperture and Power in the Microscope (continued). *Journal of the Royal Microscopical Society*, 3(6):790–812, 1883.

[274] ActiveMotif. STED Microscopy Products (https://www.activemotif.com/ images/ products/TCS_STED_CW_01_web_big.jpg), Nov. 8 2018.

[275] Matthew R G Russell, Thomas R Lerner, Jemima J Burden, David O Nkwe, Annegret Pelchen-Matthews, Marie-Charlotte Domart, Joanne Durgan, Anne Weston, Martin L Jones, Christopher J Peddie, Raffaella Carzaniga, Oliver Florey, Mark Marsh, Maximiliano G Gutierrez, and Lucy M Collinson. 3D correlative light and electron microscopy of cultured cells using serial blockface scanning electron microscopy. *Journal of Cell Science*, 130(1):278–291, 2017.

[276] Luwei Wang, Bingling Chen, Wei Yan, Zhigang Yang, Xiao Peng, Danying Lin, Xiaoyu Weng, Tong Ye, and Junle Qu. Resolution improvement in STED super-resolution microscopy at low power using a phasor plot approach. *Nanoscale*, 10(34):16252–16260, 2018.

[277] Ronan Chéreau, Jan Tønnesen, and U Valentin Nägerl. STED microscopy for nanoscale imaging in living brain slices. *Methods*, 88:57–66, 2015.

[278] S.-L. Catherine Jin and Marco Conti. Induction of the cyclic nucleotide phosphodiesterase PDE4B is essential for LPS-activated TNF-α responses. *Proceedings of the National Academy of Sciences*, 99(11):7628–7633, 2002.

[279] S.-L. Catherine Jin, François J Richard, Wie-Peng Kuo, A Joseph Ercole, and Marco Conti. Impaired growth and fertility of cAMP-specific phosphodiesterase PDE4D-deficient mice. *Proceedings of the National Academy of Sciences*, 96(21):11998–12003, 1999.

[280] Bo Ding, Jun-Ichi Abe, Heng Wei, Qunhua Huang, Richard A Walsh, Carlos A Molina, Allan Zhao, Junichi Sadoshima, Burns C Blaxall, Bradford C Berk, and Chen Yan. Functional role of phosphodiesterase 3 in cardiomyocyte apoptosis: implication in heart failure. *Circulation*, 111(19):2469–2476, 2005.

[281] Amélie Marquette, Jocelyne André, Martine Bagot, Armand Bensussan, and Nicolas Dumaz. ERK and PDE4 cooperate to induce RAF isoform switching in melanoma. *Nature structural {{}{&}{}} molecular biology*, 18(5):584–591, 2011.

[282] G MENDEL. Versuche uber Pflanzen-Hybriden. *Vorgelegt in den Sitzungen*, 1865.

[283] William E. Louch, Katherine a. Sheehan, and Beata M. Wolska. Methods in cardiomyocyte isolation, culture, and gene transfer. *Journal of Molecular and Cellular Cardiology*, 51(3):288–298, 2011.

[284] Sebastian Börner, Frank Schwede, Angela Schlipp, Filip Berisha, Davide Calebiro, Martin J Lohse, and Viacheslav O Nikolaev. FRET measurements of intracellular cAMP concentrations and cAMP analog permeability in intact cells. *Nature Protocols*, 6:427, 2011.

[285] Christiane Jungen, Katharina Scherschel, Christian Eickholt, Pawel Kuklik, Niklas Klatt, Nadja Bork, Tim Salzbrunn, Fares Alken, Stephan Angendohr, Christiane Klene, Janos Mester, Nikolaj Klöcker, Marieke W. Veldkamp, Udo Schumacher, Stephan Willems, Viacheslav O. Nikolaev, and Christian Meyer. Disruption of cardiac cholinergic neurons enhances susceptibility to ventricular arrhythmias. *Nature Communications*, 8, 2017.

[286] Michael Ibrahim, Julia Gorelik, Magdi H. Yacoub, and Cesare M. Terracciano. The structure and function of cardiac t-tubules in health and disease. *Proceedings of the Royal Society B: Biological Sciences*, 278(1719):2714–2723, 2011.

[287] Benoit-Gilles Kerfant, Dongling Zhao, Ilka Lorenzen-Schmidt, Lindsay S Wilson, Shitian Cai, S R Wayne Chen, Donald H Maurice, and Peter H Backx. PI3Kgamma; Is Required for PDE4, not PDE3, Activity in Subcellular Microdomains Containing the Sarcoplasmic Reticular Calcium ATPase in Cardiomyocytes. *Circulation Research*, 101(4):400–408, 2007.

[288] Fabien Brette, Kimiaki Komukai, and Clive H Orchard. Validation of formamide as a detubulation agent in isolated rat cardiac cells. *American Journal of Physiology-Heart and Circulatory Physiology*, 283(4):H1720–H1728, 2002.

[289] Hariharan Subramanian, Alexander Froese, Peter Jönsson, Hannes Schmidt, Julia Gorelik, and Viacheslav O Nikolaev. Distinct submembrane localisation compartmentalises cardiac NPR1 and NPR2 signalling to cGMP. *Nature Communications*, 9(1):1–9, 2018.

[290] Viacheslav O Nikolaev, Alexey Moshkov, Alexander R Lyon, Michele Miragoli, Pavel Novak, Helen Paur, Martin J Lohse, Yuri E Korchev, Sian E Harding, and Julia Gorelik. β2-Adrenergic Receptor Redistribution in Heart Failure Changes cAMP Compartmentation. *Science*, 327(5973):1653–1657, 2010.

[291] Concept Draw. Hazard Pictograms (https://www.conceptdraw.com/How-To-Guide/hazard-pictograms), Dec. 30 2018.

5. Appendix

Table 5.1: Individual Measurements for Spectral Bleedthrough Factor. HEK293a cells were transfected with a plasmid for the donor fluorophor, Cyan Fluorescent Protein (CFP). Fluorescence was detected in both CFP and Yellow Fluorescent Protein (YFP) channels.

Cell No.	YFP	CFP	YFP/CFP
1	227.456	260.695	0.872
2	226.624	259.380	0.873
3	177.747	188.445	0.943
4	205.527	225.915	0.909
5	197.347	215.396	0.916
6	189.175	204.214	0.926
7	189.175	199.273	0.949
8	191.005	207.132	0.922
9	216.442	246.060	0.879
10	252.612	296.718	0.851
11	195.156	215.506	0.905
12	196.512	217.043	0.905
13	235.335	269.407	0.905
14	236.077	276.440	0.873
15	227.513	263.137	0.864
16	275.098	334.852	0.821
17	232.439	271.233	0.856
18	213.195	245.460	0.868
19	204.454	228.017	0.896

Table 5.2: Chemicals Categorized According to GHS

Chemical	H Statements	P Statements	Hazard Pictograms
β-Mercapthoethanol	301+331, 310, 315, 317, 318, 373, 410	273, 280, 302+352, 304+340, 305+351+338, 308+310	05, 06, 08, 09
(-)-Isoproterenol hydrochloride			
2,3-Butanedione monoxime			
2-Propanol	302		07
3-Isobutyl-1-Methylxanthine	302		07
Ammonium persulfate	272, 302, 315, 317, 319, 334, 335	220, 261, 280, 305+351+338, 342+311	03, 07, 08
Ampuwa			
Bovine serum albumin	225, 302, 314		02, 05, 07
Bromophenol blue sodium salt			
Calcium chloride	319	305+351+338	07
Calcium chloride dihydrate	319	305+351+338	07
di-8-ANEPPS	302, 312, 332		07
Dimethyl sulfoxide			
di-Sodium hydrogen phosphate dihydrate			
Ethanol absolute for molecular biology	225, 319	210, 240, 305+351+338, 403+233	02, 07
Ethylenediaminetetraacetic acid (0.5 M)	319	305+351+338	07

Chemical	H Statements	P Statements	Hazard Pictograms
Fetal Calf Serum			
Forskolin	312	280	07
Glucose			
Glycerol			
Glycine			
HEPES			
Hydrochloric acid 37%	331, 314, 280	260, 280, 304+340, 303+361+353, 305+351+338, 315, 405, 403	05, 06
Insulin-Transferrin-Selenium-X (ITS)			
Laminin			
L-Ascorbic acid			
L-glutamine			
Liberase DH Research Grade			
Magnesium chloride hexahydrate			
Magnesium sulfate heptahydrate			
MEM, no glutamine, no phenol red			
Methanol	225, 331, 311, 301, 370	210, 233, 280, 302+352, 304+340, 308+310, 403+235	02, 06, 08
Moviol			

Chemical	H Statements	P Statements	Hazard Pictograms
N,N-Dimethylformamide	226, 312, 332, 319, 360D	201, 210, 302+352, 304+340, 305+351+338, 308+313	02, 07, 08
N.N,N',N'-Tetramethylethylenediamine	225 332, 302, 314	210, 280, 305+351+338, 310	02, 05, 07
PBS Dulbecco			
Penicillin/Streptomycin			
Potassium chloride			
Potassium dihydrogen phosphate			
Potassium hydrogen carbonate			
Powdered milk			
Propranolol hydrochloride	302		07
Rotiphorese Gel 30 (Acrylamide)	301, 312, 332, 315, 317, 319, 340, 350, 361f, 372	201, 280, 302+352, 304+340, 305+351+338, 308+310	06, 08
Sodium azide	300, 310, 373, 410	273, 280, 301+310+330, 302+352, 310, 391, 501	06, 08, 09
Sodium chloride			
Sodium dodecyl sulfate solution (20%)	228, 302+332, 315, 318, 335, 412	210, 261, 280, 301+312+330, 305+351+338+310, 370+378	05, 07
Sodium hydrogen carbonate			

Chemical	H Statements	P Statements	Hazard Pictograms
Sodium hydroxide solution	290, 314	280, 301+330+331, 305+351+338 308+310	05
Sodium pyruvate			
Taurine	315, 319, 335	261, 305+351+338	07
Technical Buffer Solution pH 4.01			
Technical Buffer Solution pH 7.00			
Tergitol solution Type NP-40	302, 318, 441	273, 280, 305+351+338	05, 07, 09
Tris	315, 319, 335	261, 305+351+338	07
Triton X-100 Solution 10%	302, 318, 411	273, 280, 305+351+338	05, 07, 09
Trypsin 2.5%			
Tween 20			

Figure 5.1: Hazard Pictograms According to GHS. Diagram adapted from [291].

Affidavit

Hiermit versichere ich an Eides statt, die vorliegende Dissertation selbst verfasst und keine anderen als die angegebenen Hilfsmittel benutzt zu haben. Die eingereichte schriftliche Fassung entspricht der auf dem elektronischen Speichermedium. Ich versicher, dass die Dissertation nicht in einem früheren Promotionsverfahren eingereicht wurde.

Hamburg, den 15. April 2019